

DISSERTATION

**Protein Adsorption on
Nanostructured Polymer Surfaces**



zur Erlangung des akademischen Grades Doktor-Ingenieur(in)
(Dr.-Ing.)

vorgelegt dem Rat der Physikalisch Astronomische Fakultät
der Friedrich Schiller Universität Jena
von M. Sc. Xiaoyuan Zhang, geboren
am 23.11.1988 in Qinghai, V. R. China

1. Gutachter: Prof. Dr. Klaus D. Jandt

2. Gutachter:

3. Gutachter:

Tag der Disputation:

Dedicated to Yaqing Zhang and Yuefang Hu

上善若水水善
利万物不争

於戊戌年正月
張亞清

Written by Yaqing Zhang on 20th, January 2019 in Qinghai, P. R. China

“The best virtue is like water.

Water benefits everything in the world but never contends its contribution.”

-Laozi

Statement of Authorship

Hereby, I declare that this thesis and the work presented in it are my work, and all the literature sources and materials used have been documented correctly. This thesis, in whole or in part, was not submitted to another examination board and has not been published.

All the primary sources of help have been clarified and acknowledged in the thesis. In the following circumstances, the experimental procedures were performed with the help of cooperators.

1. Prof. Mark J. Kastantin (Department of Chemical and Biological Engineering, University of Colorado Boulder, Boulder, CO 80309, USA.) for experimental work of the single protein tracking on polymer surfaces.

2. M. Sc. Alper Özogul and Prof. Dr. Enrico Gnecco (Otto-Schott-Institut für Materialforschung, Professur für Mechanik der funktionellen Materialien, Löbdergraben 32, D-07743 Jena) for the experimental work of diffusion properties on nanostructured polymer surfaces.

- 3, Dr. Thomas Dauben, Dr. Izabela Firkowska-Boden, and Mr. Felix Arendt (Otto-Schott-Institut für Materialforschung, Chair of Materials science, Löbdergraben 32, D-07743 Jena) for the platelet adhesion test and microscopic images acquisition.

No other person's work has been used without acknowledgment in the main text of the thesis.

All sources of information have been quoted as references. All presented graphs and data sets in state of the art have been quoted as references and explicitly acknowledged.

Signed: Xiaoyuan Zhang

Jena, 27th June 2019

Ehrenwörtliche Erklärung

Hiermit erkläre ich, dass diese Dissertation und die darin präsentierte Arbeit meine eigene Arbeit ist und dass alle verwendeten Quellen und Materialien korrekt dokumentiert wurden. Diese Dissertation wurde weder ganz noch teilweise einer anderen Prüfungskommission vorgelegt und ist nicht veröffentlicht worden.

Alle Kooperationspartner wurden in dieser Arbeit aufgeführt und für deren Unterstützung gewürdigt. Die folgenden experimentellen Verfahren wurden mit Hilfe von Kooperationspartnern durchgeführt.

1. Prof. Mark J. Kastantin (Abteilung für chemische und biologische Verfahrenstechnik, Universität von Colorado Boulder, Boulder, CO 80309, USA.) Experimentelle Arbeiten zur Einzelproteinverfolgung auf Polymeroberflächen.

2. M. Sc. Alper Özogul und Prof. Dr. Enrico Gnecco (Otto-Schott-Institut für Materialforschung, Professur für Mechanik der funktionellen Materialien, Löbdergraben 32, D-07743 Jena) für die experimentelle Arbeit an Diffusionseigenschaften auf nanostrukturierten Polymeroberflächen.

3. Dr. Thomas Dauben, Dr. Izabela Firkowska-Boden und Felix Arendt (Otto-Schott-Institut für Materialforschung, Lehrstuhl für Materialwissenschaft, Löbdergraben 32, D-07743 Jena) für den Thrombozyten-Adhäsionstest und die mikroskopische Bilderfassung.

Keine weiteren Arbeiten von anderen Personen wurden verwendet, ohne Sie im Hauptteil der Arbeit zu erwähnen. Alle Informationsquellen wurden als Referenzen angegeben. Die im Stand der Technik dargestellten Grafiken und Daten wurden als Referenzen zitiert und ausgewiesen.

Signiert: Xiaoyuan Zhang

Jena, 27. Juni 2019

Abstract

Human plasma fibrinogen (HPF) plays an essential role in the initial host response to biomaterials. Developing strategies for controlling the HPF-biomaterial interactions is crucial but is still in its infancy. Here, it was demonstrated that the nanostructures on polymers such as needle-like crystals (NLCs) and lamellar crystals (LCs) of isotactic polybutene-1 (iPB-1), as well as shish-kebab crystals (SKCs) of high-density polyethylene (HDPE), were capable of guiding the adsorption of HPF and their subsequent platelet adhesion.

The NLCs of iPB-1, with a lateral dimension lower than the length of the HPF major axis, supported “side-on” adsorption and trinodular conformation, confirmed by atomic force microscopy and quartz crystal microbalance with dissipation. Preferential alignment of HPF molecules concerning the axial direction of the NLCs was analyzed via an orientation analysis performed on “single-” and “multi-” protein levels. The results of the protein adsorption kinetic studies via quartz crystal microbalance revealed the surface-dependent packing density and assembly configuration of HPF.

To elucidate the relationship between single HPF adsorption and HPF layer formation, the dynamics of HPF-assemblies adsorbed on nanostructured surfaces were investigated in-situ by mapping using accumulated probe trajectories. Anisotropic diffusion of HPF was revealed on NLCs. This was ascribed to the partial detachment and thus the Sansetsukon-like nanocrawling of HPF.

To further understand the biofunctionality of the surface-immobilized HPF, platelet adhesion as a function of surfaces and conformation was investigated. It was observed that the number of platelets adhered on NLCs was significantly reduced by 90% after one-hour incubation, compared with those on LCs and SKCs. NLCs led to small platelet aggregates, which point toward the potential thrombogenicity of such nanostructured surfaces.

This study provides fundamental insight into the mechanism of topographically mediated HPF-biomaterial interactions, a promising technique to control the host response to biomaterials, and advancing the design of innovative implantable biomedical devices.

Zusammenfassung

Humanes Fibrinogen aus dem Blutplasma (HPF) spielt eine wichtige Rolle bei der initialen Reaktion des Wirts auf Biomaterialien. Die Entwicklung von Strategien zur Kontrolle der Wechselwirkungen zwischen HPF und Biomaterial ist unerlässlich, steht jedoch noch am Anfang. In der vorliegenden Arbeit wird gezeigt, dass polymere Nanostrukturen wie nadelartige Kristalle (NLCs) und lamellare Kristalle (LCs) aus isotaktischem Polybuten-1 (iPB-1) sowie Shish-Kebab-Kristalle (SKCs) aus Polyethylen hoher Dichte (HDPE) geeignet sind, um die Adsorption von HPF und die daran anschließende Blutplättchenadhäsion zu steuern.

NLCs aus iPB-1, deren laterale Abmessung geringer als die Länge der HPF-Hauptachse ist, unterstützten die „side-on“ Adsorption und die trinoduläre Konformation, was mittels Rasterkraftmikroskopie und Quarzkristall-Mikrowaagen-Daten bestätigt wurde. Darüber hinaus ergab die Orientierungsanalyse von Einzelproteinen und Proteinnetzwerken eine bevorzugte Ausrichtung von HPF-Molekülen in Bezug auf die axiale Richtung der NLCs. Die Ergebnisse der kinetischen Proteinadsorptionsstudien mittels Quarzkristall-Mikrowaage zeigten eine oberflächenabhängige Packungsdichte und Konfiguration der angeordneten HPF-Moleküle auf.

Um die Beziehung zwischen der Adsorption von einzelnen HPF-Molekülen und der Bildung von HPF-Schichten besser zu verstehen, wurden Messungen von dynamischen HPF-Anordnungen durchgeführt. Dazu wurde die Adsorption von HPF auf nanostrukturierten Oberflächen in-situ mittels Kartierung von akkumulierter Proben-Trajektorien untersucht. Anisotrope HPF-Diffusion wurde auf NLCs nachgewiesen. Dies wurde der partiellen Ablösung und somit einer „Sansetsukon-ähnlichen“ Diffusionsbewegung von HPF im Nanometerbereich zugeschrieben.

Um die Biofunktionalität des an der Oberfläche immobilisierten HPF besser zu verstehen, wurde die Adhäsion der Blutplättchen in Abhängigkeit der

Oberflächenstruktur und der HPF-Konformation untersucht. Nach einstündiger Inkubation konnte eine um 90 % verringerte Adhäsion der Blutplättchen auf NLC im Vergleich zu LC und SKC beobachtet werden. NLCs induzierten jedoch eine Aggregation der Blutplättchen, was auf eine potenzielle Thrombogenität solcher nanostrukturierter Oberflächen hinweist.

In der vorliegenden Arbeit werden grundlegende Einblicke in den Mechanismus topographisch-induzierter HPF-Biomaterial-Wechselwirkungen aufgezeigt. Die hier beschriebene Nanostrukturierung ist eine vielversprechende Technik um die Reaktion des Wirts auf Biomaterialien zu kontrollieren und liefert Ansätze zur Verbesserung des Designs innovativer implantierbarer biomedizinischer Geräte.

Table of Contents

Statement of Authorship	I
Ehrenwörtliche Erklärung	III
Abstract	V
Zusammenfassung	VII
Table of Contents	1
List of Figures	5
List of Tables	6
List of Abbreviations and Symbols	7
1 Introduction	11
2 State of the Art	13
2.1 Polymer Biomaterials	13
2.1.1 Classification of polymers	13
2.1.2 Application of synthetic polymers as biomaterials	15
2.2 Surface Nanostructuring of Polymers	17
2.2.1 Lithography and molding	17
2.2.2 Self-assembly	18
2.2.3 Melt drawing	19
2.3 Protein Adsorption on Nanostructured Polymers	22
2.3.1 Proteins	22
2.3.2 The human plasma fibrinogen (HPF)	23
2.3.3 HPF adsorption mediated by surface factors	25
2.3.4 HPF on nanostructures of molded polymers	29
2.3.5 HPF on surfaces with self-assembled polymers	30
2.3.6 HPF on melt-drawn polymers	31
2.4 Platelet Adhesion on Surfaces	33
2.4.1 Platelet adhesion on nanostructured polymer surfaces	33
2.4.2 Platelet adhesion influenced by HPF conformation	34

2.5 Brief Summary	35
3 Aims and Objectives	38
3.1 Open Scientific Questions.....	38
3.2 Hypotheses.....	38
3.3 Aims and Objectives.....	39
3.4 Scientific Significance	39
3.5 Related Publications	40
3.6 Related Presentations	40
3.7 Thesis Outline	41
4 Experimental	43
4.1 Experimental Techniques	43
4.1.1 Atomic force microscopy (AFM).....	43
4.1.2 Quartz crystal microbalance with dissipation (QCM-D).....	45
4.1.3 Mapping using accumulated probe trajectories (MAPT).....	46
4.2 Sample Preparation and Characterization.....	49
4.2.1 Preparation of nanostructured surfaces.....	49
4.2.2 Surface nanostructures by AFM	50
4.2.3 Surface chemistry determination by contact angle measurement and X-ray photoelectron spectroscopy (XPS)	51
4.3 Protein Detection on Nanostructured Surfaces.....	51
4.3.1 HPF adsorption on nanostructured surfaces	51
4.3.2 HPF observations by AFM	51
4.3.3 HPF adsorption dynamics by QCM-D.....	52
4.3.4 Single protein tracking by MAPT	52
4.4 Cell Adhesion on Nanostructured Surfaces.....	53
4.4.1 Cytotoxicity of surfaces	53
4.4.2 Platelet adhesion on surfaces.....	53
4.4.3 Platelets observation by optical microscope (OM) and scanning electron microscope (SEM).....	54
5 Results and Discussion	56
5.1 Nanocrystal Width Controlled Fibrinogen Assembly.....	56
5.1.1 Semicrystalline polymer thin films.....	56

5.1.2 HPF assembly on nanostructured polymers.....	59
5.1.3 HPF adsorption kinetics on nanostructured surfaces.....	67
5.1.4 Conclusion.....	71
5.2 Anisotropic HPF Diffusion on Nanostructured Polymers	73
5.2.1 Single HPF on nanostructured isotactic polybutene-1 (iPB-1)	73
5.2.2 Elongated structures of HPF trajectories.....	75
5.2.3 Mean residence time of HPF	77
5.2.4 Anisotropic diffusion of HPF.....	78
5.2.5 Conclusion.....	84
5.3 Cell Adhesion on Nanostructured Polymers.....	85
5.3.1 Fibroblast cell viability on nanostructured surfaces.....	85
5.3.2 Platelet morphologies on smooth surface.....	86
5.3.3 Platelet surface coverage on nanostructured surfaces.....	87
5.3.4 Platelet activation on nanostructured surfaces.....	89
5.3.5 Conclusion.....	94
6 Summary.....	96
References	99
Acknowledgments.....	123
Curriculum Vitae.....	125

List of Figures

1. The chemical structures and sketches of polymers.
2. Nanostructured amorphous polymer surfaces by compression molding.
3. Nanostructures of block copolymer.
4. Nanostructures of semicrystalline polymers by melt-drawing (MD) technique.
5. Molecular structure of human plasma fibrinogen (HPF).
6. Surface physicochemical factors that affect the HPF adsorption.
7. HPF molecule assembly on block copolymer surfaces.
8. HPF molecule assembly on nanostructured semicrystalline polymer surfaces.
9. The working principle of AFM.
10. The working principle of quartz crystal microbalance with dissipation (QCM-D).
11. The working principle of mapping using accumulated probe trajectories (MAPT).
12. Schematic of MD technique.
13. Schematic of spin-coating (SC) technique.
14. Surface topography of melt-drawn isotactic polybutene-1 (MD iPB-1) thin film.
15. Surface topography of spin-coated isotactic polybutene-1 (SC iPB-1) thin film.
16. Surface topography of melt-drawn high-density polyethylene (MD HDPE) thin film.
17. HPF assembly on MD iPB-1.
18. Quantitative analysis of HPF network assembly on MD iPB-1.
19. HPF assembly on SC iPB-1.
20. HPF assembly on MD HDPE.
21. HPF adsorption kinetics on MD and SC iPB-1 thin films.
22. Single HPF observation on MD iPB-1.
23. MAPT occupancy maps on MD iPB-1.
24. Residence time on MD iPB-1.

25. Diffusion coefficients and polarizations of HPF on MD iPB-1.
26. Surface diffusion directions on MD iPB-1 and MD HDPE.
27. Sansetsukon-like nanocrawling.
28. MTT assay of fibroblasts on MD and SC iPB-1.
29. Morphologies of attached platelets on PS.
30. Platelet surface coverages.
31. Platelets adhesion on MD iPB-1.
32. Platelets adhesion on SC iPB-1.
33. Platelets adhesion on MD HDPE.
34. Sketches of platelets adhesion on HPF adsorbed surfaces.

List of Tables

1. QCM-D data analysis.
2. Protein adsorptions on polymeric nanostructured surfaces.
3. Platelet adhesion and activation influenced by HPF adsorbed surfaces.

List of Abbreviations and Symbols

Aα, Bβ, and γ	Polypeptide chains
Aα572-574	572-574 peptide sequences in A α chain
Aα95-97	95-97 peptide sequences in A α chain
AFM	Atomic force microscopy
ANOVA	Single factor analysis of variance
AT-cut	Crystal is cut at an angle of 35°15' from the Z-axis
BCPs	Block copolymers
BSA	Bovine serum albumin
C_f	Sensitivity factor for the quartz crystal
C=O	Carbon and oxygen bond
C terminal	Peptide sequences connected to D-domains
D	Dendritic of platelets
D	Parallel motions in reference to the drawing direction
D_⊥	Perpendicular motions in reference to the drawing direction
D_{MAPT}	Diffusion coefficient
D: D sites	Associations between D domains
DNA	Deoxyribonucleic acid
DMEM	Dulbecco's modification of Eagle medium
DTT	Dithiothreitol
F_N	Normal force
FS	Fully spread of platelets
HDPE	High-density polyethylene
HPF	Human plasma fibrinogen
HSA	Human serum albumin
iPB-1	Isotactic polybutene-1
iPP	Isotactic polypropylene
iPS	Isotactic polystyrene
LCs	Lamellar crystals
MAPT	Mapping using accumulated probe trajectories
MD	Melt-drawn

MD HDPE	Melt-drawn high-density polyethylene
MD iPB-1	Melt-drawn isotactic polybutene-1
MD UHMWPE	Melt-drawn ultra-high-molecular-weight polyethylene
Milli-Q water	Pure water with a conductivity of $18.2 \text{ M}\Omega\cdot\text{cm}^{-1}$
MTT	3- (4,5-dimethylthiazol-2-yl) -2,5-diphenyltetrazolium bromide
NLCs	Needle-like crystals
N-H	Nitrogen and hydrogen bond
OD	Optical density
OM	Optical microscopy
P	Diffusion polarization
PBS	Phosphate buffered saline solution
PC	Polycarbonate
PDMS	Polydimethylsiloxane
PE-SC	Polyethylene single crystal
pH	Hydrogen ion exponent
PHMS	Polyhydroxymethylsiloxane
PI	Isoelectric point
PLGA	Poly (lactide-co-glycolic acid)
PMMA	Poly(methyl methacrylate)
PS	Polystyrene
PU	Polyetherurethanes
PUU	Polyurethaneurea
PVDF	Polyvinylidene fluoride
QCM-D	Quartz crystal microbalance with dissipation
R	Unactivated (or "resting") state of platelets
RGD	Arginine, glycine, aspartic acid
RSA	Random sequential adsorption
SC iPB-1	Spin-coated isotactic polybutene-1
SD	Spread dendritic of platelets
SDS	Sodium dodecyl sulfate
SEM	Scanning electron microscopy
SKCs	Shish-kebab crystals
TIRFM-SM	Total internal reflection fluorescence microscopy with a single

	molecule resolution
UHMWPE	Ultra-high-molecular-weight polyethylene
UV	Ultraviolet
XPS	X-ray photoelectron spectroscopy
αIIbβ3	Glycoproteins IIb/IIIa
βC and γC	Nodules in the D domains.
γ400-411	400-411 peptide sequences in γ chain
γ254-256	254-256 peptide sequences in γ chain
γXL-sites	γ chain region in each D domain
ΔD	Dissipation change
ΔD/Δf	Ratio of dissipation change and frequency change
ΔD/(-Δf/n)	Dimensional ratio
Δf	Frequency change

1

Introduction

A biomaterial is considered to be a substance, which is designed to interact with biological systems in the purpose of medical treatments. When biomaterials are implanted into the human body, protein molecules, following the arrivals of the water molecules and inorganic salt ions in the body fluid, reach the surface of biomaterials in mere seconds. [2] Subsequently, the adhesions of platelets, host cells, and macrophages are mediated by the adsorbed proteins. [3] Eventually, biological processes, such as the host responses, thrombosis, hemolysis, tissue healing, as well as infection and aseptic inflammation, are influenced by the composition of the protein layer on the biomaterial surface. [4-6] Therefore, it is of great importance to understand the molecular pathways and mechanisms mediating protein interactions with biomaterials, to achieve favorable host responses.

To this end, modern biomaterial science concentrates not only on designing specific medical materials but also on elucidating the protein assembly behavior and bioactivity of immobilized proteins. [7] Generally, adsorption of plasma proteins on implant surfaces irreversibly takes place, regardless of the material they are made from. [8] The classes, adsorption rates, adsorption amounts, and spatial conformations of the proteins affect the formation rate, morphology, and biological functions of the protein layers. [7, 8] Beneficially, the adsorbed protein layer may improve the blood and cell compatibilities of the biomaterials and favorable host responses. [9] Detrimentally, it may also activate the foreign body reaction, an irrevocable host defense mechanism, which might ultimately reject the biomaterials. [10]

Human plasma fibrinogen (HPF), which is the third abundant plasma protein, steers the critical processes in the wound healing. [11] HPF molecule comprises two distal

D-domains and one central E-domain. [11] The domains are linked by three polypeptide chains (coiled-coil segments), termed as A α , B β , and γ . [11] With alternative splicing, enzymatic modification, and proteolysis, the HPF molecules exhibit a highly heterogeneous structure and expose various interactive sites. [11] The surface functionalities of HPF play an essential role in improving the blood clotting, cellular and matrix interactions, as well as preventing the inflammatory response. [12]

Studies show that both the surface properties of the implant materials and the buffered environment significantly affect the exposure of interactive sites of HPF molecules. [13] As the buffered environment is stable in the human body, the surface properties of the implant materials dominate the behavior of HPF molecules. [13] The surface properties, which influence the HPF adsorption behavior, include surface chemistry, hydrophilicity, and topography. [14] Nowadays, the surface nanostructure attracts keen interest due to the development of the nanofabrication techniques, which can provide the topographical features mimicking the length scale of proteins. [9, 15] In no small extent, the controlling of protein adsorption on the nanostructured surfaces is beneficial for not only understanding the fundamental knowledge but also providing the valuable parameters for technological design.

2

State of the art

2.1 Polymer Biomaterials

In 1920 Staudinger suggested to the scientific community that a polymer is a macromolecule built up from smaller monomers. [16] Twenty years later, the first synthetic polymer used as biomaterial was poly(methyl methacrylate) (PMMA), which was utilized in dentistry [3] and dialysis tubing [4]. The application of PMMA as implants was recognized in World War II via wounded pilots. [17] The eyes of airplane pilots were damaged by the flying shards of PMMA but suffered much less from them, compared with those from the standard glass. [17] This indicated that the biocompatibility of PMMA was better than glass. Subsequent research provided a multitude of polymers as biomaterials and developed several generations of polymeric implant materials. [3, 4]

2.1.1 Classification of polymers

According to their origin, polymers can be divided into natural and synthetic polymers. [18] Natural polymers include deoxyribonucleic acid (DNA), proteins, and polypeptides, etc. Distinct from natural polymers, synthetic polymers are human-made polymers, composed of small molecule compounds as subunits. [19] The synthetic polymer is an ultra-large molecule, which is composed of more than thousands of atoms. It is generally created by polymerization of monomers. [19, 20] The connected monomers are the subunits or building blocks of synthetic polymers. [19, 21]

Based on structure and composition, etc., synthetic polymers can be classified into several categories. Owing to the differences in molecular structure, synthetic polymers can be divided into amorphous and semicrystalline polymers. [22] Amorphous polymers do not show ordered arrangement, i.e., the random orientation of polymer chains. [22, 23] The molecular structure of amorphous

polymers with no regularity is mostly being attributed to the chain architecture, e.g., atactic chain stereochemistry. [22, 24] Well-known amorphous polymers used as biomaterials are polystyrene (PS), [25] polycarbonate (PC), [26] and PMMA, etc. [27, 28] They display no nano- or micro-structure neither in bulk and nor in the film state. [27, 29]

Semicrystalline polymers are believed to display nano- and micro-structures. [30, 31] When the side groups are regularly spaced on the straight chains, i.e., isotactic and syndiotactic chain stereochemistries, the polymers are named as crystalline polymers. [18, 32] Notably, all the crystalline polymers only consist of partially chain alignments in the polymer crystals. [18, 33] Therefore, “crystalline” is equal to “semicrystalline” for polymers. [18, 33]

Polyethylene (PE), a typical semicrystalline polymer and biomaterial, consists of many ethylene groups connected in a chain. [34] This unique chemical structure endows PE with ability to form crystals of straight-chain alkanes (Fig. 1). Polybutene-1 (PB-1), another biomaterial, has a flexible carbon backbone with ethyl side groups. [35] Its chemical structure, which is similar to PE, assures excellent biocompatibility and usage in dilatation catheter and pressure piping, etc. [36] Isotactic polybutene-1 (iPB-1), a semicrystalline polymer, [37] is composed of regularly ordered ethyl side groups on the straight chains (Fig. 1).

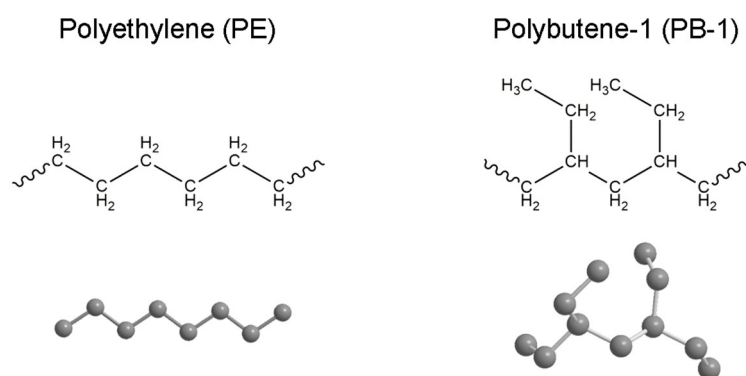


Figure 1. The chemical structures and sketches of polymers. Polyethylene (PE) and isotactic polybutene-1 (iPB-1). Only the carbon atoms are shown in the lower drawings.

Semicrystalline polymers have ordered or regulated packing molecules both in bulk and in the thin film states. [38] The well-ordered molecules provide semicrystalline polymers densely-packed crystal structures, which improve the mechanical properties of the polymers. [39, 40] By varying the crystallization conditions, the

polymer chains fold into various macroscopic morphologies, e.g., spherulites, single crystals, and long-range order crystals. [41, 42] These morphologies compose of thin lamellae, which is in the order of 100-500 Å thickness. [33] The lamellae form during polymer crystallization either from a melt or from solution. [33, 43]

Based on composition, polymers can be classified into homopolymers and copolymers. [44] Homopolymers contain one kind of mers, while copolymers contain more than one type of mers. [45] The addition of the other mers complicates the structures and morphologies of the bulk polymer. [46] Within the copolymers, which are useful in the industry or scientific work, mers can be arranged in various ways, including alternating, periodic, statistical, gradient, block, and graft copolymers. [47, 48] Among all kinds of the copolymers, block copolymers (BCPs) have drawn considerable attention as functional materials in electronics, energy, and biomedical detection, with the realization of possible applications of nanoscale polymeric domains. [47, 49, 50] This is attributed to the BCP unique property, namely microphase separation. [48, 51, 52] BCPs tend to self-assemble into well-ordered nanostructures due to their two segments with different chemical properties. [53, 54] These different segments are immiscible and are prone to form separated phases. [52] Because the blocks are covalently bonded, these phases are limited in nanoscale size. [48] Depending on various factors, several well-ordered and adjustable nanostructures form in the bulk and thin films of BCPs. [55]

2.1.2 Application of synthetic polymers as biomaterials

From the material point of view, synthetic biomaterials can be grouped into three categories, i.e., metals, ceramics, and polymers. [4] Metals, with excellent mechanical properties and fatigue resistance, are applied in load-bearing implants, such as knee or hip implants. [56] Metals and metalloids may induce toxicity due to their corrosion through body enzymes and acids. [57] Another synthetic biomaterial, ceramic, which is commonly used as orthopedic implants and dental applications, exhibits highly inert property and high compressive strength. [58] However, their brittleness, hardness, and degradation limit the application directions of ceramics. [59]

Different from metals and ceramics, polymers interest the biomaterial scientists with their i) carbon-based chains, ii) reactive groups on surfaces and

iii) viscoelasticity, apart from lightweight and acceptable mechanical properties. [3] These combined properties endow polymers with easy handling and various biological properties, such as bioinert, bioactive, and biodegradable. [60] Meanwhile, the easy handling property of polymers allows engineers to process advanced technologies to obtain structured surfaces with topographical features within a wide range, particularly in nanoscale. [61] This feature is considered to be the most advanced property of polymers over metals and ceramics. [62, 63]

The choice of synthetic polymers for biomaterials is based on its application and requirements for physical, chemical, and biological properties. [27] According to these, the polymers can be classified as biodegradable and biostable polymers. [64] These synthetic polymers as biomaterials share specific properties. [65] Namely, they are biocompatible, nontoxic, and noninflammatory, as well as have good mechanical properties. [66] For example, original PMMA, which behaves brittle under load and low wear resistance, can be improved during modification and functionalization. [67] Nowadays, PMMA and its modified formulations have been used in a wide range of biomedical fields, such as the eyeglass lenses, bone cement, soft tissue filler, and microfluidic lab-on-a-chip devices. [68-70] With increasingly inventions of various polymers in the industry, more and more polymers with excellent biocompatibility are applied in the biomedical field, such as Dacron for vascular grafts [71], polyetherurethanes (PU) for artificial hearts [72], polybutene (PB) for blood vessel dilatation catheter [73, 74], PE for sutures and acetabular cups [75, 76], as well as polyvinylidene fluoride (PVDF) for surgical meshes and sutures [77, 78]

Although polymers help to meet the patients' medical requirements, the critical problems of polymers as biomaterials are lacking epithelialization, insufficient vascularization of the cellularly colonized scaffolds, and sparse reconstruction of tissues. [17] The polymers alone are inadequate to overcome these critical problems. [27, 79] They provide a framework but lack bridges for integration with the host systems. [80] With the recent findings, it was recognized that the proteins had gained significant importance. [81] Thus, attentions have to be focused on either design of bulk polymers or design of polymer surfaces, which might drastically enhance the implant success. [82]

2.2 Surface Nanostructuring of Polymers

2.2.1 Lithography and molding

Various processing and structuring techniques can achieve the nanostructure fabrication on amorphous polymer surfaces. [83, 84] The well-developed methods in recent years are lithography and molding, such as photolithography, [85] electron beam lithography, [86] nanoimprint lithography, [87] and dip-pen lithography [88]. The created patterns range from pits, pillars, squares, lines, rings, to gradient patterns. [83, 84] These custom-designed patterns in lithography and molding have a lateral resolution of 10-100 nm. [89-93] For example, the square and lamellar patterns using an amorphous Teflon mold, shown in Fig. 2.

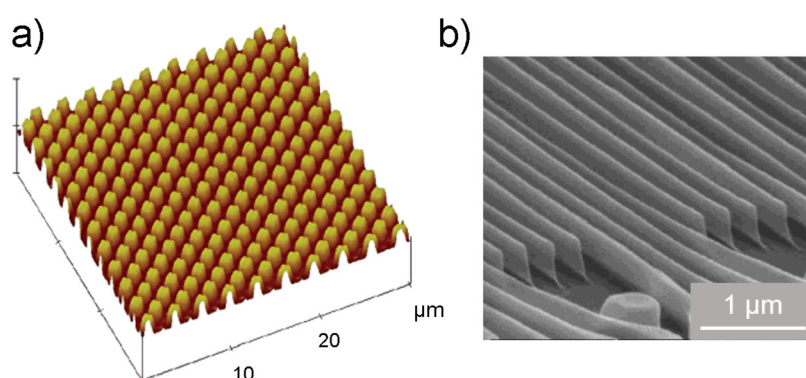


Figure 2. Nanostructured amorphous polymer surfaces by compression molding. (a) Perspective Atomic force microscopy (AFM) images of molded $1\ \mu\text{m}\times 1\ \mu\text{m}$ square patterns using the amorphous Teflon mold. (b) Perspective scanning electron microscopy (SEM) images of molded patterns using the amorphous Teflon mold. The pattern height is $\sim 500\ \text{nm}$, which leads to an aspect ratio of $\sim 6:1$. Images are reproduced from ref [92] with permission from American Chemical Society, Copyright©2004.

Among various lithography and molding techniques, photolithography is applied in a wide range of structural fabrication. [94, 95] Photolithography (optical or ultraviolet lithography) utilizes the ultraviolet (UV) light to transfer the nano- or micro-patterns from the mask to photoresist. [96] The uncovered polymer is chemically etched. [95] The reverse pattern of the mask remains on the polymer surface after all photoresist is removed. [95] The lateral resolution of the pattern can be in the sub-100 nm range, which is even smaller with extreme UV lithography. [97, 98] Detailed understandings of this technique can be found in various publications. [99-101] However, the relative high defect density and

resolution, as well as harsh processing solvents, were considered as the obstacles for applications in biomaterials. [97]

2.2.2 Self-assembly

With the deep understandings of copolymers, self-assembly of BCPs was recognized as one of the efficient ways to control nanostructure fabrication with high resolution under mild conditions. [102, 103]

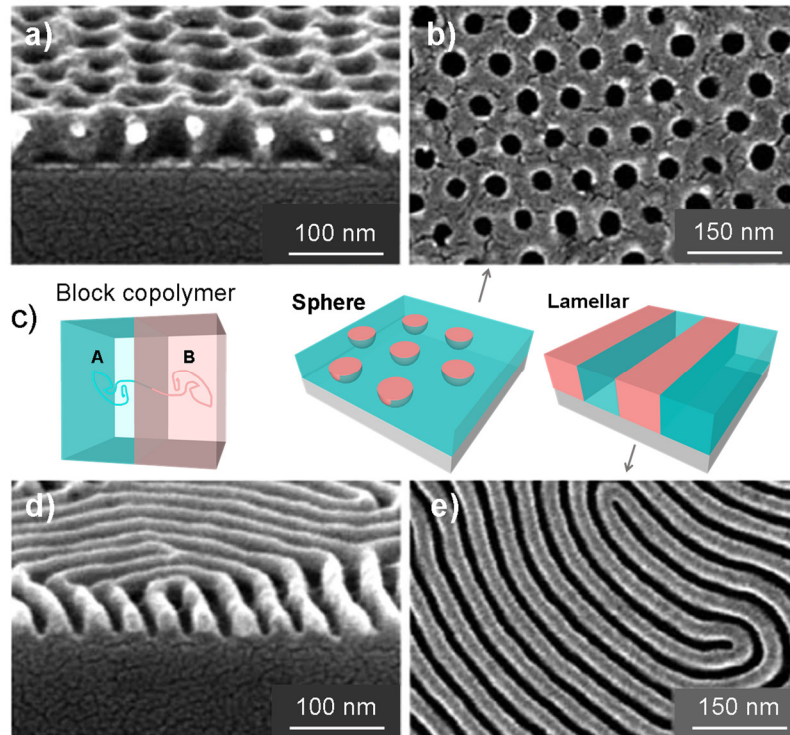


Figure 3. Nanostructures of the block copolymer. SEM images of (a,b) and (d,e) are the PS hole array pattern (sphere) and PS lamellar array pattern (lamellar) of PS-*b*-PMMA after removing PMMA, respectively. The different blocks are denoted as A and B in image c. Image a, b, d, and e were reproduced from ref [91] with the permission of the IOP Publishing, Copyright©2016.

In the thin films of BCPs, the nanostructure formation is mediated by the entropic effect of interfacial interactions, e.g., the substrate-copolymer and copolymer-air interactions. [53] In general, the perpendicular orientations of nanostructures (Fig. 3) are favorable in the applications and captured all the attention of engineers and scientists in the field of protein arrays. [91] The orientation of nanostructures is the current striving direction for self-assembly. [102] When one of the blocks has a preferential attraction to the substrate surface, the planes or axes of the nanostructures will align parallel to the substrate surfaces. [104] When there is no preferential attraction, the nanostructures will align perpendicular to the surface

plane. [104] This is the crucial point for the successful formation of nanostructures on surfaces. [103, 105]

Other than the interplay between interactions of polymer/air and polymer/substrate, the confinement effect and other factors, e.g., electric field, mechanical flow field, and temperature gradient, were considered to be able to tune the orientation. [54, 104] These approaches rely on the abilities to couple external applied bias fields to molecular or supermolecular feature, and thus achieve directional control over the nanostructures. [53, 106]

2.2.3 Melt drawing

Different from amorphous polymers, the semicrystalline polymers exhibit regularly folded morphology in the undercooled polymer melts. [31] One of the typical crystal morphology is the spherulite. [107] In this superstructure, the lamellar crystals with folded polymer chains grow radially in three dimensions. [108] The spherulites display spherical symmetry at sufficient growth rates and with a low density of nuclei. [107] It was observed that the topographies of spherulites in the thin film might offer regular nanostructures owing to the lamellae protruding out of the amorphous regions. [107] Through altering inner and outer factors, e.g., the polymer chain structure, thermal treatment, and mechanical field, the size of the lamellar crystals and thus the physical properties of the surfaces can be varied. [109] Under shear stress, all the lamellae align along the orientation direction with their c-axis parallel to this direction. [110] One example is the ultra-thin film (100-300 nm thickness) of semicrystalline polymer with the highly-oriented surface nanostructure, which is formed via the MD technique. [111, 112] This method was firstly introduced by Petermann and Gohil. [111] In this method, the polymer melt, originated from the heated polymer solution on a glass heating plate, can be drawn off the plate by a roller and form the ultra-thin film. [111] With the continuous work by Jandt *et al.*, [42, 113-116] it was demonstrated that the resulted films consisted of distinct surface nanostructures: either shish-kebab crystals (SKCs) or needle-like crystals (NLCs), depending on the polymer chains, plate temperature, and drawing speed, etc.

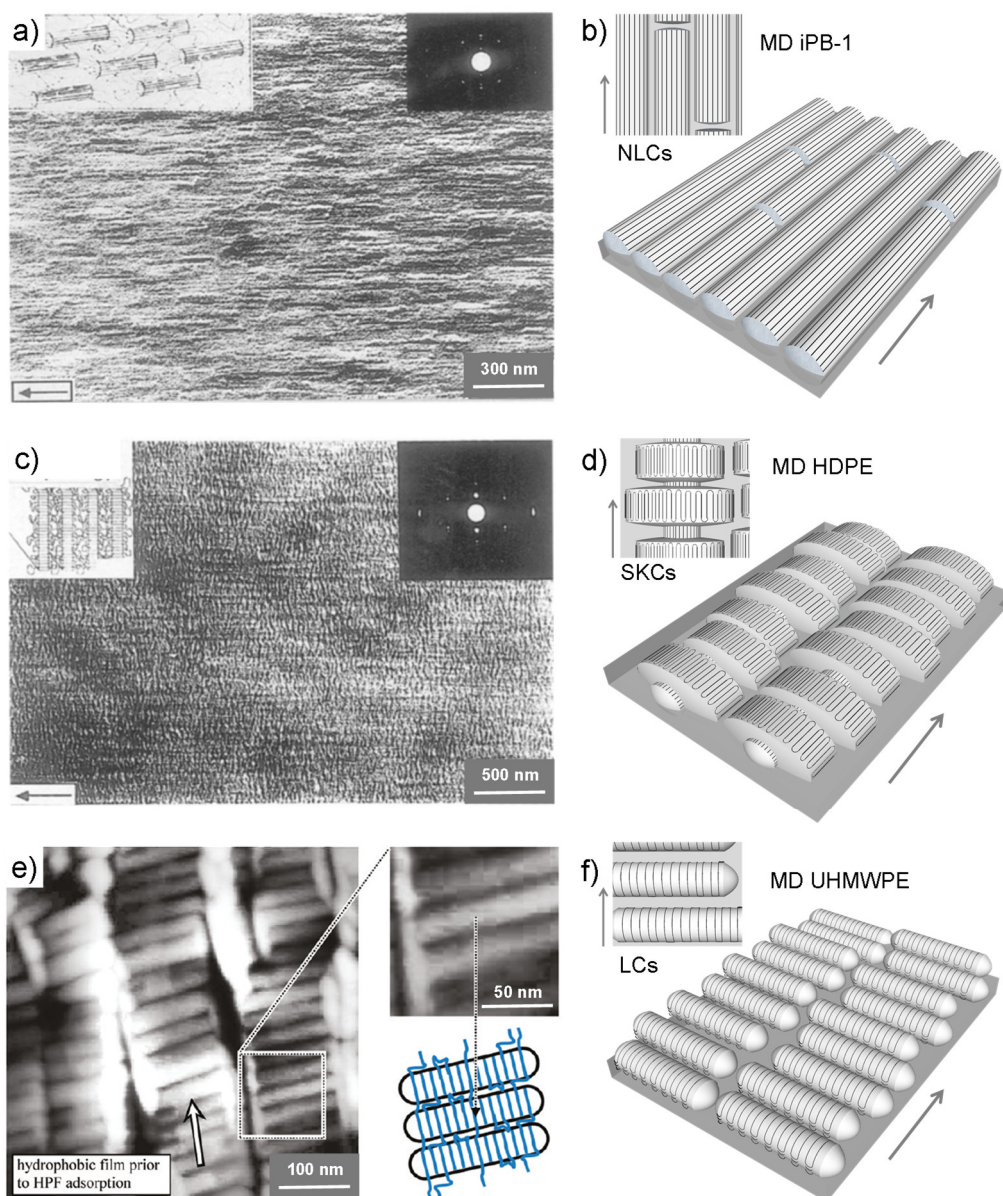


Figure 4. Nanostructures of semicrystalline polymers by MD technique. Surface morphologies of melt-drawn (a) iPB-1 (transmission electron microscopy (TEM) image in ref [114]); (c) HDPE (TEM image in ref [114]); and (e) UHMWPE (AFM image in ref [116]). The schematics of the nanostructures in b, d, and f are prepared according to the typical crystal morphologies in a, c, and e, respectively. The arrows in the images are the drawing direction. The black lines in the schematics are the polymer chains. Image a and c were reproduced from ref [114] with the permission from Chapman&Hall, Copyright©1996. Image e was reproduced from ref [116] with permission from American Chemical Society, Copyright©2011.

The NLCs were achieved by melt-drawing iPB-1, isotactic polypropylene (iPP), [117] and isotactic polystyrene (iPS) [113]. The surface of the substrate exhibited a regular arrangement similar to close-packed longitudinal needle crystals. [113, 117] As shown in Fig. 4a and b, melt-drawn isotactic polybutene-1 (MD iPB-1) exhibited a regular arrangement of close-packed longitudinal needle-crystals, which were

aligned parallel to the drawing direction. [114] The NLCs protruded out of the plane and displayed a diameter of around 25-35 nm. [42] Based on those observations, Pennings *et al.*, proposed the concept that the formation of NLCs might be attributed to simultaneous “unrolling” of polymer chains under a local flow field. [118]

The SKCs have been observed in melt-drawing high-density polyethylene (HDPE) (Fig. 4c and d). [115] Under shear conditions, the PE chains extended along one direction in the melt-drawing method. [115] Thus, the extended PE chains (“shish”) compacted along the drawing direction and the main planes of the PE lamellae (“kebabs”) overgrew perpendicularly to the drawing direction. [119] Therefore, the edges of the “kebab” protruded out from the thin film surface with several nanometers leading to highly-oriented nanostructures on the surface. [119] On the film surface, the laterally aligned lamellae appeared to form a stacked super-structure. [115] Inspired by this superstructure, Nagasawa and Shimomura explained the SKCs formation by a screw dislocation process, in which the “shish” and “kebab” crystals form simultaneously. [119] Recently, Keller *et al.* [116] in our research group found that highly oriented nanocrystalline lamellae stacked on the surfaces of melt-drawn ultra-high-molecular-weight polyethylene (MD UHMWPE) thin films (Fig.4 e and f). The well-defined lamellae thickness was 26 ± 3 nm, and the width was 103 ± 12 nm. The nanostructures of MD UHMWPE were quite similar but even regular and without visible “shish” structures, comparing to the MD HDPE. [115] The difference originated from the molecular weights of different PE. [115]

As the majority of the clinical utilization are involved in interactions with blood, interests in blood responses on artificial surfaces have lasted for a hundred years. [120, 121] There is a general belief that the interactions between implants and blood components, especially blood proteins and platelets, are essential for short-term biocompatibility evaluation of biomaterials. [122] Accordingly, precisely-defined surface nanostructures, i.e., nanopatterns, of polymers, have been suggested to be an efficient and facile strategy to control the protein adsorption behaviors and enhance their biocompatibilities. [9] The protein and the subsequent cellular behaviors were significantly influenced by the modified nanotopographies of polymeric surfaces. [123] However, the mechanism, how surface

nanostructuring determines protein behavior and cellular response, is still in its infancy. The detailed phenomena and elucidations of protein adsorption on nanostructured polymer surfaces are introduced in the next section.

2.3 Protein Adsorption on Nanostructured Polymers

Proteins, most of which are amphiphilic molecules, assembly at the water-surface interfaces rapidly and tenaciously. [7, 8] In the field of biomaterials, plasma protein adsorption can be both favorable and detrimental. [11] On the one hand, cell attachment and spreading are induced by binding sites of adsorbed proteins. [124] On the other hand, unfavorable host responses, such as platelet activation and blood coagulation are expected to be elicited. [125] At this moment, the control and prediction of the behaviors of protein adsorption are becoming the essential issues in the biomaterial field. [14] Therefore, the deep understandings of the interfacial behaviors are of critical importance for the performances of the biosensors, implants, anti-fouling materials, and drug-delivery schemes, etc. [17, 47, 57, 59]

In this section, an overview of the properties of plasma proteins, especially HPF, is provided, along with the descriptions of the conformation, structural changes, and protein-protein interactions. Moreover, the comprehensive overview of surface physicochemical factors, which greatly affect the protein adsorption behavior, its functional properties, and the following biological responses, is included and discussed in detail.

2.3.1 Proteins

Protein is termed as folded polypeptides with biological functions. [126] The polypeptides are long linear chains of amino acids, which are small organic molecules. [126, 127] Each specific polypeptide constitutes a unique sequence of amino acids. [127] The functions of protein come from both i) the type, number, and arrangement of amino acids and ii) the three-dimensional structure of the proteins. Anyone of them alone will not guarantee the biologically active form of proteins. [126-128]

Proteins have four levels in its structure: primary, secondary, tertiary, and quaternary structures. [126-128] The primary structure is the sequence of various amino acids, which is determined by the nucleotide sequence in the gene. [126] The

secondary structure is formed via hydrogen-bonding interactions between N-H and C=O groups, resulting in α helices and β sheets. [126] The tertiary structure is the folded structure of secondary structures plus loops and links. [126] The quaternary structure is the association of several folded polypeptides. [126] The optimized functions attributes to the stable tertiary structure of proteins under physiological conditions. [126, 127] The conformation of proteins involves the three-dimensional shape of the primary, secondary, tertiary, and quaternary structures. [127]

Proteins can be classified based on protein type, shape, composition, and biological functions. [129] Most of the proteins have a globular structure. [127] Some of the proteins are fibrous, in which the polypeptide chains are stretched into anisotropic shapes. [130] The proteins with a molecular weight less than 20,000 usually exhibit globular structure, with an average diameter of 20-30 Å. [131] More abundant proteins are built-up of folded structural domains, which are short polypeptide chains. [127] The cores of these domains are hydrophobic, which is essential for domain stability in aqueous solution. [126]

The biomedical and physiological functions of proteins come from the conformations of proteins and the heterogeneous domains. [132, 133] According to the biological functions, proteins can be driving into enzyme proteins, structural proteins, transport or carrier proteins, nutrient and storage proteins, contractile or motility proteins, defense proteins, regulatory proteins, and toxic proteins. [134] The prediction of protein functions can be accomplished by recognizing the protein structure and usage of structural genomics. [135] Conceptually, proteins with new functions can be created by designing the domains and conformations of protein molecules. [126]

2.3.2 The human plasma fibrinogen (HPF)

HPF is the fundamental plasma protein, which plays an essential role in hemostasis, fibrinolysis, and coagulation processes. [136-138] It is a rod-like glycoprotein with a molecular weight of 340 kDa. [12] It is mainly produced by hepatocytes. [139] It circulates in the blood plasma at the concentration of 2-4 mg/ml. [140] During inflammation, the circulation level increases to help the body's hemostatic system. [136, 138]

The observations of HPF under electron microscopy and crystallographic studies revealed that individual HPF molecule is composed of three linearly-linked domains (D-E-D domains) in a trinodular structure (Fig. 5). [141] The two distal D domains (67 kDa) consist of B β and γ chains. [142] The central E domain (33 kDa) is made of the disulfide knot and 58 cysteine residues. [142] The connectors are triple-helical coiled-coil regions, which consist of A α , B β , and γ polypeptide chains. [143] The amino termini of the three polypeptide chains are conjugated by 29 disulfide bonds. [144] The elongated HPF molecules exhibit a high aspect ratio, with 47 nm in length and 6 nm in width. [142] The HPF molecules are highly anionic with a net negative charge of isoelectric point (PI)=5.8 at the physiological condition. [145]

There are many binding sites on HPF to associate with other HPF molecules. [143, 146] The A α chains are longer than the B β and γ polypeptide chains. [147] They extend from the end of D-domains to the central E-domains and form two globular α C regions. [147] When the fibrinopeptide B is cleaved from the coiled-coil region, the A α region will dissociate from the E-domain and interact with the other A α region to promote lateral fibrinogen associations. [128, 141] The other type of branch junctions in HPF association comes from the γ chain region in each D-domain (γ _{XL} and D:D sites). [13] The γ _{XL}-sites cover the cross-linked γ chain regions in both D-domains. [148, 149] The association of γ _{XL}-sites from adjacent HPF molecules helps the alignment of the HPF molecule and fibril formation. [149] The D:D sites situate at the end of D-domains between the residues 275 and 300 of γ chains. [146] These sites act as connectors between D-domains of adjacent HPF and fibrin molecules, as well as endothelial cell adhesion. [150] Although this information about clot initiation via HPF functional sites is partially understood, the role of surface-immobilized HPF molecules on platelet adhesion is not yet conclusive. [151]

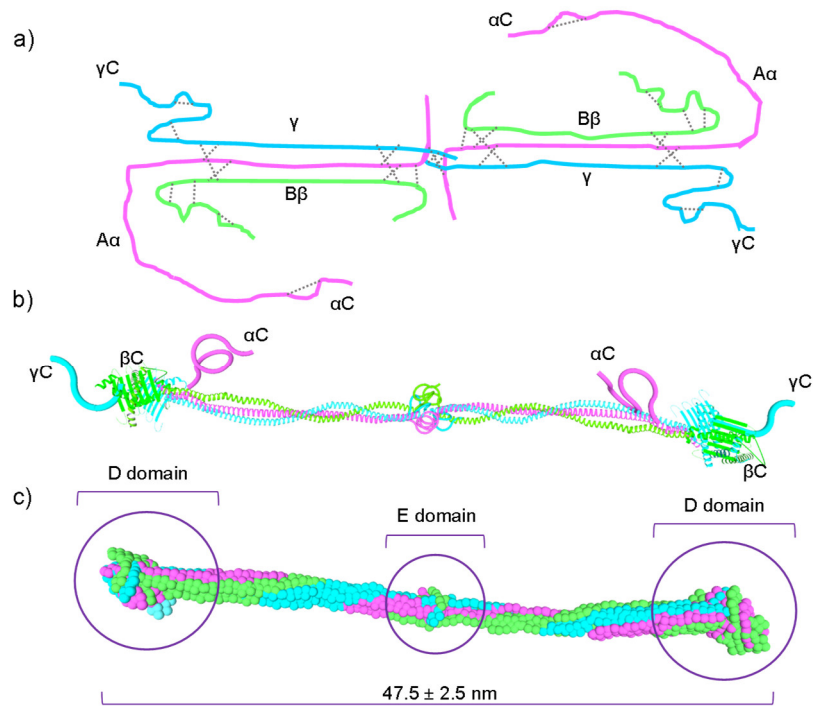


Figure 5. Molecular structure of HPF. (a and b) The composition of the polypeptide chain; (c) Schematically crystal structure of HPF molecules.

Platelet adhesion on adsorbed HPF is suggested to adjust the potential thrombogenicity of the biomaterials. [152] It was reported that there are various binding sites on the D-domains for platelets. [128] The platelets can bind to the C terminal of γ dodecapeptide by the integrin α Ib β 3 (glycoproteins IIb/IIIa) on the platelet membrane. [153] Besides the terminal γ dodecapeptide, the γ 400-411 on HPF molecules also contributes to the platelet activation and adhesion. [152] In addition to arginine, glycine, aspartic acid (RGD), A α 572-574 and possibly A α 95-97 [154] as well as receptor recognition motif, γ 254-256 asparagine-glycine-arginine [155] can result in the platelet interaction with HPF molecules.

2.3.3 HPF adsorption mediated by surface factors

Different types of functional groups in proteins, such as nonpolar, polar, negatively and positively charged residues, render protein surface highly amphiphilic property. [156] This unique property influences interfacial behaviors of protein molecules during the whole adsorption processes. [157] Generally, protein adsorption includes transport, adsorption, and desorption steps. [157] In the transport stage, distribution is the dominating step. [158] Small proteins distribute faster and arrive at the surface earlier than large ones. [159] In the adsorption stage,

the concentration of accumulated proteins is around much higher on the surface than that in the bulk solution. [160] Large proteins have a large contact area and can repel other pre-adsorbed small proteins during spreading. [161] This is the so-called Vroman effect. [162] The larger the protein is, the stronger the binding of this protein to the surface is. [163] In a circumstance, a significant amount of HPF on material surfaces was observed even when the surface was saturated with bovine serum albumin (BSA). [164] In the desorption stage, the previously-bound protein molecules detach from the surface and return into the bulk solution. [165] It was suggested that during this process, all contact points between protein and surface had been broken. [166] This high free energy requirement makes protein adsorption irreversible unless dramatic changes occur in the environment, such as high ionic strength, low pH, and detergents addition. [157, 167]

The external parameters vastly affect protein adsorption behavior. [168, 169] In the bulk solution, the driving forces of the adsorption are the entropy gains from many aspects: changes of temperature [170], pH [169], and ionic strength [168], etc. For example, the equilibrium states and kinetics of protein adsorption vary with increasing temperature. [170] The entropy gain during this process arises from the release of surface adsorbed water molecules and structural rearrangements of protein. [157] When the pH equals the isoelectric point (PI) of proteins, the numbers of negative and positive charges are in balance resulting in a net neutral protein. [171] Thus, the pH values can also influence the entropy gain by changing the electrostatic property of the proteins. [157, 167] The other major factor is the ionic strength of the bulk solution. High ionic strength increases the tendency of proteins to aggregate, due to the small Debye length between proteins. [157, 167]

From the view of the material surface, the surface physicochemical factors, such as hydrophobicity, charge/polarity, chemistry (functionalization), and topography, influence the protein adsorption to a great extent. [12] When proteins adsorb on hydrophobic surfaces, the entropy gain supports the proteins in contact with the surfaces. [145] Generally, the charged amino acids distribute in the outside part of protein molecules. [172, 173] The charge or polarity of the surfaces may either promote or inhibit the protein adsorption according to the various charges of the proteins and surfaces. [174] This process is mainly dominated by enthalpic and entropic changes within the protein-water-substrate system. [145, 167] Such

properties can drastically influence the concentration and conformation of adsorbed proteins on surfaces, which are considered to be directly accountable to multiple tissue responses and further intended integration of implanted biomaterials. [175]

Unfavorable responses include non-specific and random-oriented protein adsorptions, which imply inhibited adsorption of preferred proteins and non-ordered structures of protein layers. [176] With this, scientists dedicate their work in preventing these unfavorable protein adsorptions by functionalizing the biomaterial surfaces. [177, 178] After the chemical modification, the decreased surface energy on biomaterials allows to some extent to control the protein adsorption. [179]

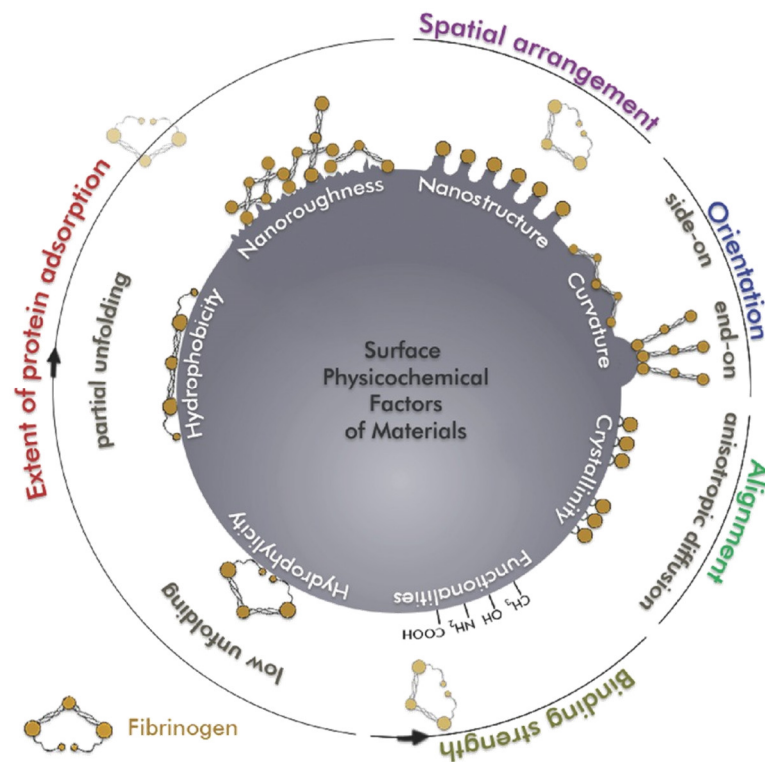


Figure 6. Surface physicochemical factors that affect the HPF adsorption. Image reproduced from ref [9], with the permission from Wiley/VCH. Copyright©2017.

With the development of micro-/nano-fabrication techniques, more and more observations showed that surface topography played a crucial part in the protein conformational changes and adsorption behaviors. [15, 180] These novel findings allow scientists to pave the way for a new generation biomaterials surfaces design. [181, 182] So far, the known surface physical factors, which influence the protein adsorption, include nanoroughness, structure curvature, protruded

structure size, and spatial arrangement. [182-185] These observations were concluded and highlighted in a review from our group (Fig. 6). [9]

In search of the topographical effect on protein adsorption, tantalum films with nearly random surface nanoroughnesses were chosen as a model system by Rechendorff *et al.* [186] The adsorption amount of HPF increased with elevating surface nanoroughnesses from 2.0 to 32.9 nm, with which the surface area was found to be increased by about 20%. [186] This was attributed to the changes of the trinodular HPF molecules in the geometrical arrangement on the surface. [186] Distinctly, for globular proteins, like BSA, nearly no change of adsorption amount was observed. The similar trends were also evidenced by simple Monte Carlo simulations. [186]

With developing nanostructuring techniques, the focus was switched from nanoroughness to curvature of the surface nanostructures, which are to some extent related. [180] [183, 184] In the beginning, silica nanospheres with diameters in the range of 15-165 nm were applied to evaluate the topographical effect on the adsorption behaviors of two distinct proteins, HPF and BSA. [180] The silica nanospheres with small radius presented a high surface curvature. [180] Considering the typical dimensions of protein molecules, HPF (46 nm in length and 4 nm in width) and BSA (14 nm in length and 4 nm in width), small nanospheres with high surface curvature led to the native conformation of globular proteins, however, denature conformation of rod-like HPF. [180] Similar trends on adsorption capacities altered by nanostructure curvatures were also found on the carbon-based nanomaterial surfaces, i.e., carbon nanotubes with descending local curvatures, and flat graphene sheet. [187] It was confirmed that the adsorption amount of BSA increases with decreasing local curvature, i.e., the highest amount of BSA was found on the graphene sheet surface. [187] Similar conclusions were suggested by molecular dynamics simulations. [180]

Considering that most of the protein dimensions are in the range of 10-1000 nm² (projected area), the adsorption of individual protein and even the formation of protein layer may be affected by the nanostructures of biomaterials, especially when the sizes of the nanostructures are comparable to the protein molecules. [188] Nanopores of PMMA films, with 15, 50, and 100 nm in size, were designed to explore the structure and elasticity changes of adsorbed HPF. [188] In the 50 nm

and 100 nm pores, the HPF concentrations displayed the highest and the lowest, respectively, which were attributed to the “end-on” and “side-on” conformations. [188] The difference between the “side-on” and “end-on” conformations depends on the orientation of an ellipsoidal HPF on the surface, i.e., long or short axis of HPF molecules is predominantly interacting with the surface (shown in section 4.1.2). [189] It seemed that HPF went through less structural changes when the pore size was comparable to the major protein axis. [189] For globular protein, lysozyme, the structural change was not affected by the pore sizes. [189]

2.3.4 HPF on nanostructures of molded polymers

Surface nanostructuring of amorphous polymer thin films is realized as an intriguing method for applications in biomedical science. [190] The tuning of surface free energy via nanostructuring on the polymer film surface may significantly influence the conformation, coverage, and adsorption kinetics of proteins. [185] Messina *et al.* found preferential immobilization of human lactoferrin on the nanopores of polyhydroxy methylsiloxane (PHMS) thin film, which was obtained from colloidal lithography. [191] By varying the hydrophobicity of the nanopores from inside to outside via plasma treatment, the assembly regions of lactoferrin changed as well. [191]

For HPF, its unique structure results in different conformations when contacting with the surfaces. [192] As was described previously, HPF is a protein with an elongated shape. The significant aspect ratio results in two main orientations of adsorbed HPF molecule, namely “side-on” and “end-on” conformations. [192] In the 50 nm pores of PMMA film surface, HPF achieved the highest adsorption amount with the “end-on” orientation due to the nanoconfinement. [6, 193]

Although it was realized that the nanostructures of molded polymers provide nanoconfinement to the proteins and can mediate the spatial protein distribution, the majority of the researches were still focused on the cellular responses and emitted the function of protein layers. [194] Considering this, surface-induced protein adsorptions, the critical mediators between implants and cells, should be emphasized and contributed more in the further step.

2.3.5 HPF on surfaces with self-assembled polymers

Due to the heterogeneous nanostructures and chemical properties of the blocks, proteins selectively interact with one of the blocks and adsorb on these preferred blocks. [195] These preferred protein-polymer interactions help the formation of various protein patterns on the nanostructured BCP surfaces. [196, 197]

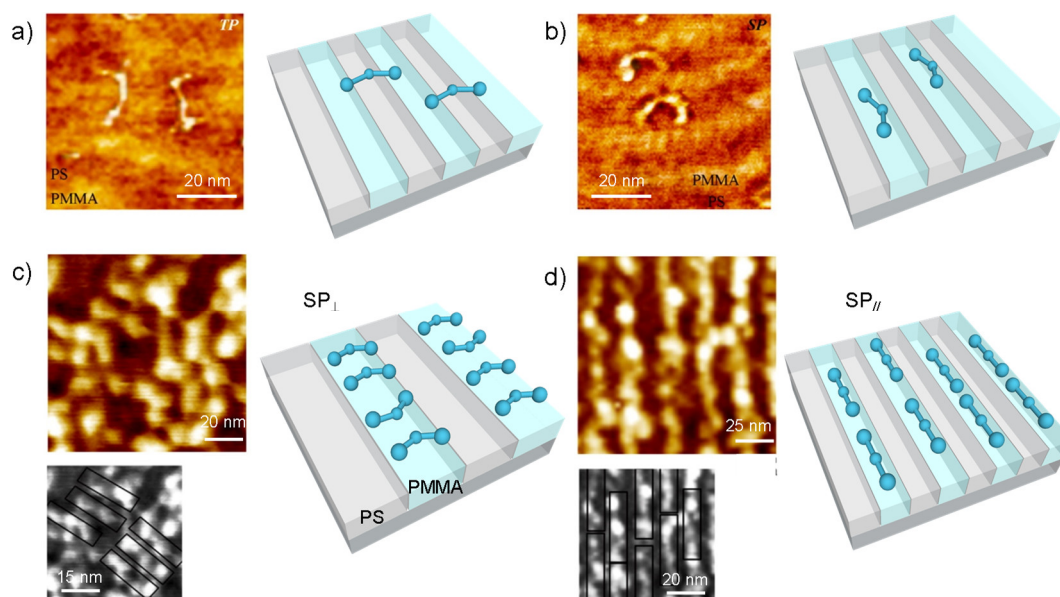


Figure 7. HPF molecule assembly on PS-*b*-PMMA block copolymer surfaces. a) Two phases (TP) and (b) single phase (SP) morphologies of HPF molecules in AFM height images; HPF alignments on PS-*b*-PMMA surfaces with varying domain sizes: (c) 45 nm and (d) 28 nm. The AFM images were reproduced from ref [198] with the permission from American Chemical Society, Copyright©2014.

Polystyrene-block-poly (methyl methacrylate) block copolymer (PS-*b*-PMMA) is the most utilized model surface for protein patterning. [199, 200] With varied block ratios, ordered lamellar with different widths can form on the surfaces of PS-*b*-PMMA thin films. [50] On the lamellar, HPF molecules selectively adsorb on PS phase, which is more hydrophobic than the PMMA phase (Fig. 7). [197, 198] When the sizes of the lamellar are smaller than the protein length, the heterogeneities gave rise to distinct protein configurations. [198] As shown in Fig. 7, HPF molecules lay across the two phases (TP), or confined in the PS phase (SP). Moreover, HPF aligned parallel (SP_{||}) or vertically (SP_⊥) to the lamellar directions, and thus resulted in relatively low adsorption amount. [188, 201]

Although a large number of studies contributed to understanding the mechanisms of protein adsorption on BCPs, they are mostly limited in the system with one kind

of proteins. [188, 199-201] To mimick the *in vivo* environment, the competitive adsorption processes are of vital importance. Recently, Song *et al.* challenged to investigate the competitive adsorption processes of HPF and BSA on PS-*b*-PMMA thin film surfaces. [202] In this dual-component protein system, the initially-immobilized BSA molecules on the PS phases were found to be replaced by late-adsorbed HPF molecules due to the Vroman effect. [202] This adsorption behaviors of proteins on BCP nanostructures suggested the potential of BCPs not only as coatings of medical devices and but also as the ideal model surfaces for protein behavior investigations. [202]

2.3.6 HPF on melt-drawn polymers

Different from BCPs, the nanostructure fabrication on semicrystalline polymers benefits from the topographical features of the polymer crystals, such as single crystals, lamellae, and spherulites. [42, 116]

Among all the polymer crystals, the single crystals possess the highest degree of crystallinity and thus the well-regulated polymer molecules on the crystal surfaces. Helbing *et al.* [203] in our research group found that on the highly-ordered single crystal surface, polyethylene single crystal (PE-SC), HPF molecules oriented along with the crystallographic directions with high chain densities in crystallographic directions of the polymer chains. [204] This unique phenomenon was explained by the similarities between α -helix chains of HPF molecules and the PE chain fold direction on the single crystal surface (Fig. 8a, b, and c). [204]

Besides, the polymer chain alignments and the arrangements of polymer crystals play also significant roles in the adsorption behavior of HPF molecules. [116, 205, 206] Keller *et al.* [116] in our group demonstrated that HPF molecules preferred to align on the crystal lamellae of MD UHMWPE films and along the major axis of the lamellae, which exhibited similar dimensions as the HPF molecules (Fig. 8d, e, and f). It indicated that the surface topographies of the highly oriented nanocrystalline lamellae influenced the conformation and aggregation of HPF molecules. [116]

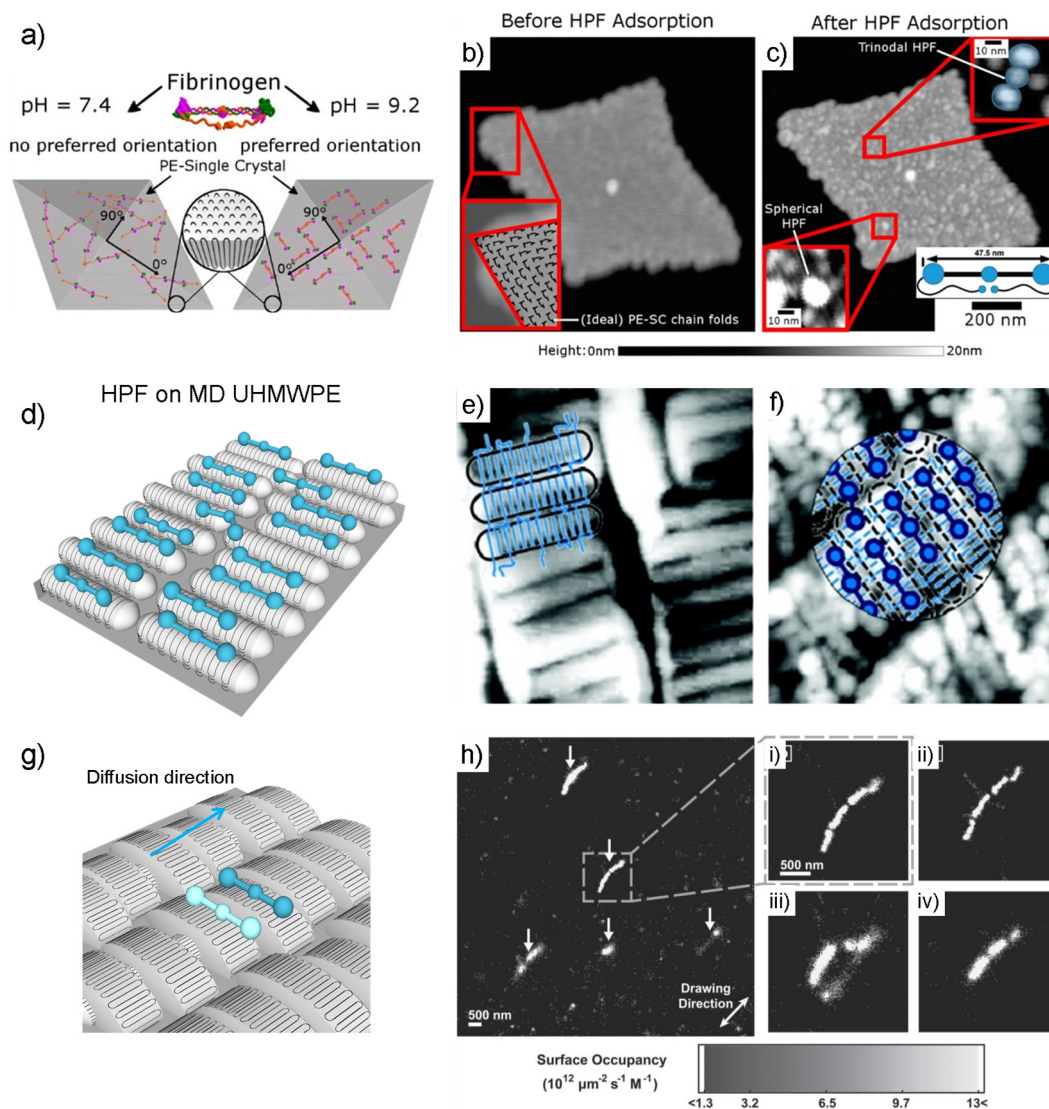


Figure 8. HPF molecule assembly on nanostructured semicrystalline polymer surfaces. a) Model of PE-SC; AFM images of PE-SC b) before and c) after the HPF adsorption, reproduced from ref [204], with the permission from American Chemical Society, Copyright©2016. d) HPF on MD UHMWPE; AFM images of MD UHMWPE e) before and f) after the HPF adsorption. Image e) and f) were reproduced from ref [116], with permission from American Chemical Society, Copyright©2011. g) Single HPF molecule diffusion on MD HDPE; h) Surface occupancy map and four magnified maps (i, ii, iii, and iv) of HPF on MD HDPE; The images in h, i, ii, iii, and iv were reproduced from ref [207], with permission from ©WILEY-VCH Verlag GmbH&Co. KGaA, Weinheim.

The mechanism behind the topographical effect may be partially elucidated by the diffusion behavior of single HPF molecules on the MD thin film surfaces. [207] Kastantin *et al.*, [207] who was in cooperation with our group, investigated the dynamic adsorption behavior of HPF on MD HDPE thin films by mapping using accumulated probe trajectories (MAPT) (Fig. 8g and h). Similar to MD UHMWPE, the surface of MD HDPE exhibited well-oriented nanocrystals on the surfaces. [119]

Through dynamically tracking the single proteins on the surfaces, HPF molecules favored diffusing along the drawing direction, i.e., the minor axis of the nanocrystals. [207] By increasing the bulk concentration, the mean residence time of fibrinogen increases from one second to several minutes, indicating the protein layer formation. [207] These observations illustrated that the protein adsorption behaviors could be fine-tuned by the surface topographical factors. [207] However, the determinations of protein biofunctionality upon adsorption to nanostructured surfaces, are still missing.

2.4 Platelet Adhesion on Surfaces

Thrombosis is the blood clot formation inside a blood vessel, preventing the abnormal arterial blood flow through the circulatory system. [208] When it exists in veins (venous thrombosis) or arteries (arterial thrombosis), it may lead to various diseases, such as cyanosis, thromboembolism, and tissue damage. [209, 210] Other than that, thrombosis may appear in medical devices, such as stents [211], intravascular catheters [212], and valves [213].

2.4.1 Platelet adhesion on nanostructured polymer surfaces

Surveys reported that the application of foreign materials, like polymer vascular stents, increased the incidence of thrombosis in 1.2 %, much higher than the control populations. [214] Meanwhile, Platelet adhesion and aggregation have been recently revealed to be connected with the thrombosis formation and thus affecting the biocompatibility of medical devices and hemocompatibility of implants. [215-217]

Different anti-thrombogenic strategies, such as anticoagulants and drug eluting polymer coatings, have been introduced to reduce the platelet adhesion and enhance the blood compatibility of biomaterials. [218, 219] Nevertheless, it was demonstrated that these anti-thrombogenic strategies might cause late stage thrombosis and prevent endothelial cell adhesion, and also is the risk for biomaterial integration. [220, 221] Current preventive methods focus on surface modifications, such as chemical modifications and passivation of surfaces. Adamson *et al.* [222] compared platelet adhesion and activation on gold surfaces modified by thiol functionalized RGD, alkane, and PEG monolayers. It was shown

that a significant reduction in the adhesion and activation of platelets were found on the alkanethiol modified gold surface due to its superhydrophobic property, comparing to RGD and PEG monolayers. [222]

Apart from the surface chemical modification, an attempt was also made to improve the anti-thrombogenic properties through topographical features. [223-225] Pham *et al.* [225] in our research group found that the platelet adhesion under shear flow conditions was significantly reduced on hemispherical microstructured polydimethylsiloxane (PDMS) surfaces, compared to the unstructured control surface. This was attributed to the high shear stress gradient generated between the tops of the microstructures and the ground areas. [225] In another work, Koh *et al.* [226] produced poly (lactide-*co*-glycolide) (PLGA) films with multi-walled carbon nanotubes in two different orientations: randomly oriented and vertically oriented. The PLGA films with vertically oriented nanotubes showed a very low level of platelet adhesion, attributing to either the presence of -COOH groups or the vertical alignment of nanotubes. [226] Further investigations addressed the influence of specific topographical structures on the adhesion of platelets. [227-230] The results showed that the platelet adhesion was significantly reduced on the structured surfaces in the size range of platelets or below. [229, 230] The reduced level of platelet activity was assumed to originate from reduced stable contact area for platelet cells. [231, 232]

2.4.2 Platelet adhesion influenced by HPF conformation

Control of HPF conformation was also recognized as one of the anti-thrombogenic strategies. [152, 233, 234] It was reported that more HPF molecules could provide more binding sites to platelets due to the recognition of GPIIb/IIIa receptors in platelet cells. [235] Xu *et al.* [236] found that polyurethane-urea (PUU) with more hard segments resulted in less HPF functionality and thus lower platelet adhesion attributing to less available binding sites on HPF layer to platelet cells.

As was described in the previous sections, the size of the nanotopographies directed the assembly of protein molecules. [188, 198, 237] Thus the amounts of proteins were assumed to affect the subsequent platelet adhesion. Lord *et al.* [238] investigated the protein adsorption influenced the platelet adhesion on stochastically nanorough surfaces with varying surface roughness. Results showed

that silica surfaces with high roughness (15 nm R_{rms}) supported significantly less HPF adsorption than the surfaces with low roughness. [238] Although all the surfaces supported the similar amounts of platelets, the surfaces with nanoroughnesses displayed round-shaped platelets and weak attachments between the surfaces and platelets. [238] This indicated that the surface nanotopographies played an essential role in protein adsorption and subsequent platelet adhesion. [238]

Recently, more and more studies indicated that the HPF conformations and availabilities of binding sites played a more critical role in platelet adhesion than the amount of HPF on surfaces. [152, 154, 226] In the work by Zhang *et al.*, [152] it was revealed that the binding sites of HPF for platelets were demonstrated to be the γ 400-411 segments, which were exposed by HPF fibers or HPF layers on hydrophilic polymer surfaces. The formed HPF fibers seemed to bind the platelets in small areas instead of uniformly across the surfaces. [152] Moreover, the HPF layer on hydrophobic surfaces appeared to improve the endothelialization while reducing the platelets adhesion, attributing to the exposed binding sites on α C chains for endothelial cells and the hidden binding sites to platelets. [152]

There is no study on the extent of HPF conformational changes and its impact on platelet adhesion independence of well-defined nanostructured surfaces, especially with the topographical features comparable to the size of HPF.

2.5 Brief Summary

In this chapter, the current state-of-the-art in controlling protein adsorption and platelet adhesion behaviors on polymeric biomaterials have been reviewed. The choice of synthetic polymers as biomaterials is defined by the end user and thoughtful considerations of their properties. Besides the biological requirements, the surface properties of polymers are being needed to guide the protein adsorption. Furthermore, the adsorbed proteins mediate cellular interactions and subsequent tissue integration.

The original design work on biomaterial surfaces, such as nanostructure fabrication, is one of the focus in current biomedical science. The creating of nanostructures on various polymer surfaces, i.e., amorphous polymers, semicrystalline polymers, and

block copolymers, could be accomplished by corresponding strategies. These nanostructures were developed to improve the biocompatibility and bio-sensing of polymeric biomaterials, other than the surface properties as wettability, charge/polarity, and functionalization.

The advances in polymeric nanostructure designs for controlled protein adsorption were highlighted, especially for the plasma protein, HPF. The unique structure and function of HPF resulted in various interactive and adsorption events on surfaces, which have attracted the most interest. The remained challenges in structural designs include developing biomaterials with much richer surface features, understanding the specific protein-surface interactions, and elucidating the platelets response to conformational changed proteins. In the next chapter, the aims and objectives of this work will be highlighted to provide a clear view of this work.

To make the above statements more understandable, the protein adsorptions on polymeric nanostructured surfaces were summarized in table 1, according to the polymers, patterns, proteins, adsorption behaviors, and conclusions. In the next chapter, the aims and objectives of this work will be highlighted to provide an overall view of this work.

Table 1. Protein adsorptions on polymeric nanostructured surfaces.

Polymers	Patterns	Proteins	Adsorption behaviors	Conclusions	Ref
Lithography and molding					
PHMS	209 and 489 nm nanopores	Human lactoferrin	The proteins were confined inside the nanopore array with higher density. The assembly regions of protein changed with the hydrophobicity of the pores.	Preferential immobilization	[191]
PMMA	70–100 nm nanowells	BSA, lysozyme	BSA adsorbed in the cavities with conformational changes. Lysozyme adsorbed outside the cavities with native conformation.	Preferential adsorption	[6]
PMMA	15, 50, 100 nm nanopits	HPF, lysozyme	HPF adsorbed in 15, and 50 nm pores with “end-on” orientation. Lysozyme adsorbed with native conformation.	Conformational changes upon adsorption	[239]
Self-assembly					
PS- <i>b</i> -PMMA	25 nm cylinders	HPF	HPF aligned parallel to the major axis of the nanodomain.	Preferential alignment	[198]
PS- <i>b</i> -PMMA	45 nm cylinders	HPF	HPF aligned perpendicular to the major axis of nanodomain.	Preferential alignment	[188]
PS- <i>b</i> -PMMA	25 nm cylinders	HPF, BSA	The initially adsorbed BSA was replaced by HPF due to the Vroman effect.	Competitive protein adsorption	[202]
Polymer crystallization					
PE single crystal	0.7 nm thick lamellae	HPF	HPF orientated along crystallographic [100] and [010] directions.	Preferential alignment	[204]
MD HDPE	30×100 nm ² SKCs	HPF	HPF diffused along polymer chain direction, i.e., melt-drawing direction.	Anisotropic diffusion	[207]
MD UHMWPE	26×103 nm ² stacked lamellar	HPF	HPF aligned along the major axis of the stacked lamellar.	Preferential alignment	[116]

3

Aims and Objectives

3.1 Open Scientific Questions

Researchers demonstrated that proteins had unique adsorption behaviors on material surfaces with nanoscale topographies, especially when the dimension of the topographical features was similar to the size of the protein. The development of nanostructure fabrication methods allowed better control of lateral resolution and geometry of structured polymer surfaces. Among these methods, the MD technique offers excellent power in highly-oriented nanostructures in a facilitated way. Unique adsorption behaviors of proteins have been observed on nanostructured MD polymer surfaces. It was elucidated that these surfaces own specific controlling factors, such as nanostructure, spatial arrangement, and crystallinity.

Inspired by these unique phenomena, the following questions raised:

- a. Could the physical factors, width, and curvature, of polymeric nanostructures play an essential role in the assembly and conformation changes of HPF?
- b. Could the spatial arrangement of polymeric nanostructures influence the alignment and orientation of single HPF molecules?
- c. How are the subsequent biological responses mediated by the nanostructures with the surface-immobilized HPF?

The better understandings of these adsorption behaviors would lead to topographically-controlled protein assembly, which can be utilized in modeling blood-contacting surfaces of biomaterials.

3.2 Hypotheses

In this thesis, the following three hypotheses were tested.

- a. The physical factors, i.e., the width and curvature of polymer crystals on the nanostructured polymer surfaces, influence the HPF conformation change, ordered layer formation, and adsorption dynamics.
- b. The nanostructured MD iPB-1 surfaces mediate the alignment and diffusion of a single HPF molecule.
- c. The conformation and thus bioactivities of the adsorbed HPF molecules, which affect the adhesion and activation behaviors of platelets, depend on the nanostructure of the underlying polymeric surface.

3.3 Aims and Objectives

This work aimed to gain more in-depth insight into the adsorption behavior of HPF on topographically distinct nanostructures of iPB-1 and HDPE surfaces.

Three objectives were applied in this thesis:

Firstly, to investigate the effect of crystal width and curvature, the concentration- and time-dependent protein adsorption on nanostructured iPB-1 surfaces in combination with protein adsorption kinetics are characterized using quartz crystal microbalance with dissipation (QCM-D) and AFM.

Secondly, to understand the influence of spatially arranged nanostructure on single HPF molecules, the alignment and diffusion of single HPF molecules on highly-oriented nanostructured iPB-1 surfaces are detected via AFM and MAPT.

Thirdly, to evaluate the bioactivities of the surface-immobilized HPF molecules, platelet adhesion and activation on nanostructured polymer surfaces are obtained through optical microscopy and SEM.

3.4 Scientific Significance

The research of protein adsorption on nanostructured polymer surfaces allows biomaterial scientists a deeper understanding of biomaterial design. Physical processes to modify materials surfaces may, i) efficiently improve the biocompatibilities of the biomaterials; ii) significantly reduce the cost of biomaterial implants by surface modification; and iii) additionally inspire more cross-disciplinary researches in nanostructured surfaces.

The experimental evidence in this work may provide the comprehensive elucidations of protein-surface interactions, confirmation of present theories, and

inspiration of new biomaterial design. Therefore, the work described in this thesis will be relevant not only for advancing the knowledge of controlled protein adsorption on the blood contact materials but also for practical interests in the developments of bio-devices and biomaterials.

3.5 Related Publications

(1) *Xiaoyuan Zhang*, Christian Helbing, Matthias M.L. Arras, Klaus D. Jandt,* and Izabela Firkowska-Boden. Nanocrystal Width Controls Fibrinogen Orientation and Assembly Kinetics on Poly (butene-1) Surfaces, *Langmuir*, 2017, 33(26), 6563-6571.

(2) Izabela Firkowska-Boden, *Xiaoyuan Zhang*, Klaus D. Jandt,* Controlling Protein Adsorption through Nanostructured Polymeric Surfaces, *Advanced healthcare materials*, 2018, 7(1), 1700995.

(3) *Xiaoyuan Zhang*,* Izabela Firkowska-Boden,* Matthias M.L. Arras, Mark J. Kastantin, Christian Helbing, Alper Özogul, Enrico Gnecco, Daniel K. Schwartz and Klaus D. Jandt,* Fibrinogen Diffuses via Anisotropic Nano-Crawling on Nanostructured Isotactic Polybutene-1 Surfaces, *Langmuir*, 2018, 34(47), 14309-14316.

+ These authors contributed equally to the work.

3.6 Related Presentations

(1) *Xiaoyuan Zhang*, Izabela Firkowska-Boden, Christian Helbing, Klaus D. Jandt, Fibrinogen Assembly on Nanostructured Polybutene-1 Surfaces, Chinese German Chemical Association (CGCA®) 30th annual conference, 19. -22. 04. 2018, Berlin, Germany.

(2) *Xiaoyuan Zhang*, Izabela Firkowska-Boden, Christian Helbing, Klaus D. Jandt, Nanocrystal Width Controls Fibrinogen Assembly on Polybutene-1 Surfaces, Jena School for Microbial Communication (JSMC) Symposium 2017, 16. -17. 10. 2017, Jena, Germany.

(3) *Xiaoyuan Zhang*, Matthias M. L. Arras, Christian Helbing, Klaus D. Jandt, Tracking the Diffusion of Single Fibrinogen on Nanostructured Polybutene-1 Surfaces, CGCA® 29th annual conference, 16. -17. 06. 2017, Bremen, Germany.

(4) *Xiaoyuan Zhang*, Matthias M.L. Arras, Christian Helbing, Klaus D. Jandt, Anisotropic Diffusion of Single Fibrinogen Molecule on Highly-oriented Nanostructures Tracked by MAPT, JSMC Symposium 2016, 15. 12. 2016, Jena, Germany.

(5) *Xiaoyuan Zhang*, Christian Helbing, Matthias M.L. Arras, Klaus D. Jandt, Fibrinogen Adsorption on Nano-structured isotactic Polybutene-1 Thin Films, Ministry of Education of the P. R. China 'Chunhui' Plan 2016, 03. -08. 07. 2016, Peking, Ningbo, and Shanghai, P. R. China.

(6) *Xiaoyuan Zhang*, Christian Helbing, Matthias M.L. Arras, Klaus D. Jandt, Human Plasma Fibrinogen on Nanostructured Polybutene-1 Thin Films, CGCA® 28th annual conference, 10. -11. 06. 2016, Düsseldorf, Germany.

(7) *Xiaoyuan Zhang*, Christian Helbing, Matthias M.L. Arras, Klaus D. Jandt, Human Plasma Fibrinogen on Nanostructured Polybutene-1 Thin Films, CGCA® South forum 2016, 05. 03. 2016, Tübingen, Germany.

(8) *Xiaoyuan Zhang*, Protein Patterns on Polymer Surfaces, CGCA® East forum 2015, 06. 12. 2015, Leipzig, Germany.

(9) *Xiaoyuan Zhang*, Matthias M. L. Arras, Christian Helbing, Klaus D. Jandt, Human Plasma Fibrinogen on Nanostructured Polybutene-1 Thin Films, JSMC Retreat 2015, 26. 11. 2015, Bad Sulza, Germany.

3.7 Thesis Outline

The following descriptions are the highlighted subjects presented in this thesis.

Chapter 1 introduces the significance of protein adsorption behavior on surfaces.

Chapter 2 provides state of the art referring to the applications of the polymer as biomaterials, surface nanostructuring methods for polymers and protein adsorption behaviors on nanostructured polymer surfaces.

Chapter 3 addresses the open questions, hypotheses, aims, objectives, and scientific significance of this thesis.

Chapter 4 describes the theories of the MD technique, QCM-D measurement, and MAPT method, which are essential for better understandings of protein adsorption on surfaces. Meanwhile, detailed information about the sample preparation and characterizations are provided.

Chapter 5 presents the HPF adsorption and cell adhesion behaviors on nanostructured surfaces.

Section 5.1 displays the topographical effect of two distinguished crystalline nanostructures on the adsorption behaviors, such as conformation change and orientation, of HPF molecules. The distinct adsorption and assembly configurations of HPF molecules on iPB-1 surfaces were determined as a function of crystal lamellae dimensions.

Section 5.2 mainly reports that the nanostructured surfaces can control protein adsorption on the molecular level. An enhanced understanding of HPF adsorption on nanostructured surfaces was present by combining MAPT and AFM to study the adsorption dynamics and static characteristics.

Section 5.3 shows that the surface-immobilized HPF molecules can regulate the platelet adhesion. The amounts, as well as the morphologies of the adhered platelet cells, are characterized and discussed with the changing of protein conformation and assembly configurations.

Chapter 6 summarized the work in this thesis and emphasized the importance of protein adsorption on biomaterial surfaces.

4

Experimental

4.1 Experimental Techniques

4.1.1 Atomic force microscopy (AFM)

This section introduces the empirical knowledge and theoretical understandings of AFM. After the invention by Binnig *et al.*, [239, 240] AFM became the dominant instrument to investigate the surface properties in the microns to the sub-nanometer range. It can provide three-dimensional topography information as well as stiffness, friction force, and lateral stiffness on surfaces by monitoring and adjusting the tip-surface interactions (Fig. 9a).

AFM consists of a scanning component, cantilever mounted with a sharp tip, optical detection system, and feedback control. [241-243] In the general setup, the motion of cantilever in three dimensions is controlled by a piezo scanner. [241] The deflection, oscillation, and twisting of the cantilever are reflected by the laser beam, which is pointed toward the back side of the cantilever and to the photodiode detector. [241] To adjust the tip-surface interactions, close-looped feedback control is applied, and thus, all feedbacks are analyzed for user-defined purposes. [242] Therefore, by raster scanning the tip over the surfaces, images with different surface properties can be obtained. [242, 243]

The imaging modes of AFM are classified into two categories, static and dynamic modes. [241] In the static mode, the tip is set to contact with material surface, in which repulsive force between the tip and surface is dominant. [244, 245] Although topography and friction images with high resolution can be achieved, mechanical damage to soft surfaces as biomolecules and polymers is inevitable. [246] In the dynamic mode, the tip is several nanometers away from the surface, in which the attractive forces are dominant. [247-249] At this intermediate distance, changes of oscillation amplitude, frequency, and phase are detected. [243] Take tapping mode

for instance, the amplitude is kept constant through the detection by lock-in amplifier and feedback by adjusting the tip-surface distances (Fig. 9c and d). As a result, topography and phase images can be possessed depending on the motion of cantilever and driving oscillation. [250, 251] This mode is suitable for soft imaging materials as polymers and biomolecules. [252-254]

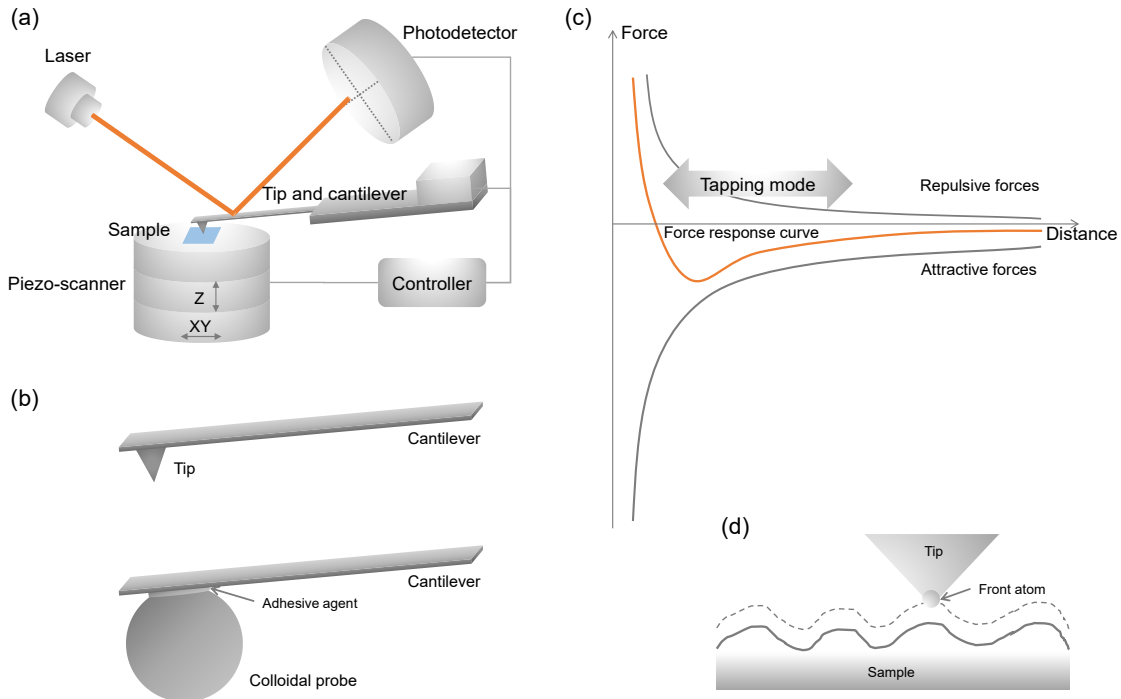


Figure 9. The working principle of AFM. (a) Sketch of AFM. (b) Typical AFM tip and colloidal probe. (c) Tip-surface interactions. (d) Tip close to the surface when scanning.

The typical tips used in AFM are from silicon or silicon nitride, with the radius of several nanometers (Fig. 9b). As is known that the AFM with the contacting mode can simulate friction properties on the surface. [255, 256] However, the sharp tip used in this mode damages the surface of soft materials easily and thus influence the measured friction forces. [257, 258] Nowadays, spherical colloidal probes mounted on the cantilever are applied to overcome these disadvantages. [259] This can be attributed to i) large contact area to distribute the pressure onto the surface, ii) high signal-to-noise ratio to acquire friction information, and iii) improved quality of adhesion values. [259, 260] Therefore, more and more researchers are utilizing colloidal probes to elucidate the tribological properties of surfaces with nanostructures. [261]

4.1.2 Quartz crystal microbalance with dissipation (QCM-D)

Over the last few decades, QCM-D has been extensively applied in various fields, such as proteins, polymers, surfactants, and cell attachments on surfaces in aqueous conditions. [6, 41, 262] In the biomedical fields, it is widely used to provide the protein adsorption kinetics and to obtain better understandings of protein-surface interactions. [263, 264] In principle, QCM-D performs as an ultra-sensitive balance for small molecules adsorbed on the surfaces (Fig. 10 a, b, and c).

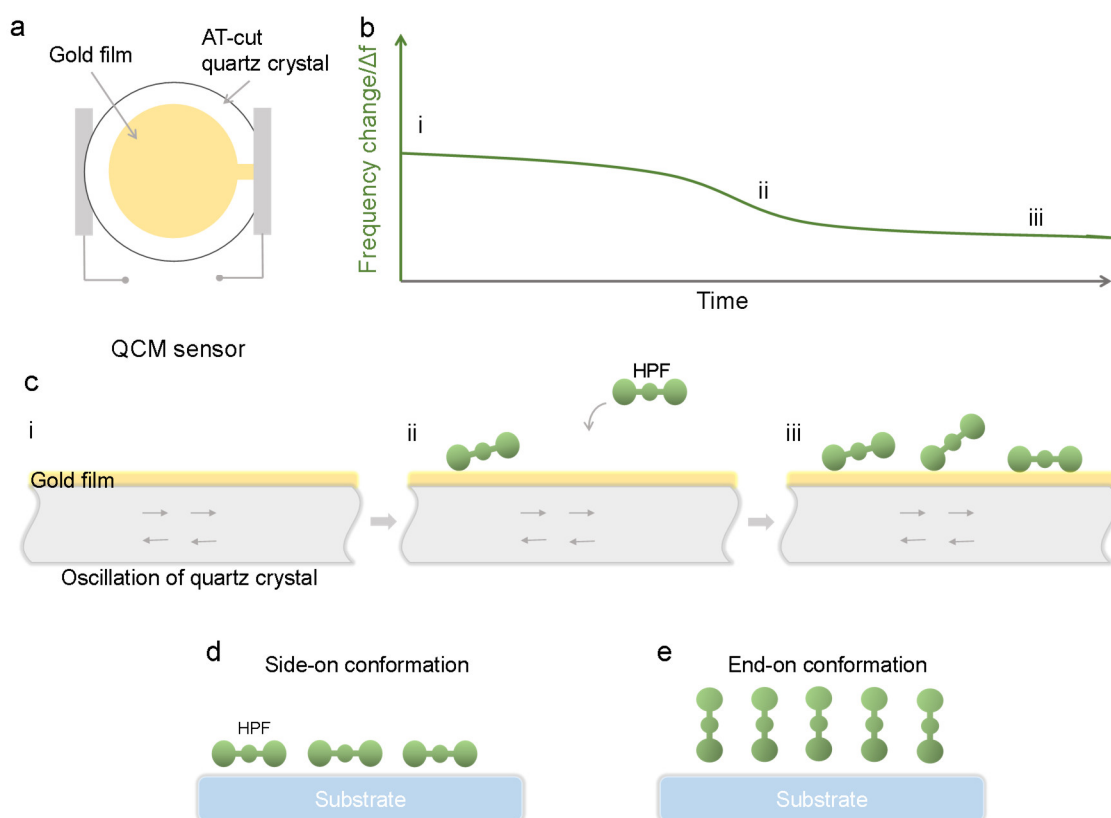


Figure 9. The working principle of QCM-D. (a) Sketch of QCM chips. (b) Detected frequency change as a function of time. (c) Schematically drawings of HPF adsorption on QCM chips at the stages i, ii, and iii. (d) “Side-on” and (e) “end-on” conformations of HPF.

The quartz crystal disc can oscillate at the resonance frequency under alternating voltage. [262] The signals of frequency changes (Δf) and dissipation changes (ΔD) can be transferred to the computer via the pair of gold electrodes on the front and back side of the discs. [265-267] Δf decrease and ΔD increases when the small molecules adsorb on the surfaces (Fig. 10b and c).

The obtained Δf can be converted to adsorbed mass by the Sauerbrey equation. [268-270] Mass changes (Δm) is equal to $-C_f \times \Delta f$, where C_f is the sensitivity factor for the crystal ($56.6 \text{ Hz} \cdot \mu\text{g}^{-1} \cdot \text{cm}^2$ for a 5 MHz AT-cut quartz crystal at room

temperature, taken from QCM-D Stanford Research). [1, 266, 271] ΔD value is calculated into the dimensional ratio, $\Delta D/(-\Delta f/n)$, where n is the number of overtones, for determining the validity of the Sauerbrey equation in the conditions applied. [272] When the dimensional ratio is much smaller than $4 \times 10^{-7} \text{ Hz}^{-1}$ for 5 MHz sensors, the ΔD concerning Δf is small, and the viscoelastic ΔD of energy can be neglected. [19, 27, 41, 273] In this case, the adsorbed protein layer can be assumed rigid, and the Sauerbrey equation is valid. [6, 169, 272, 274, 275]

Following the concept given by Hu *et al.*, a monolayer or multilayer film can be obtained by comparing the experimental mass with the theoretical protein monolayer. [276] Take HPF for instance, the theoretical monolayer coverage mass was calculated to be 540 ng/cm^2 by the random sequential adsorption (RSA) model. [187, 189] In the model, the HPF molecule can be assumed to be a rod with 6 nm diameter and a length of 45 nm. [156, 187] Two adsorption situations, “side-on” (Fig. 10d) and “end-on” (Fig. 10e) adsorption are the main basis of the theoretical calculations of maximum monolayer mass per unit area. [180, 187, 188] The surface occupied by one molecule is 270 nm^2 (projection area) for “side-on” adsorption. [180, 187, 188] The total covered mass for HPF “side-on” adsorption is $m_0 = 5.7 \times 10^{-19} \text{ g}$. [180, 187, 188] Accordingly, the monolayers in both conformations present the masses ranging from 210 (“side-on” adsorption) to 1570 ng/cm^2 (“end-on” adsorption). [156]

4.1.3 Mapping using accumulated probe trajectories (MAPT)

Tracking the individual proteins on the water-surface interfaces is the basis for elucidating the protein adsorption, desorption, and diffusion behaviors. [277] However, it is inaccessible for traditional and ensemble-averaged methods, such as AFM, TEM, and QCM-D, etc. [192] Therefore, novel characteristic techniques are needed by biomaterial scientists.

MAPT, which was recently developed for the direct observation of fundamental physical interactions, is a promising method to characterize the diffusive behavior of single HPF molecules at the solid-liquid interface. [207, 277-280] Total internal reflection fluorescence microscopy with single-molecule resolution (TIRFM-SM), which is the core component of MAPT (Fig. 11a), has recently shown its ability to provide a time-resolved spatial mapping of protein-surface interactions. Thus it

was utilized to investigate protein diffusion dynamics on specific regions of interest that are defined by distinctive dynamic features. [207, 277, 281]

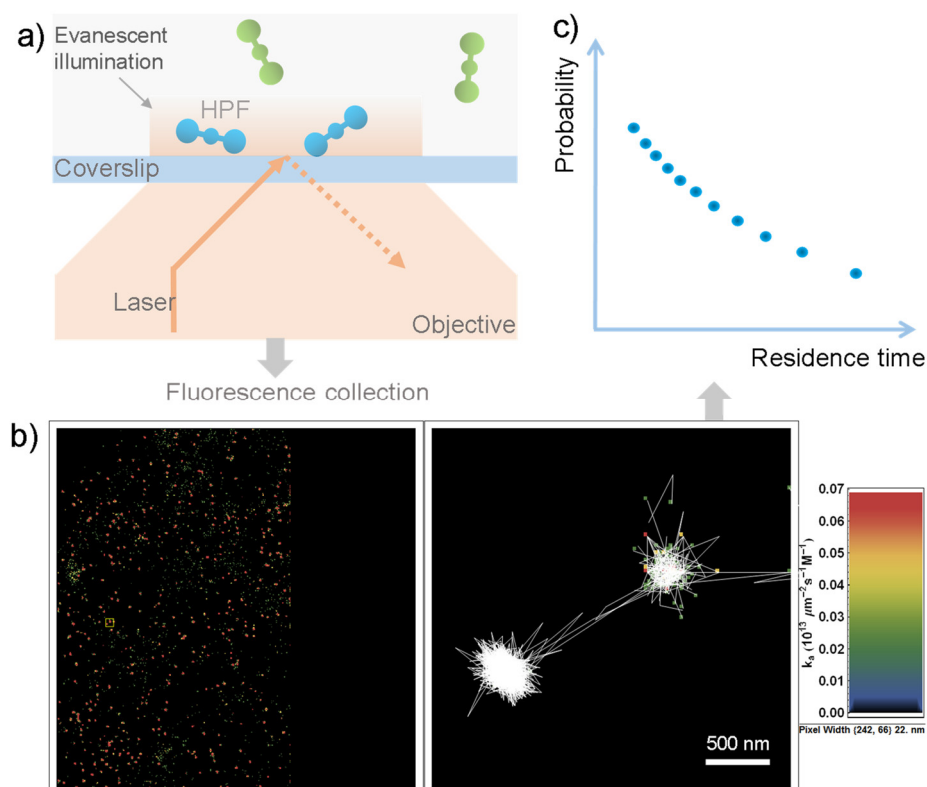


Figure 11. The working principle of MAPT. a) Data collection by TIRFM-SM; b) Occupancy map and zoomed several steps for HPF on MD iPB-1 surfaces. The connected white lines indicate the direction and distance of the diffusing HPF molecules; and c) cumulated residence time of single molecules, which are simulated from the number of steps.

The evanescent and exponentially decaying field of light, generated in TIRFM at the solid-liquid interface, penetrates the liquid for only about 100 nm (Fig. 11a). This phenomenon perfectly suits to observe solid-liquid interfacial events. The evanescent field also significantly minimizes the background emission from fluorophores in the vicinal bulk solution and thus strongly improves the spatial and temporal resolution of single molecule detection. [278, 279, 281] With continuous spatial localization tracking and the following computational analysis, the dynamic behavior of single protein molecules can be identified, independent of transport in solution. [279] Therefore, the adsorption, desorption, and diffusion behaviors of fluorescently labeled HPF molecules at the liquid-solid interface can be tracked and permit detailed analyses involving the differences in dynamics on different spots of the surface. [207, 281]

The main data analysis procedures are described as follows. After acquiring consecutive frames under certain conditions, a two-stage tracking program is performed. [279] The first stage includes identification of objects by convolving each frame with a disk matrix, background subtraction, user-defined thresholding procedure, and morphological transform. [277] The position of objects ($\sum_i x_i F_i, \sum_i y_i F_i$) is calculated by the centroid intensity, where (x_i, y_i) is the position of the i th pixel, and F_i is its intensity. [280] The second stage is creating molecular trajectories. [277] When identified objects are located on sequential frames within a distance of fewer than 4 pixels (910 nm), the object is considered as the same. [280] A trajectory is formed by connecting these objects in the sequential frames. [277] The objects only appear in one frame or much smaller than the diffraction limit is ignored to reduce the noises. [280]

The field of view is divided into square bins of a specified size for determining surface occupancy maps (i.e., the density of observed HPF locations per area, time, and the bulk concentration of labeled HPF), shown in Fig. 11b. High occupancy indicates that one object stays at the same location or that multiple objects reside sequentially in the same location. [207] One molecule residing in a bin for 0.2 s corresponds to a surface occupancy of $1.3 \times 10^{12} \mu\text{m}^{-2}\text{s}^{-1}\text{M}^{-1}$. [207] The surface residence time for an identified object can be obtained by multiplying the number of consecutive identified frames with the duration time of each frame, shown in Fig. 11c. The mean residence time is the average value of all the mean residence times from specific-selected trajectories divided by the number of selected trajectories using the occupancy map. [207] More than 200 trajectories need to be chosen for each mean residence time. [207] The standard deviations come from the half-width of the mean residence time histogram of the randomly-selected trajectories. [207]

To analyze the anisotropy of diffusion, each motion is separated into two components, one parallel and one perpendicular to the major direction, respectively. [279] The diffusion coefficient in the two directions is determined as the mean squared-displacement divided by $2\Delta t$, in which Δt is the acquisition time of 0.2 s, and the factor of 2 was appropriate for diffusion in one dimension. [279] Positional uncertainty of $0.0125 \mu\text{m}^2\text{s}^{-1}$ is subtracted from the mean diffusion coefficient in both the parallel and perpendicular directions. [207] Positional

uncertainty is estimated by selecting a subset of immobile objects over long time intervals and observing the apparent squared displacement in $\Delta t=0.2$ s. [207, 277] The uncertainty is determined as the standard deviation of the mean residence time. [207]

4.2 Sample Preparation and Characterization

4.2.1 Preparation of nanostructured surfaces

Isotactic polybutene-1 (iPB-1) with a molecular weight of $570 \text{ kg}\cdot\text{mol}^{-1}$ and HDPE with a melt index of $2.2 \text{ g}/10 \text{ min}$ ($190 \text{ }^\circ\text{C}/2.16 \text{ kg}$) were purchased from Sigma-Aldrich Chemie GmbH (Schnelldorf, Germany). p-xylene (synthesis grade) was purchased from Merck KGaA (Darmstadt, Germany).

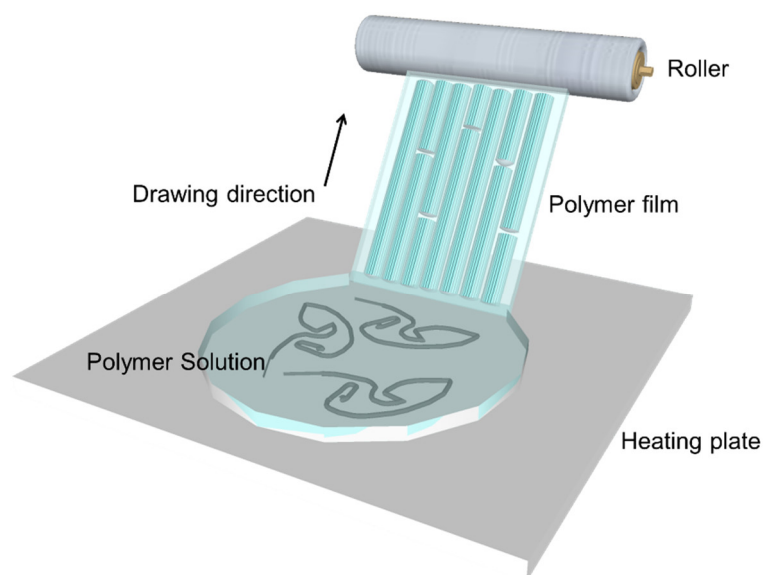


Figure 12. Schematic of MD technique. With the evaporation of polymer solution on the heating plate, polymer melt forms. The polymer thin film is collected between the roller and polymer melt.

The NLCs of iPB-1 were created by the MD technique (Fig. 12). The iPB-1/p-xylene solution was prepared at a concentration of 1 wt % and heated to $120 \text{ }^\circ\text{C}$. The main procedures for melt drawing technique are as follows. The hot solution was poured on a glass plate with a temperature of $125 \text{ }^\circ\text{C}$, which was the optimized temperature for long needles and flat surfaces. A thin iPB-1 film was drawn off the glass plate by a roller at a speed of $6 \text{ cm}\cdot\text{s}^{-1}$. The MD iPB-1 thin films were attached on glass slides for further investigation using a trace amount of solvent.

The originally self-supporting MD iPB-1 thin film was fixed on a metal ring to store it for further use temporarily. Subsequently, the melt-drawn thin films were mounted on glass coverslips and the silicon wafer, cut into 1 cm×1 cm pieces. MD HDPE was prepared similarly as MD iPB-1, but with a plate temperature of 130 °C.

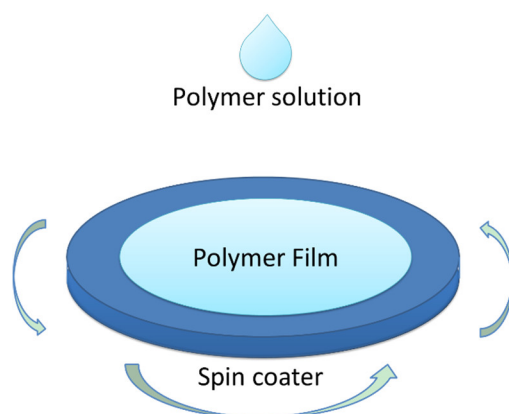


Figure 13. Schematic of SC technique. The polymer solution is dropped on the substrates. The plate, fixed with the substrate, spin with a speed of 2000 rpm to form the thin polymer film.

To obtain the lamellar crystals (LCs) of iPB-1, spin coating technique (Fig. 13) was applied. This is one of the most facilitate method to form thin films on chosen substrates. The procedures performed in this work were as follows. iPB-1 solution (1.0 wt % in p-xylene) was spin-coated on silicon wafers at 2000 rpm and thoroughly dried at ambient temperature for three days.

4.2.2 Surface nanostructures by AFM

Topography and phase images of surfaces before protein adsorption were recorded using a Multimode™ III scanning probe microscope (Digital Instruments, Veeco, Santa Barbara, CA, USA) at ambient temperature in air. Standard silicon cantilevers were purchased from Bruker (model RTESP, Veeco, Santa Barbara, CA, USA). They featured a resonance frequency in the range of 315-364 kHz in the air, a spring constant in the range of 20-80 N·m⁻¹, and a typical tip radius of less than 10 nm (average 7 nm). The sample size was 1×1 cm².

The friction properties of both MD iPB-1 and MD HDPE surfaces were measured with JPK nanowizard 4 AFM (JPK Instruments AG, Germany) under dry conditions. The colloidal probe SiO₂ with a diameter of 10.2 μm, equipped on ContAl-G cantilever, was used in this experiment. The friction forces were measured under

different loads, 10, 20, 30, 40 and 50 nN in 2 μm scan size. The sample size was $1\times 1\text{ cm}^2$. The measured lateral force directions were 0° (in the drawing direction of the melt-drawn films) and 90° (perpendicular to the drawing direction).

4.2.3 Surface chemistry determination by contact angle measurement and X-ray photoelectron spectroscopy (XPS)

The contact angle analysis was performed with a DSA10 drop shape analysis system (Krüss GmbH, Hamburg, Germany). Double-distilled water was used in this study. The images of the water drops on the surfaces were recorded and analyzed via the drop shape analysis system. At least three samples and three areas were measured in each group at ambient temperature. The distilled water volume was around 10 μL , and the dosing rate was 6.5 $\mu\text{L}/\text{min}$. X-ray photoelectron spectroscopy (XPS) analysis of pure iPB-1 films was conducted on an EA200-ESCA-system (SPECS) using nonmonochromatic Mg $K\alpha$ radiation ($h\nu=1253.6\text{ eV}$).

4.3 Protein Detection on Nanostructured Surfaces

4.3.1 HPF adsorption on nanostructured surfaces

HPF was purchased from Calbiochem (Merck KGaA, Darmstadt, Germany). Phosphate buffered saline solution (PBS) was purchased from Invitrogen (Thermo Fisher Scientific, Germany). A stock solution of HPF in PBS was prepared at a concentration of $1000\text{ mg}\cdot\text{L}^{-1}$. The stock solution was then diluted with PBS into 10^{-10} , 10^{-4} , 10^{-3} , 10^{-2} , 10^{-1} , 1, 10, and $100\text{ mg}\cdot\text{L}^{-1}$. For each HPF concentration, 2 mL PBS solution of the respective HPF concentration was pipetted on the polymer films and left for 30 min adsorption under quasi-physiological conditions at 37°C . [6, 282] Protein adsorption experiments were carried out under quasi-physiological conditions (37°C , $\text{pH}=7.4$). The sample size was $1\times 1\text{ cm}^2$. After 30 minutes exposure to HPF solution, the films were rinsed twice with pure PBS solution and Milli-Q water to remove non-adsorbed protein and PBS residues from the film surface. The films were then dried at ambient temperature in air.

4.3.2 HPF observations by AFM

Topography and phase images of surfaces after protein adsorption were recorded by the same procedure as described in section 6.1.2.

4.3.3 HPF adsorption dynamics by QCM-D

The adsorption kinetics of HPF to the nanostructured surfaces were measured with QCM-D (Q-Sense, Goteborg, Sweden). Quartz crystals with a fundamental frequency of 5 MHz were purchased from Quartz Crystal Microbalance (Q-Sense, Goteborg, Sweden) with gold electrodes and used as purchased or coated with iPB-1 films. Before use, they were cleaned by treating with piranha solution for 10 min and immediately washed thoroughly with Millipore water. UV-treatment was applied as a final stage of cleaning gold chips. Also, the melt-drawn iPB-1 films were attached to QCM-D chips by using solvent vapor to ensure the tight bonding of the film. To obtain the LCs on chips, iPB-1 solution (1.0 wt% in p-xylene) was spin-coated on QCM-D chips at 2000 rpm and fully dried at ambient temperature for three days. The diameter of the chips were 14 mm.

The sensor plate was installed into the QCM-D chamber (KSV instruments, Helsinki, Finland) connected with a temperature controller (Oven Industries, Inc. Mechanicsburg, PA), which was set to 37.0 ± 0.1 °C. During rinsing and exchange of PBS buffers, the liquids were pumped through the chamber with a flow rate of 100 $\mu\text{L}/\text{min}$. Twenty minutes were required to obtain a stable frequency baseline. For protein adsorption, the HPF solution was pumped into the sensor with a flow rate of 20 $\mu\text{L}/\text{min}$. During the QCM-D measurement, the Δf and ΔD were simultaneously recorded at its first five overtones ($n=3, 5, 7, 9, 11$). [283, 284]

4.3.4 Single protein tracking by MAPT

For the TIRFM-SM measurement, the HPF molecules labeled with AlexaFluor 488 were purchased from Molecular Probes Inc. (Eugene, Oregon, United States). The buffer concentration of labeled HPF was 10^{-10} $\text{mg}\cdot\text{L}^{-1}$, resulting in sufficiently sparse images to permit accurate localization and trajectory segmentation of individual HPF molecules. To study the effects of crowding, a high concentration (1 $\text{mg}\cdot\text{L}^{-1}$) solution was prepared, composed primarily of unlabeled HPF, in which the concentration of labeled HPF molecules was still 10^{-10} $\text{mg}\cdot\text{L}^{-1}$. Single molecule detection was carried out by TIRFM-SM measurements. The Nikon TE-2000 microscope with a 60 \times objective was equipped with a custom-built prism-based illumination system, flow cell and 491 nm diode pumped solid state laser. The frame acquisition time was 0.2 s for each 800-frame movie. All experiments were

carried out under quasi-physiological conditions (37 °C, pH=7.4). The sample size was 1×1 cm². The signal-to-noise ratio, 3.5±1, was determined by the ratio of the maximum intensity of each identified object to the root mean squared value of background intensity. The data acquisition was performed by Prof. Mark J. Kastantin in university of Colorado Boulder in the USA. The sample preparation, data analyzation, and mechanism elucidation were achieved in the group of Chair of Materials Science in Jena in Germany.

4.4 Cell Adhesion on Nanostructured Surfaces

4.4.1 Cytotoxicity of surfaces

The 3-(4,5-dimethylthiazol-2-yl)-2,5-diphenyltetrazolium bromide (MTT, Sigma, Poole, UK; 1.25 mg/mL in Dulbecco's modification of Eagle medium (DMEM)/Ham's medium) assay were used to determine the fibroblast cell viability on iPB-1 surfaces. The cells were seeded at 2×10³ cells/well in 96-well plates and cultured in serum-free medium for 24 hours. At the incubation, the serum-free medium was removed. 100 µL of MTT with different concentrations were added into the medium. The cells were then incubated at 37 °C for four hours. To form the formazan precipitate, the medium was solubilized overnight by 20% sodium dodecyl sulfate (SDS) and 50% dimethyl formamide. The light absorbance of dissolved formazan was measured at 570 nm using a Power Wave HT spectrophotometer (Bio-Tek Instruments GmbH, Bad Friedrichshall, Germany).

4.4.2 Platelet adhesion on surfaces

The MD iPB-1, Spin coated isotactic polybutene-1 (SC iPB-1), and MD HDPE films were prepared as mentioned before. To fix the samples, PDMS was firstly coated on the clean coverslips. The PDMS blend was made from two components of a silicone elastomer kit (Sylgard 184 Silicone Elastomer Kit, Dow Corning, Midland, Michigan, USA). In this case, the base component was mixed with a thermally-sensitive crosslinking component in a ratio of 10:1 in a plastic vessel. The viscous mixture was mixed continuously in a polystyrene tumbler for 10 minutes until no more bubbles appeared. The finished mix was then spin-coated on the glass coverslips. For the spin coater, the settings for coating with iPB-1 were retained. The PDMS-coated coverslips were placed in an aluminum foil-covered glass vessel. A

heat treatment took place in a vacuumed oven at 120 °C for about two hours. They were then cooled in the oven for 12 h to room temperature and stored for later fixation of the films. The MD iPB-1 and MD HDPE films were then transferred to the PDMS/glass substrates.

The HPF solutions and the nanostructured surfaces were ready for experiments. A total of 105× samples were used for the tests: 35× SC iPB-1, 35× MD iPB-1, and 35× MD HDPE. Two different concentrations of protein solutions (0 mg/L as control and 1 mg/L) were used, as well as three different incubation times (5, 30, and 60 min) for the platelet concentrate-covered samples. The experiments were carried out for each parameter pair with five samples.

The platelet concentrate was purchased from the University Hospital Jena (Germany). The donor blood required for this was taken 48 hours before the start of the experiments. Twenty-four hours later, after checking for unacceptable residues and sources of infection, the blood was centrifuged. The buffy coats from a total of four donors were assembled into a platelet concentrate (2×10^{11} platelets per 250 mL). Then the concentrate was stored at 22 °C in constant motion.

1 mL of HPF solution was added to according films. After that, the samples were kept at 37 °C in the incubation cabinet for half an hour. Twenty samples per material were covered with one concentration at a time. Subsequently, the HPF solutions were removed, and the samples were rinsed with 1 mL of PBS. After that, all samples, including those without HPF pretreatment, were covered with 1 mL of the concentrate. After the incubation, the samples were placed in the incubation cabinet for 5, 30, and 60 min at 37 °C.

At the end of each time, the samples were rinsed twice with 1 mL of PBS. Subsequently, 25% glutaraldehyde solution (Sigma Aldrich, Schnelldorf, Germany) was diluted with PBS in 1:10. In each case, 1 mL of the resulting solution was added to the samples. The mixture was removed from the samples after 18 hours.

4.4.3 Platelets observation by optical microscope (OM) and scanning electron microscope (SEM)

The samples were examined after completion of the experiments for evaluation with the light microscope Leica DM2700M (Leica Mikrosysteme Vertrieb GmbH, Wetzlar, Germany) and with the Zeiss Auriga 60 SEM (Carl Zeiss Microscopy, Jena,

Germany). All data were expressed as the mean \pm standard deviation for n=5. Before the number and area percentage analysis, the LM and SEM images were transferred into 8-bit images. To further enhance the contrasts between background and platelet cells, the backgrounds of the images were subtracted via the "Subtract background" function with a rolling ball radius of 50.0 pixels. After that, the number of platelets on surfaces were analyzed through particle analysis function in ImageJ software (ImageJ 1.52i, 64-bit) on the binary (black and white) images. While the area percentage analysis was accomplished via the over/under threshold adjustment. Single factor analysis of variance (ANOVA) technique was used to assess the statistical significance of results between groups of platelet adhesion on nanostructured surfaces. The statistical analysis was performed with the software OriginPro (version 9.1G 64-bit) at a confidence level of 95%.

5

Results and Discussion

5.1 Nanocrystal Width Controlled Fibrinogen Assembly

Aiming at fabricating nanostructures approaching the dimension of HPF, different nanostructuring techniques were applied to the corresponding polymers. This section presents the (i) AFM analysis of the surface nanotopographies of pristine MD and SC films, and adsorption behavior of HPF molecules, as well as (ii) HPF adsorption kinetics by QCM-D.

5.1.1 Semicrystalline polymer thin films

To create chemically alike yet nanostructure distinct on polymer surfaces with topographical features smaller or comparable to the length of HPF molecule, iPB-1 thin films were fabricated by the MD and SC techniques. As shown in Fig. 14, the native surface of MD iPB-1 features a specifically arrangement of close-packed longitudinal NLCs, which are aligned parallel to the film drawing direction. The peak-to-peak distance between the NLCs is 27 ± 10 nm, where the width of the crystal is 22 ± 8 nm. The crystals protrude out of the interconnected amorphous regions of the film with an arithmetic average roughness of 2 ± 1 nm. As a result of strong shear forces, the iPB-1 polymer chains are packed parallel to major NLC axis, i.e., the film drawing direction.

On the contrary to MD iPB-1, the surface nanotopography of SC iPB-1 is composed of LCs (Fig. 15). The SC iPB-1 LCs have a lateral peak-to-peak distance of 62 ± 12 nm and a width of 50 ± 11 nm. The width of the LCs segments, highlighted by the dashed white lines on the enlarged LCs phase image in Fig. 15c, is 40 ± 10 nm. The crystals protrude out of the surfaces with an arithmetic average roughness of 4 ± 1 nm. In the study of Mellbring *et al.*, [285] sheaf-like crystals were observed in SC HDPE thin films with a thickness below 100 nm. The observed sheaf-like crystals in spherulites exhibited similar nanostructures as the LCs in SC iPB-1 (with a thickness of

72.2±15.1 nm) from this work. Meanwhile, the boundaries of the spherulites in the ultra-thin film were diffuse and not clear, different from the typical spherulite structures in thick films. Therefore, the formation of the LCs in SC iPB-1 might be attributed to higher secondary nucleation rate for edge-on crystals in contact with the substrate, analogous to sheaf-like crystals in SC HDPE.

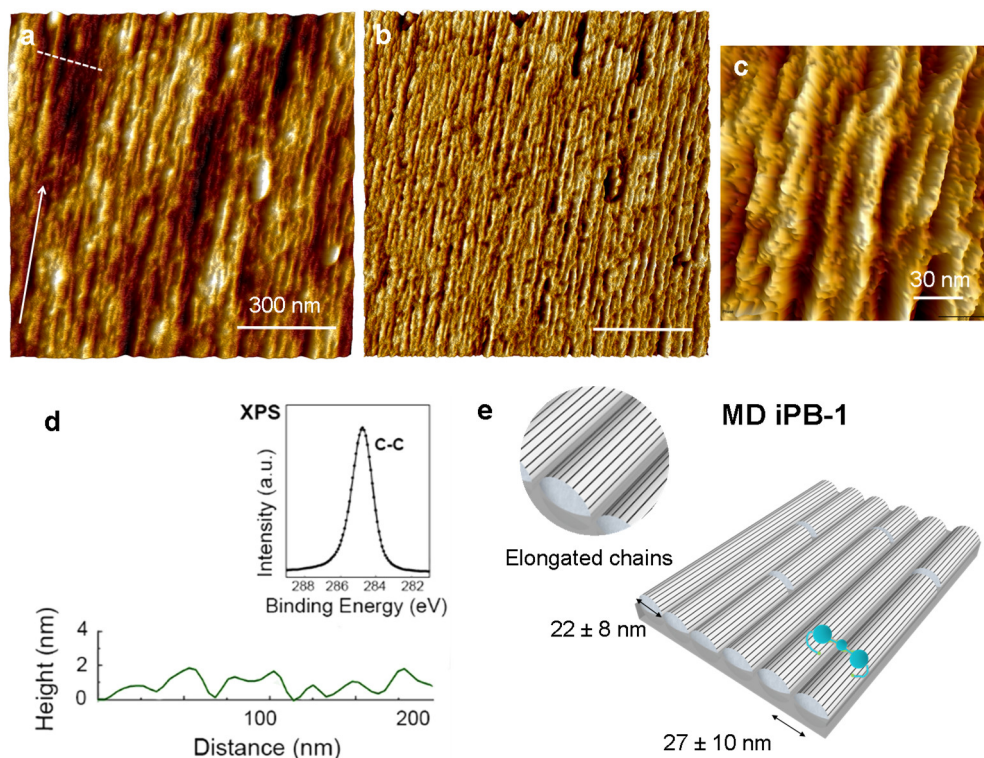


Figure 14. Surface topography of MD iPB-1 thin film. AFM (a) height, (b) phase images, and (c) enlarged phase image of the NLCs. (d) Height versus distance profile measured along the white dashed lines in height image as well as the C(1s) XPS spectrum. (e) Schematic illustration of the lateral dimensions of the NLCs, the arrangement of the polymer chains in the crystals, and their relation to the size of the single HPF molecule. Note, the two red balls and blue balls in the middle are D- and E-domains, respectively. The dark blue lines joining the domains are coiled chains of α , β , and γ chains. The dark blue lines outside of D-domains are α chains with sensitive ends.

To eliminate the possible effects of surface chemistry on the surfaces, XPS spectra was performed on the MD and SC iPB-1 surfaces. It is important to note that the C(1s) XPS spectra placed above the topography line profiles in Fig. 14 and 15 show no measurable differences in the surface chemistry between MD and SC iPB-1 surfaces. The similar chemical properties were also proved by the water contact angle of MD iPB-1 ($103.04 \pm 3.16^\circ$) and SC iPB-1 ($106.2 \pm 1.96^\circ$). The lateral dimension of the NLCs is smaller than the major axis of an HPF molecule, whereas the lateral dimension of the LCs corresponds to the length of the HPF molecules.

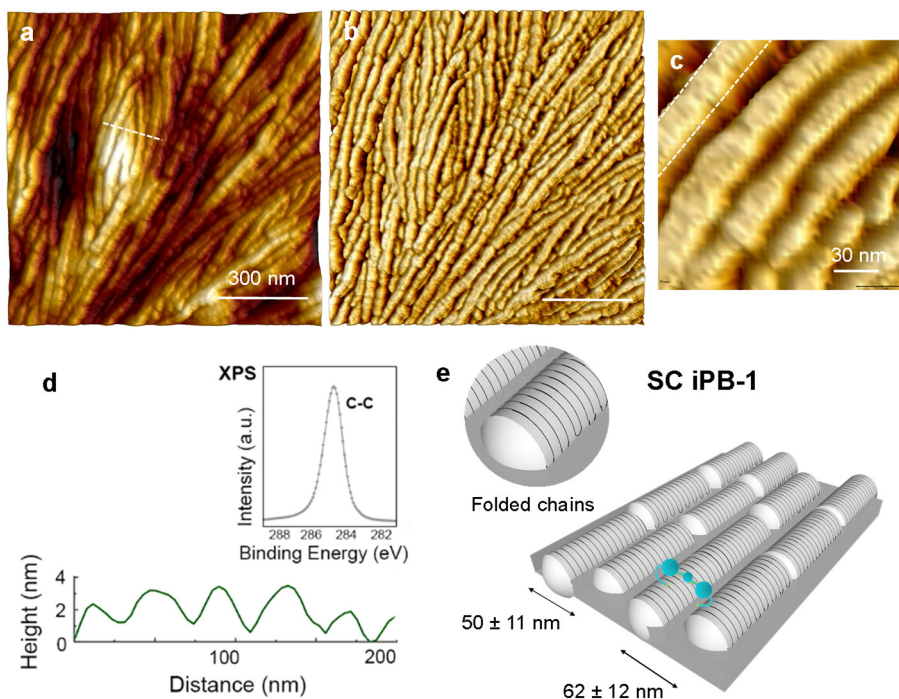


Figure 15. Surface topography of SC iPB-1 thin film. AFM (a) height, (b) phase images, and (c) enlarged phase image of the LCs (dashed white lines highlight the segmented structure of the LCs). (d) Height versus distance profiles measured along with the white dashed line in the height image as well as the C(1s) XPS spectrum. (e) Schematic illustration of the lateral dimensions of the LCs, the arrangement of the polymer chains in the crystals, and their relation to the size of the single HPF molecule.

The surface nanotopography of MD HDPE exhibits SKCs (Fig. 16), yet they have a more regular arrangement in comparison to LCs of SC iPB-1. The kebab crystals have a lateral peak-to-peak distance of 33 ± 9 nm, a width of 13 ± 2 nm, and are 100 ± 19 nm long. The major axis of the kebab crystals aligns perpendicular to the film drawing direction, i.e., lamellar crystals grow on the crystalline needle backbones, and protrude out of the surfaces with an arithmetic average roughness of 3 ± 1 nm. The HDPE chains orient parallel to the drawing direction. [114]

Different from LCs of SC iPB-1, the kebabs of MD HDPE exhibit higher length but lower width values. The larger length/width ratio (~ 10) leads to the unique morphologies on MD HDPE surfaces. Comparing to the protein, both the length and width of the HPF molecules are relatively smaller than those of MD HDPE kebabs. Moreover, the water contact angle of MD HDPE is measured to be $99.4 \pm 1.25^\circ$, indicating that MD HDPE is slightly more hydrophilic than MD iPB-1 ($103.04 \pm 3.16^\circ$) films.

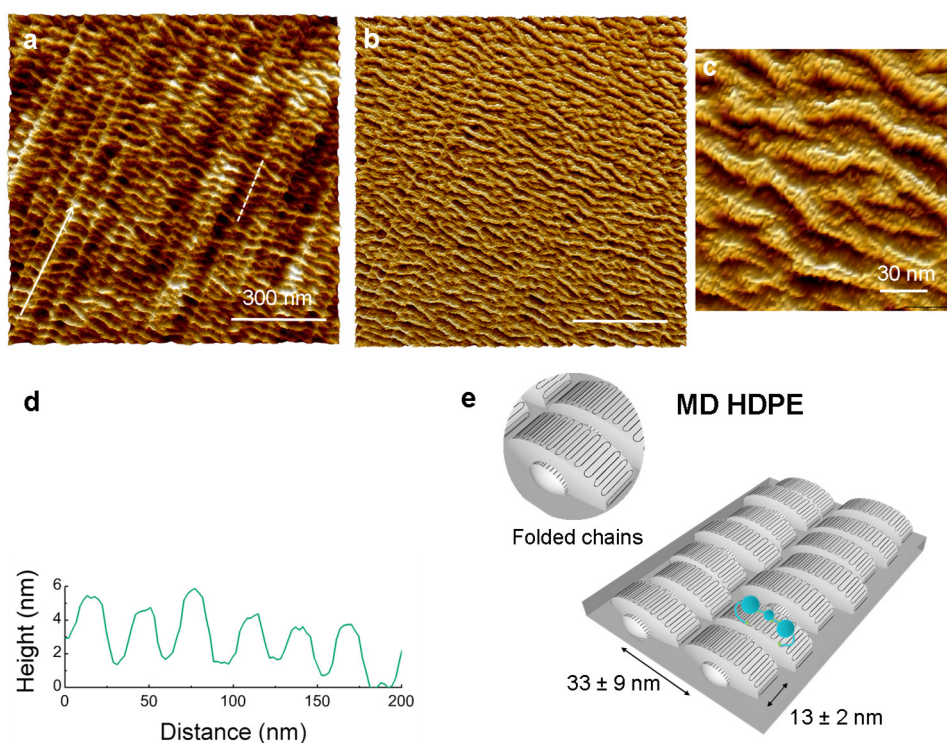


Figure 16. Surface topography of MD HDPE thin film. AFM (a) height, (b) phase images, and (c) enlarged phase image of the SKCs (dashed white grid highlights the segmented structure of the SKCs). (d) Height versus distance profiles measured along the white dashed lines inserted in the height images. (e) Schematic illustration of the lateral dimensions of the SKCs, the arrangement of the polymer chains in the crystals, and their relation to the length of the single HPF molecule.

5.1.2 HPF assembly on nanostructured polymers

To investigate protein-surface interactions and the assembly behavior of protein-protein associations, the nanostructured polymer surfaces were exposed to three HPF buffer concentrations, namely $0.0001 \text{ mg}\cdot\text{L}^{-1}$, $0.001 \text{ mg}\cdot\text{L}^{-1}$, and $1 \text{ mg}\cdot\text{L}^{-1}$. The height and phase images of a series of MD iPB-1 surfaces with NLCs after HPF adsorption are displayed in Fig. 17. For the ultra-low HPF concentration of $0.0001 \text{ mg}\cdot\text{L}^{-1}$, only star-like structures composed of several molecules can be seen. These structures are magnified and schemed in Fig. 17a and b.

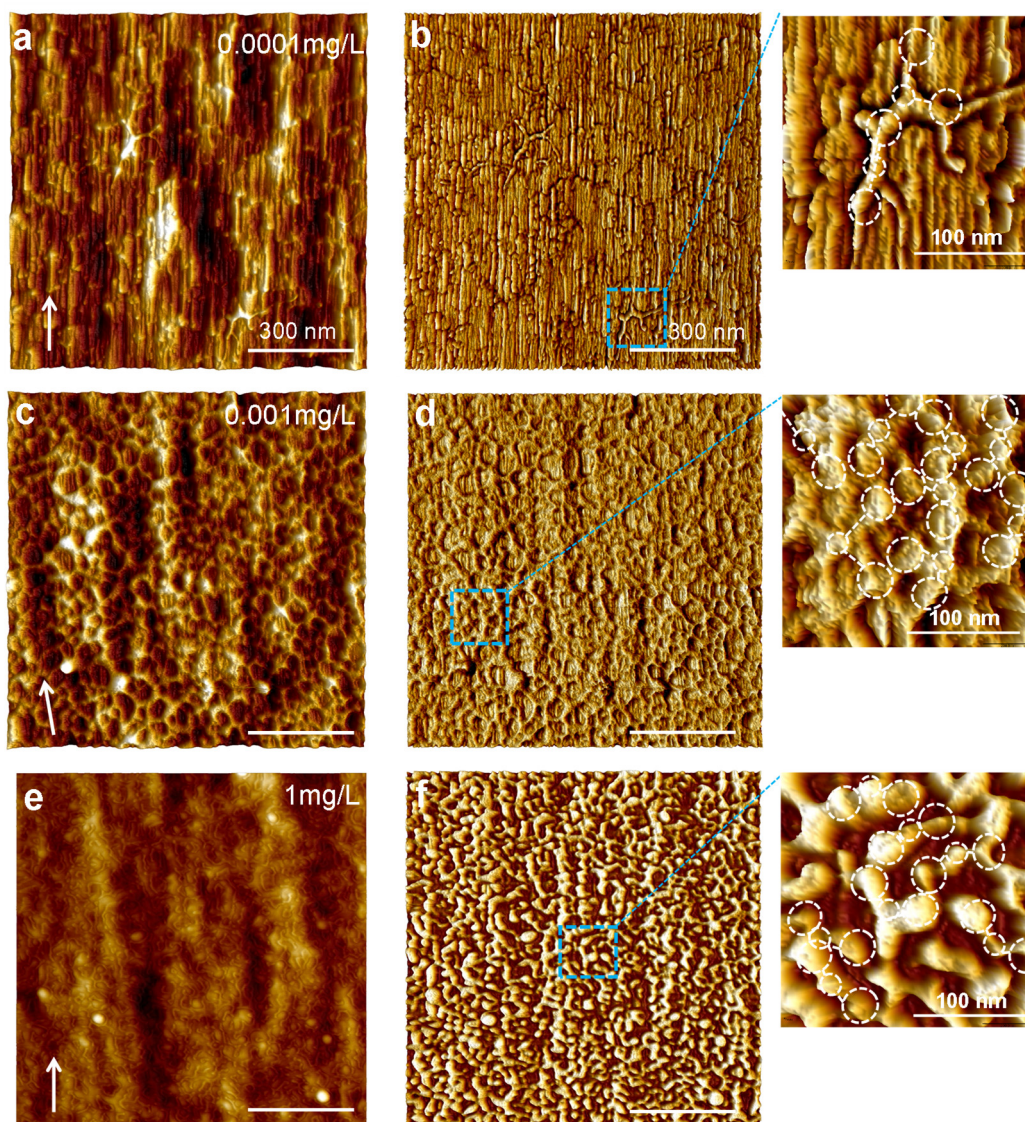


Figure 17. HPF assembly on MD iPB-1. AFM height (left) and phase (middle) images of HPF adsorbed on MD iPB-1 with different HPF concentrations: (a and b) $0.0001 \text{ mg}\cdot\text{L}^{-1}$, (c and d) $0.001 \text{ mg}\cdot\text{L}^{-1}$, and (e and f) $1 \text{ mg}\cdot\text{L}^{-1}$. The arrows indicate the film drawing direction. Magnifications of typical regions in the phase images are shown on the right side of AFM images. The sketches of HPF structures are shown on the corresponding magnified AFM images. The HPF molecules are sketched by the small dashed white circles in the middle (E-domain) and the two big dashed white circles at the ends (D-domains) and white linker lines (coiled-coil regions).

With increasing concentration ($0.001 \text{ mg}\cdot\text{L}^{-1}$), and thus increased protein-protein interaction, the proteins assembled into a network structure over the entire NLCs surface. The characteristic feature of this network is a ring-like network, termed by Sit and Marchant, [286] an “eyelet” structure, with protein-free, centered voids. Based on Fig. 17c and d, it can be assumed that three or more HPF molecules are partially involved in one “eyelet”. The extracted height of the HPF molecules within the network, $1.94\pm 0.84 \text{ nm}$, corresponds well to the reported dimensions of the

HPF molecule D and E domains, namely 2.9 ± 0.3 and 1.8 ± 0.3 nm, respectively. [287] It also confirms a single HPF layer of the “side-on” adsorbed molecules. Notably, the uniform “eyelet” network layer is similar to that on HOPG reported by Gettens *et al.* [282], as well as on MD UHMWPE surfaces. [116] Yet, on these surfaces, the “eyelet” network formed at much higher HPF concentrations, namely $5\text{ mg}\cdot\text{L}^{-1}$, compared to MD iPB-1. Furthermore, at the concentration of $1\text{ mg}\cdot\text{L}^{-1}$, the underlying structure of NLCs is not visible (Fig. 17e and f).

To show the HPF “eyelet” network in relation to the underlying NLC nanotopography, a zoomed AFM image was displayed in Fig. 18a and b. The zoomed AFM image shows that the “eyelets” can be structured by ellipses with different dimensions. It was found that the majority of the major axes are arranged parallel to the drawing direction, indicating the interactions between protein and NLCs on the surface. Since the protein “eyelet” consists of several HPF molecule domains, it can be speculated that the orientation of the “eyelet” originates from the arrangement of the proteins along the drawing direction, i.e., the NLC long axis.

To test this hypothesis, the orientation angles, θ , between the “eyelet” major axis and the drawing direction, are statistically analyzed and illustrated in Fig. 18b. Furthermore, the polar plot as a function of the “eyelet’s” major axis is performed to be the angle distribution. In the plot, $\theta=0^\circ$ and 90° correspond to the major axis of “eyelet” parallel and perpendicular to the drawing direction, respectively (Fig. 18c). From the plots, it can be found that the major axis of the “eyelets” mostly aligned parallel to the drawing direction. The orientation factor was calculated to be $f=0.82$ with Herman’s orientation function. [288] In the function, $f=1$ corresponds to a perfect uniaxial orientation to one direction, and $f=0$ corresponds to the random orientation.

Besides the “eyelet” orientation, their length distribution and the assembly structure of protein molecules are performed to provide more information on protein assembly behavior. The lengths of the “eyelet” major axis oriented parallel to the NLC nanostructure vary between 25 nm and 60 nm, shown in Fig. 18c.

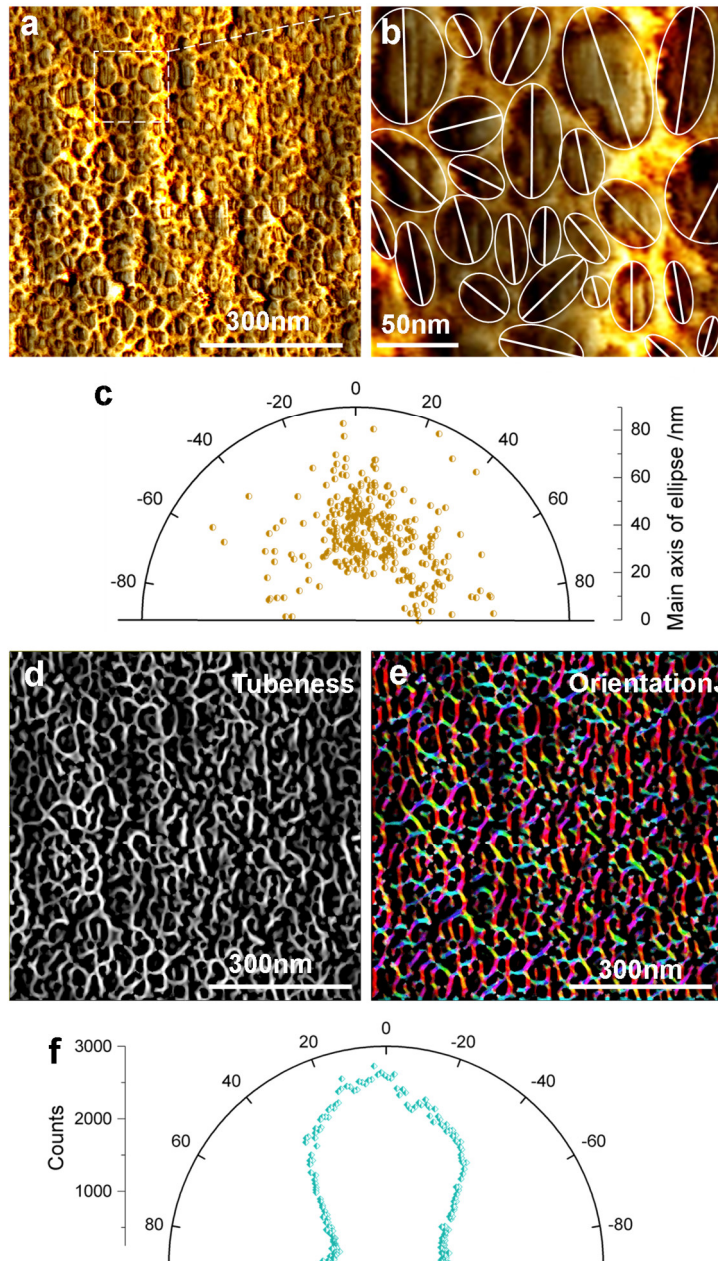


Figure 18. Quantitative analysis of HPF network assembly on MD iPB-1. (a,b) Overlaid height and phase image with HPF network and “eyelet” structure represented by solid ellipses. (c) Polar plot with the orientation angle, θ , distribution of “eyelets” major axis as a function of axis length and “single” HPF molecule. (d,e) Extracted HPF network and its color-coded orientation obtained with ImageJ. (f) Polar plot with the orientation angle, θ , distribution of “single” HPF molecule.

These measured lengths fall in the range of reported HPF molecule length, 53 ± 3.4 nm and analogous to the “eyelet” on MD UHMWPE film. [116] To be specific, an “eyelet” with two HPF proteins is 24 nm long, in which the proteins are touching each other at the D-domains at each end and having a 90° bend in the E-domain. This would be the smallest “eyelet” in the networks. Thus, observing that the

“eyelet’s” length distribution disappears below 25 nm, it can be assumed that more than two HPF molecules form the “eyelet” on the MD iPB-1 surface. In combination with the high aspect ratio of the eyelets’ major to the minor axis, 1.6 ± 0.1 , this indicates that the HPF end-to-end interaction and associated alignment.

Illustrating the “eyelet” orientation on the surface, one can shift the focus to examining the orientation of individual network segments. This information can be extracted from the local orientation of the protein network using 2D image processing analysis with ImageJ software (shown in Fig. 18d). By using the “Tubeness” plug-in, a clear image of the HPF network from the AFM height profile is extracted. The processed images are then analyzed by the OrientationJ plug-in, which is developed by Razakhaniha *et al.* [289] This plug-in allows evaluating the local orientation of every single pixel of the image. Therefore, the local orientation of the network structure can be visualized on the color-coded image presented in Fig. 18e. In the plot, the HPF molecules in the networks with the same orientation angles represent one color. And thus, the protein segments oriented parallel to the NLCs are processed in red color.

The distribution of the molecule’s orientation angle, θ , is presented on the polar plot (Fig. 18f). As shown by the black filled circles, the distribution peaks at $\theta\approx 0^\circ$, which points toward preferred alignment of the HPF molecules along the NLCs axis. Interestingly, the calculated Herman’s orientation factor, $f=0.61$ indicates a lower degree of orientation of “single” HPF molecules in comparison to the assembly structure of several molecules, i.e., “eyelets”. This discrepancy in orientation (factors) may be explained by the simplified assumption that the locally oriented network segment corresponds to a single HPF. Likely, a different local orientation is ascribed to the molecules shared by adjacent “eyelets”.

The observed orientations of the “eyelets” and “single” proteins indicate that the MD iPB-1 surface mediates the arrangement of HPF molecules into anisotropic network structures. The orientation mechanism can be proposed as (i) preferred adsorption of HPF molecules on crystalline regions compared to amorphous ones, [116] and (ii) the high aspect ratio (above 10) in combination with the low width of the lamellae crystals. Both factors induce an alignment along the NLC axis, whereas the small amorphous regions between the NLCs allow for interaction between the adjacent HPF molecules. For the high HPF concentration of $1\text{ mg}\cdot\text{L}^{-1}$,

the protein-protein interactions outweigh the topographical factor, and the network anisotropy disappears. The close-up in Fig. 17a shows that the “eyelet” network structure is still present, although with significantly smaller voids.

On the SC iPB-1 surface with LCs, the structures of isolated proteins and the overall HPF assembly are drastically different, displayed in Fig. 19. At ultra-low HPF concentration of $0.0001 \text{ mg}\cdot\text{L}^{-1}$ (Fig. 19a and b), a few HPF individual molecules with globular shapes can be seen on the surface. This globular structure indicates strong protein-surface interactions and feeble “end-to-end” protein-protein interactions. Whereas, the “end-to-end” interactions are characteristic for HPF molecules on the MD iPB-1 surface at the concentration of $0.001 \text{ mg}\cdot\text{L}^{-1}$ (Fig. 19c and d). Thus, the dominant HPF-LC interactions can be explained by the low aspect ratio of the LC, ~ 1 , which is contrary to the NLCs, may act as interaction barrier.

Apart from the aspect ratio, the surface curvature, K , is another important topographical features, distinguishing the MD and SC iPB-1 surfaces. The curvature in this work is defined as the geodesic curvature, whose curve is projected onto the tangent plane of nanocrystals. In comparison to NLCs on MD iPB-1 (tubular diameter of 22 nm, $K=0.09 \text{ nm}^{-1}$), the LCs on SC iPB-1 exhibit a diameter of 50 nm, displaying a twice smaller surface curvature ($K=0.04 \text{ nm}^{-1}$). Theoretical studies on HPF adsorption onto tubular structures, such as carbon nanofibers, with different curvature (width), have shown that protein adsorption increases with a decrease in the local curvature. [290] Another study, investigating HPF and human serum albumin (HSA) adsorption, suggested that the surface curvature modified the protein conformation upon binding. [180] That is to say, the surfaces with low surface curvature, such as particles with a diameter above 30 nm, facilitated the “end-on” conformation (section 4.1.2) of HPF on surfaces.

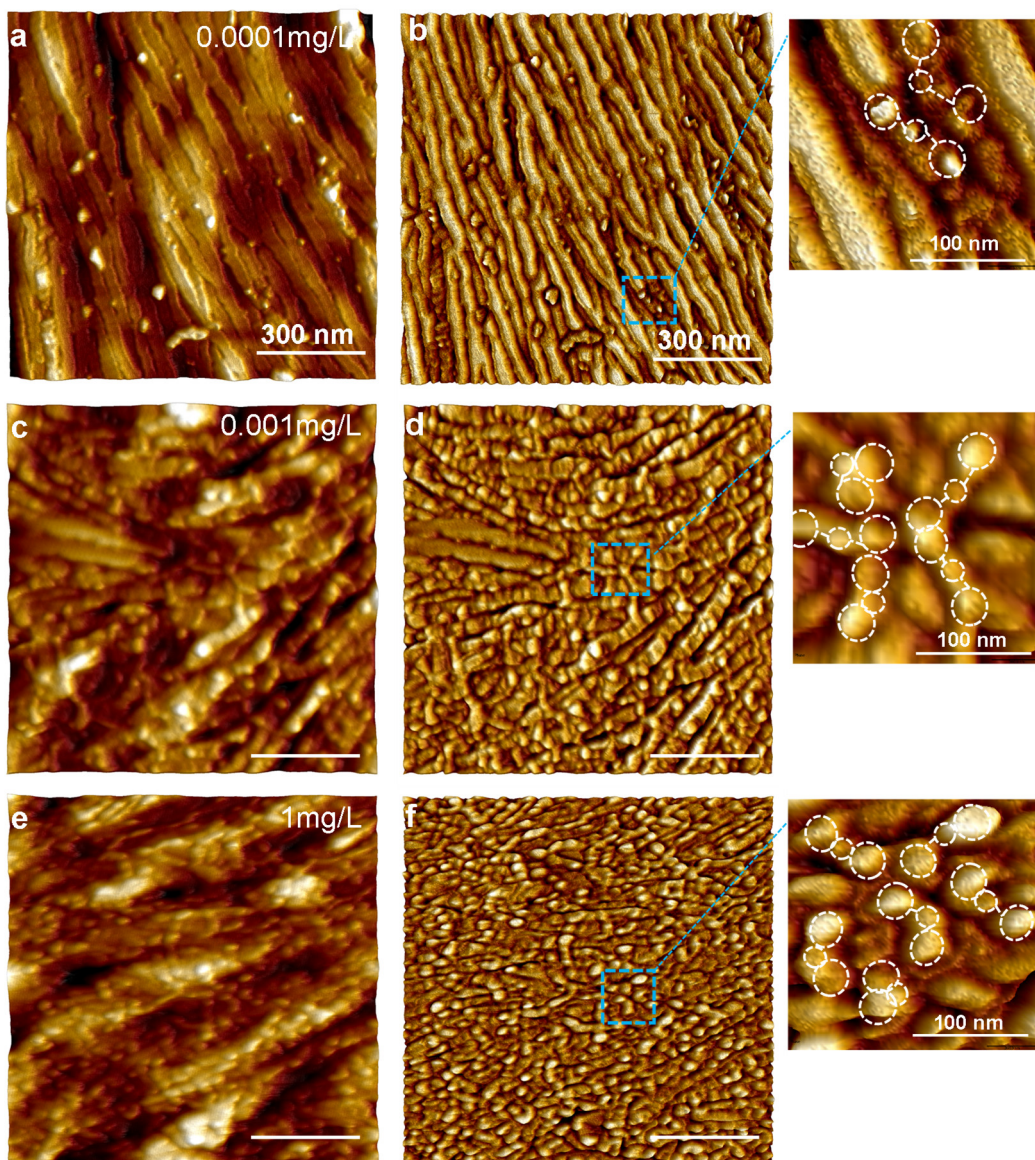


Figure 19. HPF assembly on SC iPB-1. AFM height and phase images ($1\ \mu\text{m}\times 1\ \mu\text{m}$) of HPF adsorbed on SC iPB-1 surface from PBS solution with different HPF concentrations: (a) 0.0001; (b) 0.001; and (c) $1\ \text{mg}\cdot\text{L}^{-1}$, respectively. The arrows indicate the drawing direction. Magnifications of typical regions in the phase images are shown on the right side of AFM images. The sketches of network structures of HPF molecules are shown under corresponding magnified AFM images. The sketches of HPF structures are shown on corresponding magnified AFM images. The HPF molecules are sketched by the small dashed white circles in the middle (E-domain) and the two big dashed white circles at the ends (D-domains) and white linker lines (coiled-coil regions).

The above studies suggest that HPF upon adsorption on LCs will not assemble into ordered network structures but instead will create a densely packed layer. The assumed high surface coverage is indeed well visible in Fig. 19e and f ($1\ \text{mg}\cdot\text{L}^{-1}$), where the underlying LCs structure is no more apparent. Based on these AFM

observations, it can be concluded that the LCs having a lateral size comparable to the HPF major axis, may promote “end-on” protein assembly.

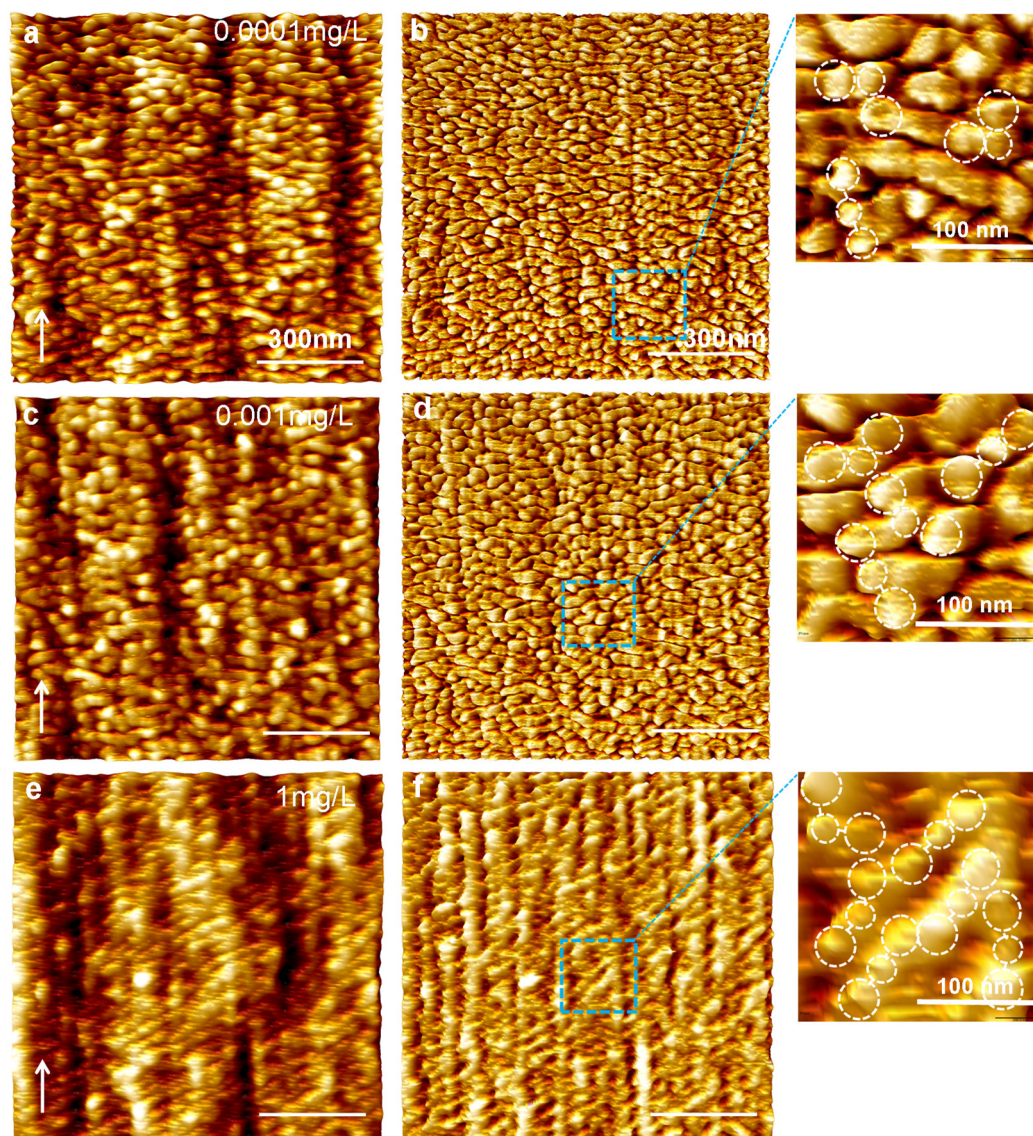


Figure 20. HPF assembly on MD HDPE. AFM height and phase images ($1\ \mu\text{m}\times 1\ \mu\text{m}$) of HPF adsorbed on MD HDPE from PBS solution with different HPF concentrations: (a,b) 0.0001; (c,d) 0.001; and (e,f) $1\ \text{mg}\cdot\text{L}^{-1}$, respectively. The arrows indicate the drawing directions. Magnifications of typical regions in the phase images are shown on the right side of AFM images. The sketches of HPF structures are shown on corresponding magnified AFM images. The HPF molecules are sketched by the small dashed white circles in the middle (E-domain) and the two big dashed white circles at the ends (D-domains) and white linker lines (coiled-coil regions).

Like MD iPB-1, MD HDPE was also considered as a model surface for protein adsorption behavior study. This is owing to its highly-oriented and well-defined nanostructures. Slightly different surface chemistry between nanostructured iPB-1

film surfaces and MD HDPE make the comparisons more difficult from a purely topographical point of view.

At an HPF concentration of $0.0001 \text{ mg}\cdot\text{L}^{-1}$ (Fig. 20a and b), HPF molecules can be seen on the MD HDPE surface. The underlying surface morphology is still visible. Similar to HPF molecules on MD iPB-1 and SC iPB-1, single HPF prefers to align along with the kebab crystals in the case of MD HDPE. At a concentration of $0.001 \text{ mg}\cdot\text{L}^{-1}$ (Fig. 20c and d), the surface is covered by HPF molecules, between which the connections are not visible. This indicates that the HPF molecules do not form networks, which is distinct from that on MD iPB-1 (uniform ring-like networks) and SC iPB-1 (star-like connections). At a concentration of $1 \text{ mg}\cdot\text{L}^{-1}$ (Fig. 20e and f), a dense HPF layer can be discerned on the surface. Notably, the HPF molecules form a layer on the kebab crystals. Comparing to the original surface structure, the nanotopography of the underlying shish is still visible.

5.1.3 HPF adsorption kinetics on nanostructured surfaces

Aiming at elucidating how the nanostructured surfaces modulate protein-surface interaction, the adsorption kinetics of HPF on nanostructured iPB-1 films were investigated using QCM-D. For this, the MD and SC iPB-1 films were directly attached to gold QCM electrodes (see Experimental Section 5.2.3). The HPF adsorption kinetics on MD HDPE thin films could not be performed, as the MD HDPE film could not be firmly attached to the QCM chip.

The changes of the resonance frequency (Δf) upon adsorption of HPF on MD and SC iPB-1 surfaces were displayed in Fig. 21a. For all concentration levels, the addition of HPF led to a decrease in the Δf over time, which reflects the increase in adsorbed protein mass on the surfaces. Thus, the appearance of a significant difference in Δf between MD and SC iPB-1 is attributed to a different amount of adsorbed proteins. As the HPF molecules fill the surface, the adsorption process slows down, reaching the adsorption saturation (plateau). The time needed to reach surface saturation depended mainly on protein concentration, and it occurred between 40 min and 2 h.

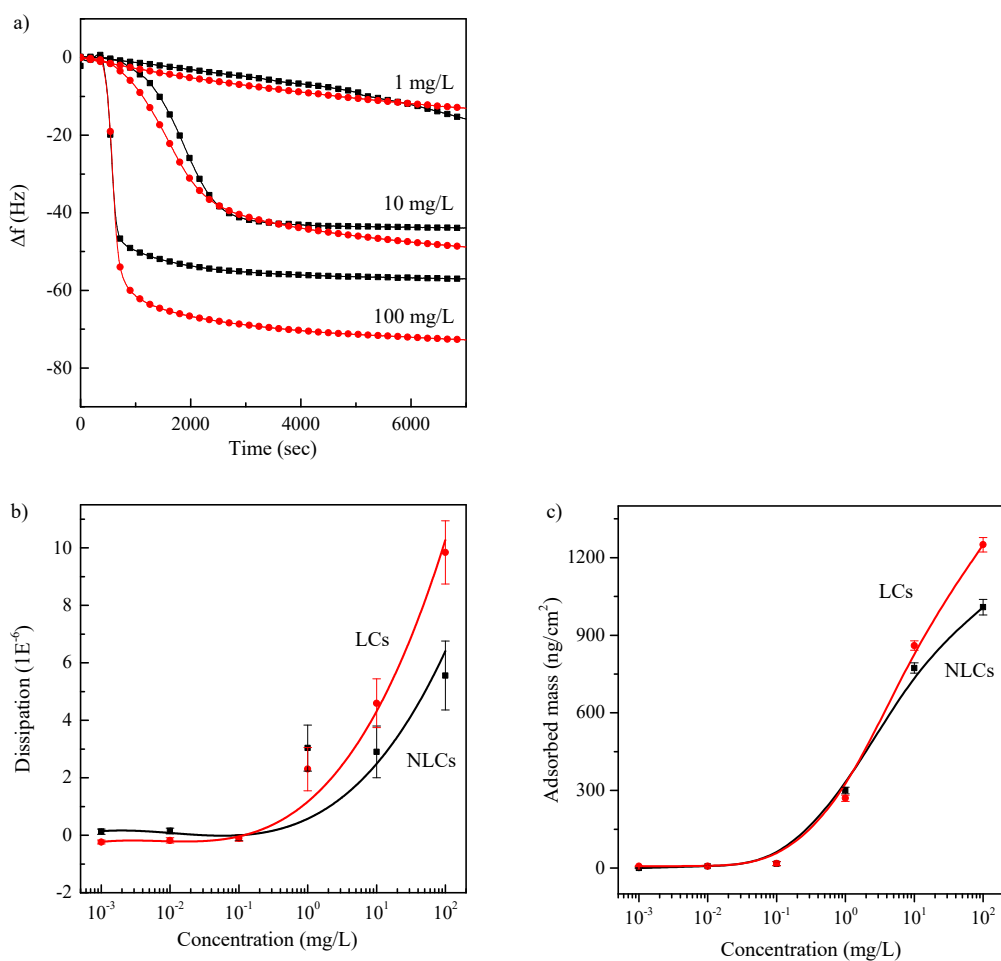


Figure 21. HPF adsorption kinetics on MD and SC iPB-1 thin films. (a) Typical Δf upon adsorption of HPF on MD iPB-1 (black square and line) and SC iPB-1 (red sphere and line) surfaces at the concentration of 1, 10, and 100 mg·L⁻¹. (b) The ΔD upon adsorption of HPF on MD and SC iPB-1 at various concentrations after two hours' adsorption time. (c) The average adsorbed mass of HPF on MD and SC iPB-1 surfaces at multiple concentrations.

Notably, at a concentration of 1 mg·L⁻¹, HPF adsorbed slowly on both films and reached no saturation within the measurement time. Interestingly, Δf for HPF on MD iPB-1 reached a plateau value (10 and 100 mg·L⁻¹) and stayed constant after approximately 50 min of exposure to the protein solution. Conversely, on SC iPB-1, HPF seems to adsorb more than that on MD iPB-1, which appears in a late stage small linear decrease of Δf (see data for 100 mg·L⁻¹). As is well known that, the HPF layer formation is mainly determined by the hydrophobic and electrostatic interactions. Since there is neither a difference in hydrophobicity (difference in the measured water contact angle below 3%) nor in surface chemistry (XPS spectra revealed no measurable changes), the increase in adsorption amount can be attributed to the distinct iPB-1 surface nanotopographies.

According to the observations, the Δf values being higher for SC iPB-1, it is proposed that (i) the surface diffusion of the molecules allows the rearrangement of the randomly adsorbed proteins into a more tightly packed layer, [189] (ii) the hydration of the layer increases, or (iii) a multilayer forms. The latter explanation can be validated by comparing the experimental mass with the theoretical mass of the protein monolayer. The mass of the adsorbed proteins can be obtained by converting the observed frequency shift to a mass uptake by the Sauerbrey equation (see section 5.2), while the validity of the latter depends on whether the adsorbed layer can be considered rigidly coupled to the iPB-1 modified QCM electrode (viscoelastic adsorbed layer will dampen the crystal's oscillation).

To distinguish the nature of the adsorbed layer from viscoelastic or rigid adsorbed protein layers, the ΔD profiles (Fig. 21b) are utilized to calculate the $\Delta D/(-\Delta f/n)$ dimensional ratio and compared to the $4 \times 10^{-7} \text{ Hz}^{-1}$ threshold suggested by Reviakine [274]. For both nanostructured films, the dimensional ratio falls in the range of $(3.2-7.6) \times 10^{-9} \text{ Hz}^{-1}$. Thus, the HPF layer can be considered to be rigidly coupled on the surface, and the Sauerbrey model is deemed to be valid for the samples under investigation.

The calculated mass uptakes, Δm , of HPF molecules on MD and SC iPB-1 as a function of concentration are shown in Fig. 21c. For the lowest HPF concentration, the adsorbed mass is close to zero. While an increase of Δm from 200 to 1300 $\text{ng}\cdot\text{cm}^{-2}$ is observed for the protein concentration in the range of 0.1-100 $\text{mg}\cdot\text{L}^{-1}$. On different surfaces, the adsorbed mass varies substantially. The overall adsorbed mass on the SC iPB-1 is higher, compared to that on MD iPB-1. The Δm difference between MD and SC iPB-1 varies between 12% and 25% for 10 and 100 $\text{mg}\cdot\text{L}^{-1}$, respectively. It is worth to note that the influence of a possible variation in film thickness on the adsorption of protein is negligible. [291] The combination of the results from QCM-D and AFM jointly indicate that the lateral dimensions of the iPB-1 nanostructures (nanocrystals) affect the adsorption behavior and arrangement of HPF molecules.

Table 2. QCM-D data analysis. Comparison between the experimentally determined mass of iPB-1 adsorbed HPF and theoretical protein surface coverage based on assumed HPF orientation and size (47.5 nm [3]).

iPB-1 film	Mass change Δm (ng·cm ⁻²)	Random sequential adsorption RSA (ng·cm ⁻²) “side-on” [1]	RSA (ng·cm ⁻²) “end-on” [1]	Ratio of dissipation change and frequency change $\Delta D/\Delta f$ (10 ⁻⁹ cm ² ·ng ⁻¹)
MD iPB-1	1009 ± 30			3.63
		210	1570	
SC iPB-1	1250 ± 28			3.05

* The results refer to samples with the HPF buffer concentration of 100 mg·L⁻¹.

To gain better understandings on the effect of the nanotopographies on HPF orientation, the experimental Δm was compared to the theoretical mass of the HPF monolayer. This theoretical mass is calculated by the RSA model and can distinguish HPF layer formation from mono- and multi-layer. [275, 276] The experimental mass and the theoretical values are summarized in Table 2. As was explained in the section 4.1.2, the orientation of HPF molecule on the surface can be classified into “side-on” and “end-on” orientations, depending on the arrangements of HPF major axis parallel or perpendicular to the surface. [292] Obviously, a higher protein area density in an adsorbed monolayer is possible with “end-on” orientation. As described by the RSA model, monolayer area densities with the “side-on” and “end-on” orientations are ranging from 210 to 1570 ng·cm⁻². [1, 275, 276] Based on the theory of Roach *et al.*, [6] the “end-on” orientation of HPF molecules after the initial adsorption stage would favor the adsorption of additional molecules because of increased hydrophobic interaction between HPF molecules aligned parallel to each other. In this work, the experimentally determined masses of adsorbed proteins on iPB-1 nanostructures at the HPF concentrations up to 100 mg·L⁻¹ are within this range (see Table 2).

On the MD iPB-1 surface, Δm for the protein concentration of 100 mg/L indicates that the adsorbed proteins preferred the “end-on” packing configuration. One should keep in mind that the mass value obtained via the measured frequency shift of the QCM also includes water in the protein adlayer, coupled via direct hydration

or water entrapped in cavities formed between and near the adsorbed proteins. [293, 294]

The information about the water content can be extracted from $\Delta D/\Delta f$, measured at saturation. [286] As shown in Table 2, the ratios demonstrate that notably more water is entrapped in the HPF layer on MD iPB-1 than that on SC iPB-1. Consequently, these findings reveal different assembly behaviors of HPF molecules, in which HPF molecules undergo distinct packing configurations upon interactions with nanotopographies. This effect is consistent with the one concluded from the AFM results. The overall observations provide more detailed information about how the studied nanostructures influence protein-surface interaction. Meanwhile, based on these results, the adsorption behavior of isolated HPF molecules, as well as assembly characteristic of several HPF molecules should be visible.

5.1.4 Conclusion

This section demonstrates that lateral variations in the nanoscale surface topography are essential contributors to dictate the protein conformation, orientation, and assembly structure. It was also shown that the effect of surface periodicity is compounded by variations in crystal lamellae aspect ratio and surface curvature. The surface topographies of MD and SC iPB-1 predominantly affected not only the adsorption amount but also the ensemble morphology of HPF assemblies. At the same HPF concentration, lower HPF molecule concentrations were needed to form a dense layer on the MD iPB-1 and, thus, resulting in decreased adsorption amount compared to the SC iPB-1 surface. Different from both iPB-1 surfaces, HPF formed a dense layer with no clear “eyelet” networks on MD HDPE. Overall, these findings support the first hypothesis, i.e., the physical factors, the width and curvature of polymer crystals on the nanostructured polymer surfaces, influence the HPF conformation change, ordered layer formation, and adsorption dynamics.

These findings indicate that the adsorption and assembly behaviors of the HPF depend significantly on the nanostructures. Meanwhile, the nanocrystal dimension is the relevant topographical parameter that modulates the adsorption processes. These observations enrich our knowledge of the role of the nanocrystal dimensions as a trending feature to design the biomaterial surfaces. Besides, the recognized

connections between the physical factors and protein adsorption may further direct the mediation of cellular behaviors via surface-induced protein assembly.

5.2 Anisotropic HPF Diffusion on Nanostructured Polymers

In the previous section, the HPF assemblies on nanostructured surfaces were observed directly under static conditions via AFM. The lack of direct observation of HPF assembly, as well as anisotropic HPF network formation on MD iPB-1, led us to hypothesize that the diffusion of single HPF molecules may facilitate the ordered protein layer formation on MD iPB-1. To test this hypothesis, the adsorption and diffusion dynamics of individual HPF molecules on nanostructured MD iPB-1 were investigated by AFM and MAPT. Permanently, MAPT was applied to obtain dynamic in-situ information about mean residence time, diffusion coefficient, and diffusion polarization of single HPF molecules on the iPB-1 NLCs surface. Additionally, the protein dynamics on MD iPB-1 were compared to HPF dynamic on MD HDPE.

5.2.1 Single HPF on nanostructured isotactic polybutene-1 (iPB-1)

The iPB-1 films were exposed to ultra-low (10^{-10} mg·L⁻¹) and highly concentrated (1 mg·L⁻¹) aqueous solutions of HPF molecules. The latter was chosen as a concentration at which HPF molecules are known to assemble into a compact protein layer (see section 6.1). The AFM phase images show time-dependent adsorption behavior of HPF molecules (Fig. 22).

The individual HPF molecules adsorbed on the nanostructured iPB-1 surface can be seen for the ultra-low HPF concentration, as shown in Fig. 22. After 2 minutes of adsorption, only a few HPF molecules with a trinodular conformation can be identified on the MD iPB-1 (Fig. 22a and b). After 10 minutes, multiple individual HPF molecules can be seen with the typical trinodular conformation on the MD iPB-1 (Fig. 22c and d). After 30 minutes of adsorption, in general, most of the three HPF domains (two D-domains and one E-domain in the middle) adsorb on the ridges of the NLCs (Fig. 22e and f). It can be assumed that the HPF molecules align along the NLCs, where three domains are in one straight line along the drawing direction for the ultra-low concentration case (10^{-10} mg·L⁻¹). The increasing amount of HPF molecules adsorbed parallel to the NLCs over time shows that the underlying nanostructure and adsorption time contribute to the single HPF molecules alignment on the NLCs. Alignment of single HPF molecules on nanostructured surfaces was also observed on MD UHMWPE and PS-*b*-PMMA block copolymers, presumably due to topographical and chemical confinement, respectively. [116,

188] This controlled protein adsorption on nanostructured polymer surfaces can be described in detail in the review of Firkowska-Boden *et al.* [9]

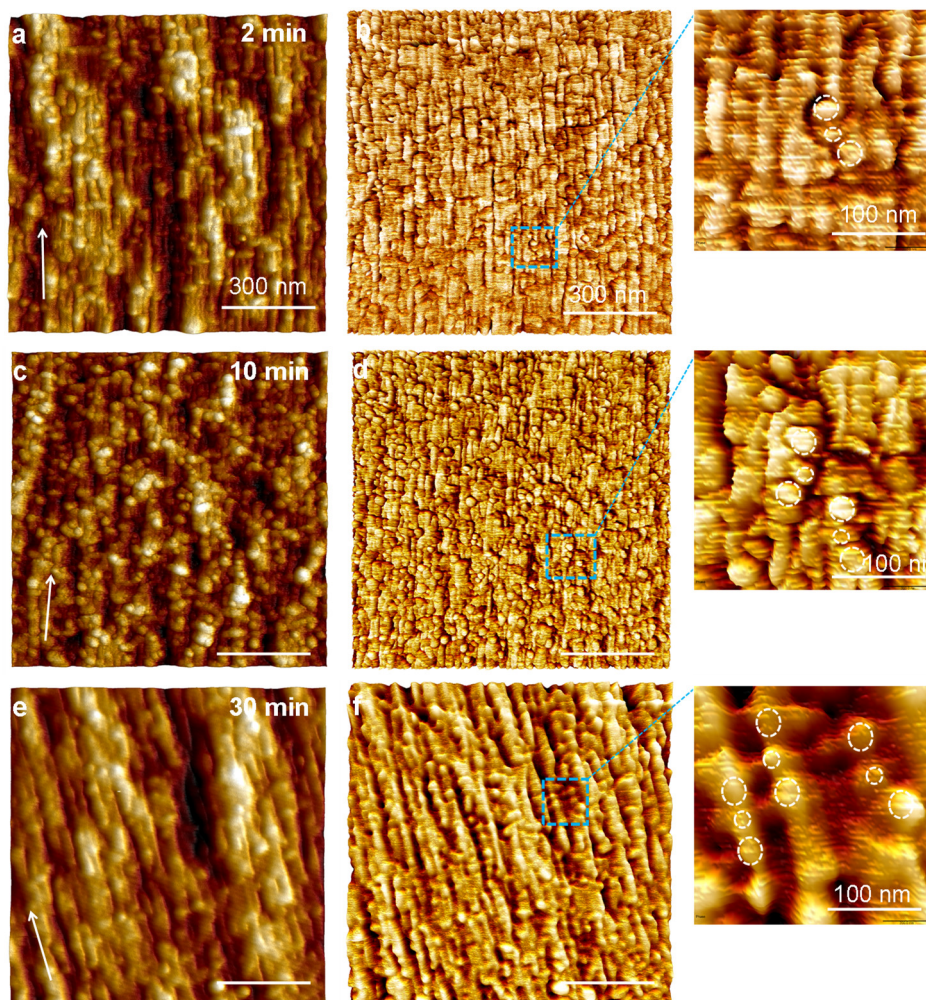


Figure 22. Single HPF observation on MD iPB-1. AFM height and phase images show HPF adsorption behavior on the MD iPB-1 after different adsorption times at an HPF concentration of 10^{-10} mg·L $^{-1}$, after (a,b) 2 min; (c,d) 10 min; and (e,f) 30 min, respectively. White arrows indicate the drawing direction. Magnified regions with characteristic features are shown below each large image. To the right of each magnified image, a model of adsorbed HPF is depicted.

Although the information from AFM provides direct evidence of HPF preferential adsorption on the crystalline parts of the MD iPB-1 film, namely on the NLCs, this static observation alone does not allow us to probe the adsorption and diffusion mechanism of this confinement on single HPF molecules. The inclusion of MAPT into the dynamic analysis is therefore critical to obtain a fundamental understanding of HPF molecules-NLC interactions and HPF layer formation.

5.2.2 Elongated structures of HPF trajectories

MAPT occupancy maps of single HPF molecules on MD iPB-1 at protein concentrations of 10^{-10} and $1 \text{ mg}\cdot\text{L}^{-1}$ are shown in Fig. 23. As described in the Experimental section 5.2.4, these maps were calculated by accumulating observations of at least 10^5 molecular trajectories and assigning observations to specific spatial locations (i.e., bins). The individual molecular trajectories were subjected to further analysis, whereby the mean residence time, diffusion, and polarization coefficients were calculated by computational analysis of these trajectories.

The overall occupancy maps for the two concentrations were shown in Fig. 23a and c. The zoomed maps (Fig. 23b and d) show representative surface occupancy maps (i.e., the density of observed HPF locations per area, time, and the bulk concentration of labeled HPF) on the MD iPB-1 exposed to 10^{-10} and $1 \text{ mg}\cdot\text{L}^{-1}$ HPF, respectively. The occupancy maps reveal specific high-occupancy areas (red color), which may result from one protein residing in the same area for significant time intervals or many HPF passing through that area (rear case).

The high-occupancy areas of MD iPB-1 at ultralow protein concentration represent a mix of compact features with a roughly circular shape and elongated structures. The latter are 2-3 μm in length and 100-250 nm in width and segmented into smaller regions along their length, as shown on the close-up in Fig. 23b (right image). These elongated structures suggest that the HPF molecules diffuse to relatively large distances on the NLC surfaces. Interestingly, the orientation of the elongated structures is perpendicular to the drawing direction of the film (i.e., perpendicular to the major axis of the NLCs), which points toward a preferential mobility direction of the HPF molecules. Similar elongated structures were observed by Kastantin *et al.* [207] on MD HDPE. These structures, in contrast with the structures recorded on MD iPB-1, were elongated parallel to the drawing direction of the MD HDPE film surfaces. Another striking difference between occupancy maps of MD iPB-1 and MD HDPE films is that high HPF concentration ($10 \text{ mg}\cdot\text{L}^{-1}$) is required for the appearance of the elongated structures on MD HDPE surfaces.

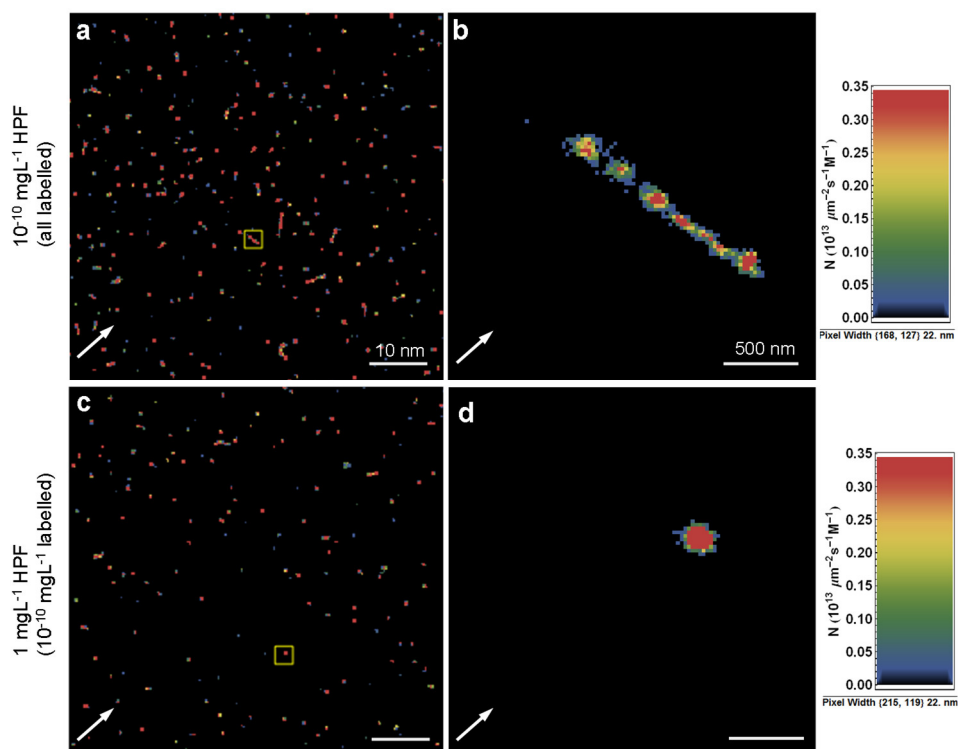


Figure 23. MAPT occupancy maps on MD iPB-1. Occupancy maps of MD iPB-1 surfaces exposed to (a) 10^{-10} $\text{mg}\cdot\text{L}^{-1}$ and (c) 1 $\text{mg}\cdot\text{L}^{-1}$ HPF concentration. White arrows indicate the alignment direction of the NLCs long axis. The representative images at each concentration are shown in the right panel (b,d). The red color corresponds to a high number of steps when HPF molecules diffuse. The concentration of labeled HPF molecules is the same, 10^{-10} $\text{mg}\cdot\text{L}^{-1}$, in (a,b) and (c,d).

From previous AFM characterizations of HPF adsorption onto MD UHMWPE, it is known that at this concentration, the HPF molecules form an ordered layer where HPF is confined in a single row on the crystalline lamellae. [116] Thus, it has been suggested that elongated structures of high-occupancy areas originate from an ordered protein layer formation. Here, the lack of HPF layer formation (Fig. 22a) for an ultralow protein concentration indicates that the pronounced HPF confinement and distinctive protein diffusion seem to be the dominant contributors to the elongated structures. The HPF diffusion on MD iPB-1 will be discussed further below in the section on direction-dependent diffusion.

A MAPT image of the MD iPB-1 film exposed to a high concentration of unlabeled HPF is shown in Fig. 23c and d. The concentration of labeled HPF is the same as in the ultra-low concentration experiments. Again, high occupancy areas are identified as isotropic features with the roughly circular shape, which are distinct from the anisotropic features (elongated trajectories) at ultra-low concentration. A possible explanation for the observation is: on the MD iPB-1 surfaces at 1 $\text{mg}\cdot\text{L}^{-1}$, HPF formed

a compact layer which hindered diffusion of single HPF molecules. This could be confirmed by the AFM study in section 5.1.1. At a high HPF concentration, i.e., $1 \text{ mg}\cdot\text{L}^{-1}$, protein molecules assembled into an ordered network. The diffusion of the HPF molecules within the protein layer was restricted due to enhanced protein-protein interactions. Similar isotropic features of HPF molecules have also been observed on MD HDPE surfaces at a high concentration of $10 \text{ mg}\cdot\text{L}^{-1}$. [116]

5.2.3 Mean residence time of HPF

To quantify the time of one HPF molecule residing on the surface, the images of residence times were performed and further processed into mean residence times. Figure 24a and c show the representative images of high and low occupancy areas, respectively. At the ultra-low concentration of $10^{-10} \text{ mg}\cdot\text{L}^{-1}$, in low occupancy area, images of residence times are multi-colored circular trajectories, representing a brief stay of HPF molecules on the surface. In the high occupancy area, the residence times of HPF molecules features mostly red-colored elongated trajectories, indicating that HPF molecules adsorb and desorb many times (hopping), and also diffuse in a long distance for a long time. [207]

The measured mean residence times are different for both concentrations. At ultra-low concentration, the mean residence time of trajectories in the low occupancy area was $0.3\pm 0.1 \text{ s}$. Similar mean residence times were observed for HPF on MD HDPE, bare fused silica, poly (ethylene glycol) and trimethylsilane surfaces. [207, 279] In contrast, most of the labeled HPF molecules reside on the surface for nearly $6.0\pm 2.2 \text{ s}$ in the high occupancy area, more than an order of magnitude longer than that in the low occupancy area. The longest residence time observed was 256.4 s in high occupancy areas. This mean residence time is also higher than that in the low occupancy area for HPF molecules on MD HDPE at 5×10^{-4} and $10 \text{ mg}\cdot\text{L}^{-1}$ (mean residence time $1.1\pm 5 \text{ s}$ and $1.4\pm 5 \text{ s}$, respectively). [207] The confinement of NLCs to HPF molecules plays an imperative role in higher mean residence time on MD iPB-1 surface. At ultra-low concentration, the protein-surface interaction is the major effect in the long residence time on the MD iPB-1 surface.

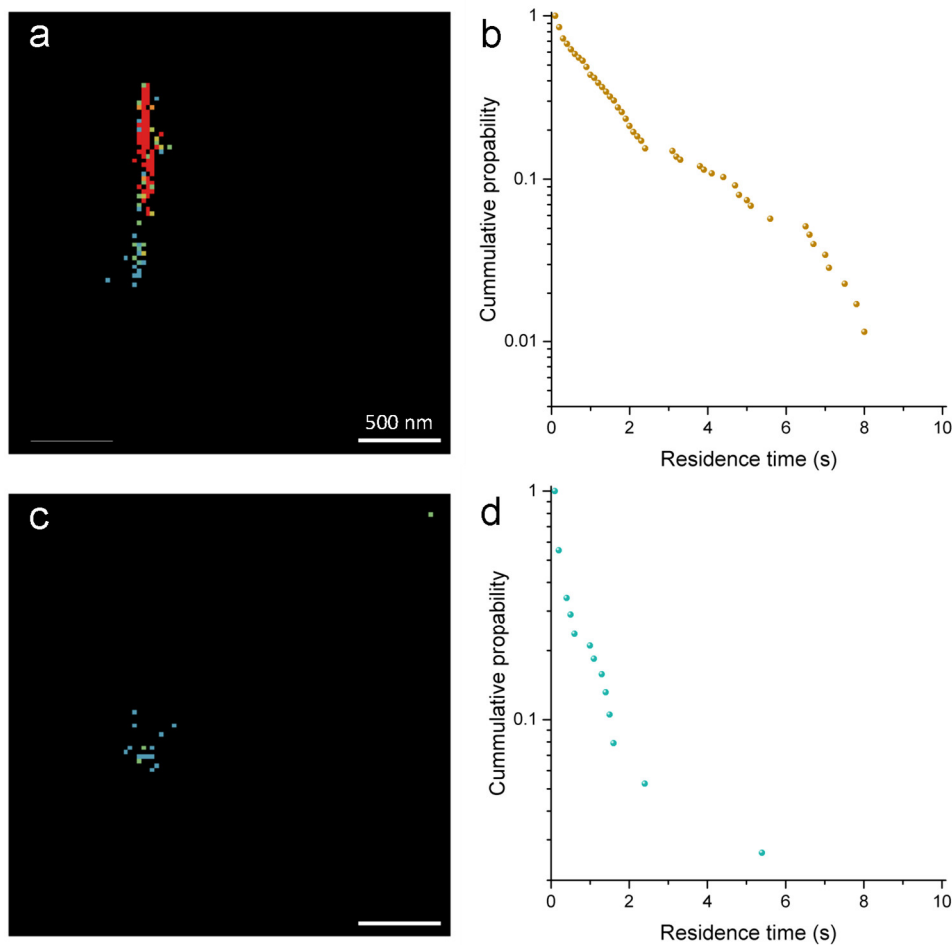


Figure 24. Residence time on MD iPB-1. Maps of (a) high and (c) low occupancy areas. (b) and (d) are the corresponding residence time values for high and low occupancy areas at the concentration of 10^{-10} mg·L⁻¹, respectively.

At high concentration, the mean residence time in the low occupancy area was 0.2 ± 0.1 s. While the mean residence time in the high occupancy area was 6.4 ± 3.0 s. The longest residence time observed was 230.9 s, equal to that at the ultra-low concentration in the high occupancy area. The long mean residence time of single HPF molecules on the MD iPB-1 surface could be attributed to protein-protein interactions, i.e., the non-covalent linkages (D-E contact and α C domain) and formation of an HPF layer.

5.2.4 Anisotropic diffusion of HPF

The diffusion polarization and coefficients are extracted from the trajectory maps to describe the diffusion direction of the HPF molecules. The individual diffusive motions of the labeled HPF molecules were separated into parallel (D_{\parallel}) and vertical motions (D_{\perp}) about the MD iPB-1 film drawing direction. The diffusion polarization (P) was calculated as $P = (D_{\parallel} - D_{\perp}) / (D_{\parallel} + D_{\perp})$. Thus, a positive (or negative) value of P

represented preferential diffusion parallel (or perpendicular) to the NLC major axis. The two-dimensional diffusion coefficient (D) was calculated as $D_{\text{MAPT}}=(D_{\parallel}+D_{\perp})/2$ on the whole trajectories. [207]

The D and P values are shown in Fig. 25, which are calculated by D_{\parallel} and D_{\perp} . The directionality of HPF diffusion was indicated by the P value, which was in the range of -1 to 1. High positive P values reflect the fast diffusion of HPF molecules along the NLC major axis (drawing direction). [207] Interestingly, the measured P values were negative, indicating that HPF molecules diffused faster perpendicular to the drawing direction. The P value at the ultra-low HPF concentration (-0.219 ± 0.09) was higher than that at higher concentration (-0.067 ± 0.04). This was due to i) the rapid perpendicular diffusion of HPF molecules perpendicular to the drawing direction; and ii) the relatively low D_{MAPT} value of HPF molecules at high concentration. Thus, for ultra-low concentrations, the nanostructure of MD iPB-1 influenced the HPF diffusion. Interestingly, the HPF diffusion on MD iPB-1 is distinct from that on MD HDPE. [207] At ultra-low concentration, the P values of HPF molecules approached zero. Therefore, the authors stated that nanostructured HDPE alone has a minor effect on the HPF diffusion direction, and the ordered layer formation is the major determinant in diffusive motion. [207] The results presented here strongly indicate that the nanostructured MD iPB-1 surface has a notable influence on HPF diffusion direction at an ultra-low concentration (single HPF level) indeed.

The coefficient D_{MAPT} is informative to provide the direction-independent diffusion behavior of single HPF molecules on MD iPB-1 thin films. The D_{MAPT} value at ultra-low concentrations ($0.074\pm 0.020 \mu\text{m}^2\cdot\text{s}^{-1}$) was significantly higher than that at high concentration ($0.028\pm 0.025 \mu\text{m}^2\cdot\text{s}^{-1}$), indicating that HPF molecules diffused faster when there were more space and fewer protein-protein interactions. The values at the ultra-low concentration are smaller than that on MD HDPE at $5\times 10^{-4} \text{mg}\cdot\text{L}^{-1}$ by a factor of 1.5, which could be attributed to the higher attraction of NLCs to HPF molecules. In contrast, the D values at the high concentration were similar to those on MD HDPE at $10 \text{mg}\cdot\text{L}^{-1}$, suggesting HPF layer formation. [207]

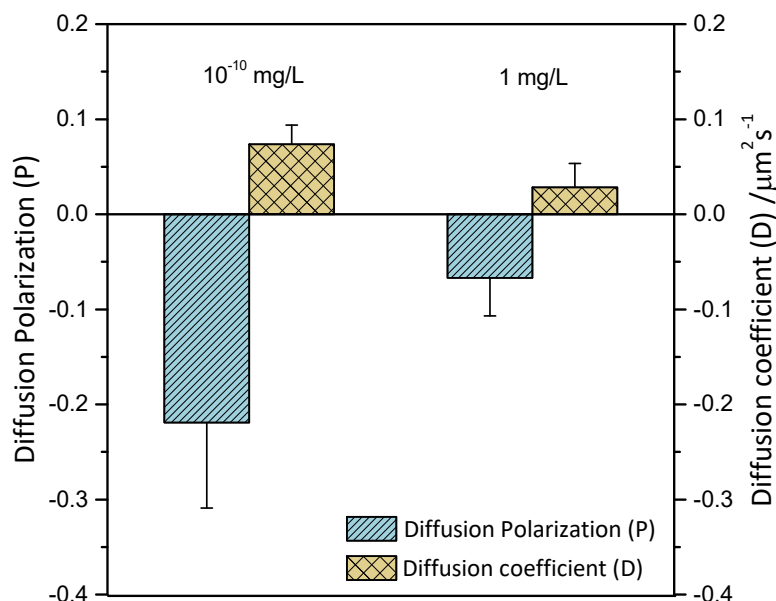


Figure 25. Diffusion coefficients and polarizations of HPF on MD iPB-1. D_{MAPT} and P of HPF molecules at 10^{-10} and $1 \text{ mg}\cdot\text{L}^{-1}$. The diffusion coefficients indicate the direction-independent HPF diffusion. Whereas, the diffusion polarizations display the anisotropic diffusion of HPF on the polymer surface.

It was assumed that subtle variations in chemical and topographical properties between MD iPB-1 and MD HDPE could lead to different HPF adsorption and diffusion behaviors. Chemically, the weak inductive effect of ethyl groups to iPB-1 chains, which results from the ethyl group on the central carbon backbone, leads to a slightly electropositive surface. [18] HPF molecules exhibit a negative net charge under physiological conditions [284], which will be selectively attracted on the iPB-1 surfaces. This can be used to explain the high amount of HPF assembly on the MD iPB-1 surface at the ultra-low concentration of $10^{-10} \text{ mg}\cdot\text{L}^{-1}$. The topographical effect of the two surfaces will take over the slight chemical difference and become the main influencing factor for HPF diffusion direction.

The topographical property mainly reflects on two aspects: surface friction property and topographical confinement. To explore the possibilities of the connections between surface frictional behavior and single HPF diffusion behavior, both the MD iPB-1 and MD HDPE surfaces were measured against SiO_2 colloidal probe using AFM under series of loads, 10-50 nN. The friction force on MD iPB-1 in 0° (the drawing direction), 45° (45° to the drawing direction), and 90° (perpendicular to the drawing direction) under 10 nN loads were 1.10 ± 0.05 , 1.31 ± 0.22 , and 1.75 ± 0.26 with arbitrary units, respectively. The lateral force

directions are shown in Fig. 26. The friction force on MD HDPE at 0°, 45°, and 90° directions were 0.77 ± 0.09 , 1.08 ± 0.05 , and 1.33 ± 0.23 with arbitrary units, respectively. This arbitrary unit came from the unknown torsional spring constants.

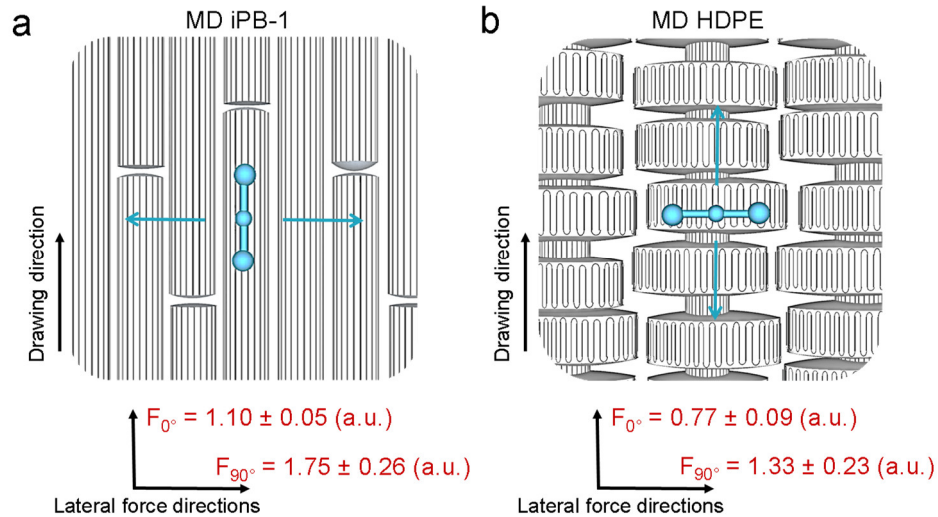


Figure 26. Surface diffusion directions on MD iPB-1 and MD HDPE. The illustration of HPF molecules diffusing on the (a) MD iPB-1 and (b) MD HDPE surfaces. The cyan cylinders represent the (a) NLCs on the MD iPB-1 and (b) SKCs on the MD HDPE surfaces. The black lines on the cylinders represent the chain direction in the crystals which are parallel to the drawing direction. The blue-colored three spheres jointed in a line are illustrated as the single HPF molecule with its typical trinodular shape. The blue arrows represent the preferred diffusion direction of HPF molecules. The coordinates below the sketches show the lateral force directions, 0° (in the drawing direction) and 90° (perpendicular to the drawing direction) on both surfaces.

On both surfaces, the friction forces increased linearly with the increasing loading forces, whose tendency was similar to that between various AFM probes and polymer surfaces. [295] The results show that friction forces on MD iPB-1 are higher over the whole load range from 10 to 50 nN comparing to that on MD HDPE under dry conditions by a factor of around 1.2. It is interesting to notice that, the friction forces in 0° (the drawing direction) on both MD iPB-1 and MD HDPE surfaces were always found the lowest compared to the other directions.

To identify the connection between friction force and HPF diffusion direction, the low friction force directions to the HPF diffusion direction were compared on both surfaces. For MD iPB-1, the preferred HPF diffusion direction is perpendicular to the drawing direction, which is the higher friction force direction. For MD HDPE, the preferred HPF diffusion direction is equal to the lower friction force direction. It can be concluded that the significant variations between the directions indicate

that the HPF molecular diffusion seems to be less influenced by the friction force. Therefore, the topographical confinement of the nanostructured surfaces to the HPF molecules will be taken into account as the significant factor for directionality of the HPF diffusion.

The variation of friction (friction force measured at normal force $F_N=10$ nN) concerning crystalline area orientation is finally compared to the HPF-preferred diffusion directions for both surfaces (see Fig. 26). Interestingly, the preferred HPF diffusion direction on MD iPB-1 surface corresponds to the direction with the highest friction. In contrast, the preferred HPF diffusion direction on MD HDPE is equal to the lowest friction direction. From the MAPT and AFM friction measurement results, it can be concluded that HPF nanoconfined in the crystalline regions of the nanostructured surfaces diffuses perpendicular to its major axis independent of the anisotropic friction characteristics of the surface.

One proposed explanation for the preferential HPF diffusion perpendicular to its major axis is the conformational flexibility of the molecule in the coiled-coil regions facilitated by the two hinges (Fig. 27). [296] According to molecular dynamic simulations of HPF, the existence of the two hinges provides high bending motions of the coiled-coil regions without resulting in noticeable conformational changes to the rest of the molecule. [141] From this perspective, HPF molecules resemble the running mode of the Sansetsukon, an ancient Asian weapon, which consists of three wooden staffs connected with a flexible rope. With the observation of the preferred diffusion of HPF perpendicular to the major axis of the needle crystals (evident from Fig. 23) and considering the intramolecular flexibility structure of HPF molecules, an assumption can be deduced. Namely, the Sansetsukon-like nanocrawling diffusion (partial detachment) perpendicular to the major axis of the topographically confined HPF molecules is supported by the bending motions at the hinges of the HPF molecule.

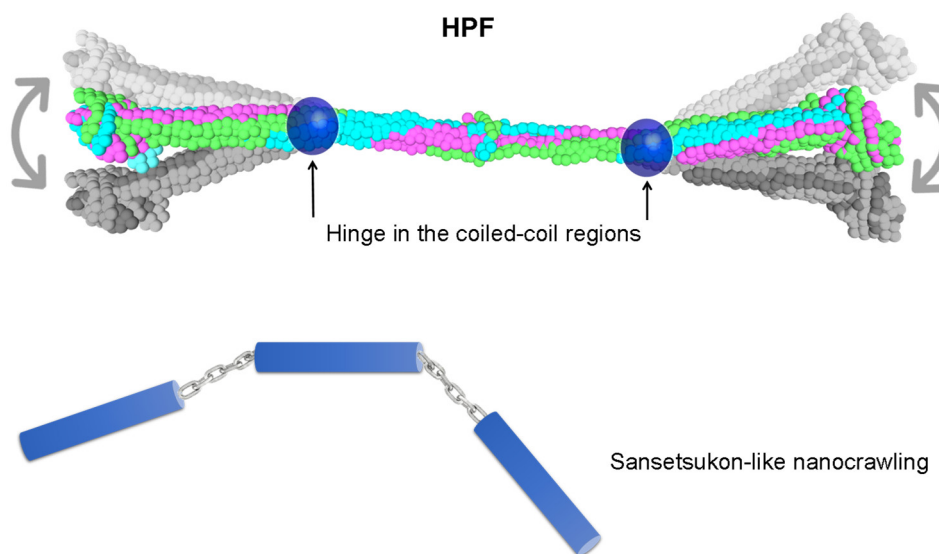


Figure 27. Sansetsukon-like nanocrawling. The schematic drawing of the HPF molecule with the marked hinge in the coiled-coil regions, which are related with the bending twisting of the adsorbed HPF molecule, similar to sansetsukon. Dark and light grey drawings are the bent molecule after the original blue drawing of HPF molecule.

Diffusion along the major axis of the crystals accompanying with the HPF motions by minor axis would require considerable stretching/contraction of the HPF molecules, which would lead to conformational changes of the entire molecule. This assumption is supported by recent studies of HPF adsorption on nanostructured diblock copolymer surfaces. [237, 297] Owing to the chemical heterogeneity of the polymeric blocks, negligible surface diffusion of HPF along the structure major axis and HPF minor axis was observed. Based on this unique direction-dependent diffusion of HPF on MD iPB-1 (Fig. 27), a flying diffusion mechanism and thus complete protein detachment can be ruled out from the elucidations. Meanwhile, it can be assumed that such diffusion mechanism would reduce the barrier to protein diffusion along the NLCs, resulting in isotropic diffusion. Also, a rolling diffusion mechanism, i.e., HPF molecule rolling along its minor axis toward the adjacent crystal surfaces would likely be sterically hindered by the β C and γ C nodules in the D-domains. [298] The applicability of nanostructured surfaces in creating functional biomaterials can be demonstrated by this anisotropic diffusion nature of HPF molecules observed on chemically alike yet topographically different polymeric surfaces. For instance, the unidirectional nanoconfinement of HPF and its anisotropic mobility may be practical for lowering friction and improving the wear resistance of polymeric joint implants. [299]

5.2.5 Conclusion

In this section, direct insight into single protein dynamics using MAPT allowed to reveal the anisotropic diffusion of HPF on nanostructured MD iPB-1 surfaces. Notably, this anisotropic diffusion was dominated by the confinement of NLCs and HPF layer formation on MD iPB-1 surfaces. At ultra-low concentration, the single HPF molecules preferably diffused along the minor axis of the NLCs, i.e., perpendicularly to the drawing direction. This indicates that MD iPB-1 has a significant effect on the direction of HPF diffusion at ultra-low HPF concentration. Similarly, the single HPF molecules prone to diffuse along the minor axis of SKCs on MD HDPE surface. This mechanism is based on the intrinsic flexibility of HPF in the coiled-coil regions. These observations support the second hypothesis of this thesis, namely, the highly-oriented nanostructures on the MD iPB-1 surfaces mediate the alignment and anisotropic diffusion of a single HPF molecule. It can also be concluded that nanostructured surfaces that encourage this characteristic surface mobility are more likely to lead to the formation of ordered protein assemblies and may be useful for advanced biomaterials. Therefore, the further question lies in how the subsequent biological responses mediated by the nanostructures and the surface-immobilized protein molecules are.

Based on these results, it is believed that the nanostructured polymer surfaces, providing both nanoconfinement and highly-oriented surface arrangement to protein molecules, are prone to result in ordered protein layers. These observations may function as a reference template for other nanostructured surfaces, including nonpolymeric materials. At the same time, the gained knowledge can inspire more work on protein-mediated surface-cell interactions, which have been long-time neglected. From a practical view, these understandings may contribute to the development of innovative biomaterials and biosensor fabrications.

5.3 Cell Adhesion on Nanostructured Polymers

In the previous chapters, the nanostructures of iPB-1 and HDPE were found to be able to mediate the HPF conformational changes. Therefore, it can be assumed that the influenced conformations of HPF may lead to various exposed binding sites and affect the subsequent platelet's adhesion and activation. Based on this hypothesis, the cytotoxicity of the polymeric surfaces was first evaluated. Then the platelets adhesion behaviors on HPF-adsorbed MD iPB-1, SC iPB-1, and MD HDPE thin films were investigated. Consequently, the morphologies of the platelets were characterized by SEM.

5.3.1 Fibroblast cell viability on nanostructured surfaces

The MTT assay, a colorimetric assay, is commonly used to evaluate the effects of different materials on cell viability. The MTT reagent, a 3-(4,5-dimethylthiazol-2-yl)-2,5-diphenyltetrazolium bromide salt, can be reduced by cellular oxidoreductase enzymes from tetrazolium dye to insoluble dark blue formazan, shown in Fig. 28a. Therefore, the concentration of formazan can reflect the existence of the living cells.

Generally, the MTT assay of fibroblast cells gives a linear relationship between optical density (OD, 590 nm) of formazan and number of cells, shown in Fig. 28b. This direct relationship will be the standard curve for counting the cell numbers, which are cultured with samples. In this standard curve, the higher the OD value is, the more living cells present in the culture medium.

The OD values of formazan, shown in Fig. 28c, demonstrate the viable cell numbers on MD and SC iPB-1 films, which are pre-adsorbed by HPF at the concentration of 0 and 1 mg·L⁻¹, respectively. All the OD values for the nanostructured iPB-1 films are higher than that for the control sample (PS), indicating the good biocompatibilities of these films. Besides, the fibroblasts cultured on MD iPB-1 films with and without HPF layers exhibit slightly lower cell viability than that on SC iPB-1 films. This suggests that SC iPB-1 films have a positive effect on fibroblast cell viability, compared to MD iPB-1 films. It needs to be clarified that, as HDPE is a well-known biomaterial, its excellent cell viability via MTT assay is confirmed and fully evaluated in other works. [300, 301]

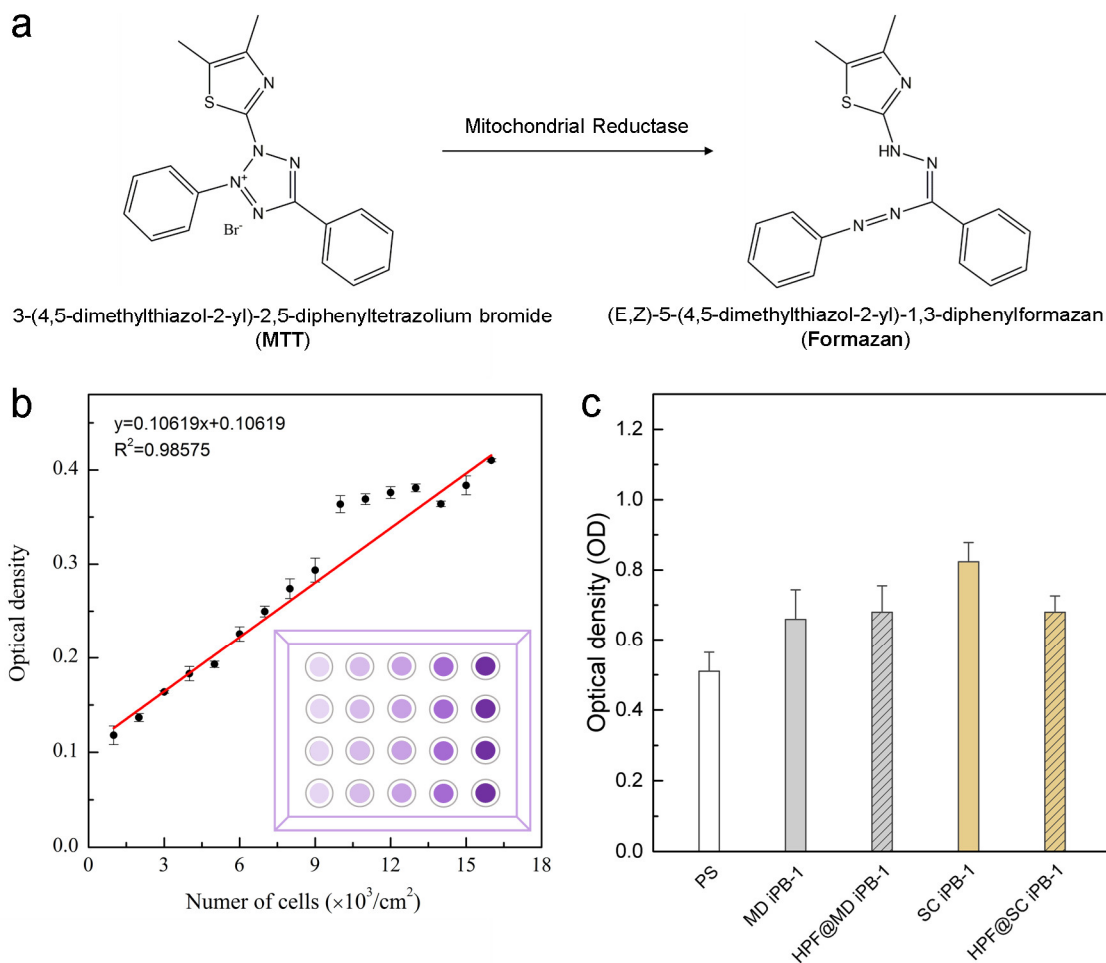


Figure 28. MTT assay of fibroblasts on MD and SC iPB-1. a) The principle of MTT assay; b) standard curve of MTT assay; and c) optical density of different substrates, MD iPB-1 and SC iPB-1 with and without HPF pretreatment.

5.3.2 Platelet morphologies on a smooth surface

The anucleate platelets, which are generated from megakaryocytes in the bone marrow and with the function as major actors in coagulation, contain a number of surface receptors, adhesion molecules, and granules. Platelets keep in the inactivated (or "resting", R) state, retaining a plump, discoid shape, in the circulation system. [302] Upon activation through multiple pathways, the morphologies of the inactivated platelets are changed, and the granules in the platelet cells are released. [222] The HPF molecules bind to the GPIIb/IIIa receptors on the platelet cell membrane. In general, there are three distinct morphological groups, i) dendritic (D), ball-shaped with filopods; ii) spread dendritic (SD), hemisphere-shaped with filopods; and fully spread (FS), extensively spread. The

platelet cells in different activation status were investigated by SEM and shown in Fig. 29.

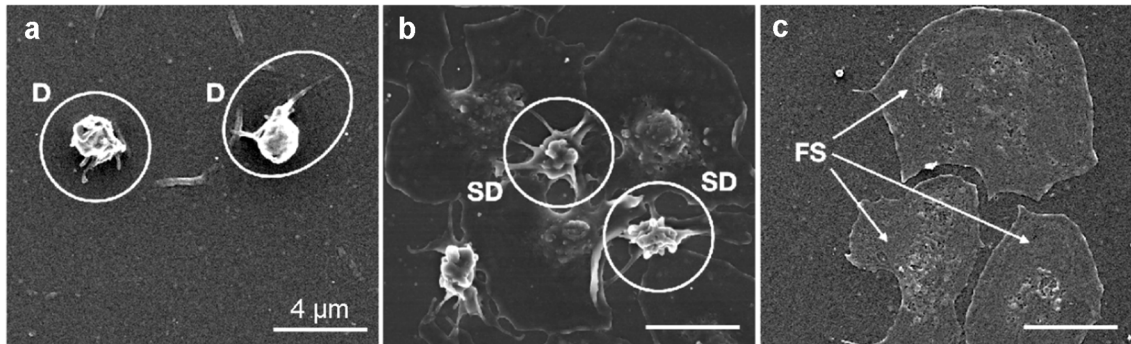


Figure 29. Morphologies of attached platelets on PS. SEM images of the Dendritic "D", Spread Dendritic "SD", and Fully Spread "FS" activation stage on culture dish after (a) 5 and (b,c) 30 minutes.

These observations illustrate the typical scenario of platelet morphological changes during adhesion on solid surfaces. The first activation stage is referred to D. When contacting with the material surface, the cytoskeleton of the ball-shaped and inactivated platelet cells is everted, to increase the surface area of the cells. After that, the filopods form on the cell surfaces and adhere to the material surface. In the second stage of SD, the platelet cells gradually flatten to a hemispherical shape. The numerous stunted filopods are expressed and covered more area on the material surfaces. At the FS stage, the cells show widened cytoplasm and flattening. The more flattened the cells are, more firmly, the platelet cells adhere to the material surface. [303]

5.3.3 Platelet surface coverage on nanostructured surfaces

To understand the interactions between the platelets and surfaces, the LM images were firstly processed to obtain the surface coverage as an indicator for platelet adhesion. The surface coverages of the adhered platelets are summarized in Fig. 30. In each case, the occupied area percentages of all R, D, SD, and FS platelet cells are plotted over the adhesion time. The number counts of FS cells on the polymer thin films were difficult to be analyzed from the LM images due to the ultra-low contrast between inner parts of FS cells and substrates.

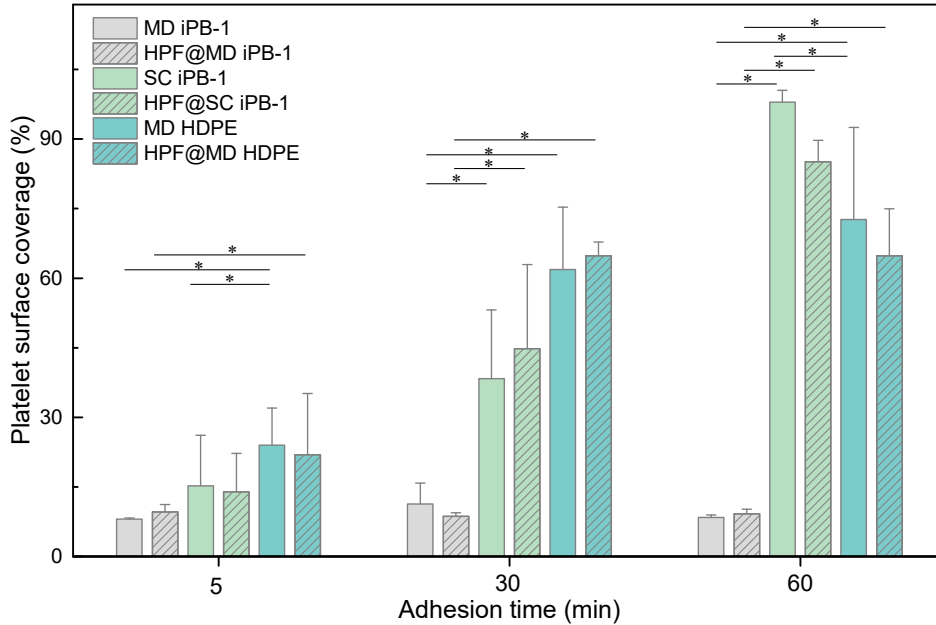


Figure 30. Platelet surface coverages. Area percentages of platelets on MD iPB-1, SC iPB-1, and MD HDPE surfaces, as well as the HPF-adsorbed surfaces (HPF concentration of $1 \text{ mg}\cdot\text{L}^{-1}$). The stars indicate a significant difference ($P < 0.05$).

On MD iPB-1 surfaces, the area percentages of platelets keep constant at around 10% in one hour. This indicates that only a few platelets adhered to the surface and thus only a few of them were activated. Comparing the MD and SC iPB-1 films, no significant difference between platelet surface coverages can be observed after 5 minutes of adhesion time. Notably, significantly more surface areas of SC iPB-1 surfaces were covered by platelets as the adhesion time increases. In contrast, on the MD HDPE surfaces, the platelet cells occupied around one fourth the surface area in the initial 5 min. This indicates that more platelet cells adhered and activated on the MD HDPE surfaces at the beginning, compared to the MD and SC iPB-1 surfaces.

Moreover, there were no significant differences between the nanostructured surfaces and the surfaces pretreated with 1 mg/L HPF solutions. The question arises as to why adhesion and activation of platelet cells were not affected by the pretreatment of HPF on surfaces. This can be caused by the high amount of HPF molecules in the platelet concentrate (pool TK), which contained around $0.26\text{-}0.68 \text{ mg}\cdot\text{mL}^{-1}$ of HPF molecules. This HPF concentration in platelet concentrate was more than 300 times higher than that ($1 \text{ mg}\cdot\text{L}^{-1}$) for the pre-treatment on surfaces. As was measured by QCM-D (Fig. 21a), the HPF adsorption saturated in

five minutes and formed a dense layer on polymer surfaces under the HPF concentration of $100 \text{ mg}\cdot\text{L}^{-1}$. Therefore, the ultra-high concentration of HPF in platelet concentrate led to immediate saturation of HPF adsorption on polymer surfaces. And thus, the influence of the pre-treated HPF molecules fell into a decline due to these dense HPF layers on all surfaces. For the samples treated with other fibrinogen solutions (0.01 or $0.1 \text{ mg}\cdot\text{L}^{-1}$), values were not shown. The trend was that there were no significant differences between the surfaces, which were pre-treated by HPF solutions of different concentrations. Aiming at better elucidating the effects on platelet adhesion from the distinct underlying nanostructures, morphologies, and distributions of platelet cells on surfaces were systematically evaluated via SEM images.

5.3.4 Platelet activation on nanostructured surfaces

To acquire detailed information about the morphological changes of platelets on the surfaces, the dehydrated samples of MD iPB-1 were explored with SEM, shown in Fig. 31a. The adhesion test images include representative exposures for each sample type after 5, 30, and 60 minutes of platelet adhesion. Based on the relatively low platelet adhesion, it can be assumed that on MD iPB-1 films, the activation and thus the stimulation of new cells occurs only after a considerable delay. The number of platelets increases slightly from 5 to 30 minutes, while it keeps constant after that. Moreover, the morphology of the cells changes from R/D via D/SD to network-like structures of SD cells at 60 minutes. Notably, no FS cells could be detected on MD iPB-1 surfaces.

To extract more information on morphological changes of platelet cells on surfaces, the surface coverage and cell numbers of the four cell types (data from SEM) are summarized in Fig. 31b and c. On MD iPB-1, the R and D cells adhered from the beginning, and a few of them are activated into SD and FS cells. With the increased adhesion time, the MD iPB-1 surfaces are gradually covered by the developed SD cells. After 60 min incubation, the total surface coverage is not more than 50% of the surface area. It needs to be pointed out that networks of SD platelets, sometimes small agglomerates, formed on the MD iPB-1 surfaces (Fig. 31a) after 30 minutes' platelet adhesion. SD platelet networks appear later (after 60 minutes) on MD iPB-1 surfaces.

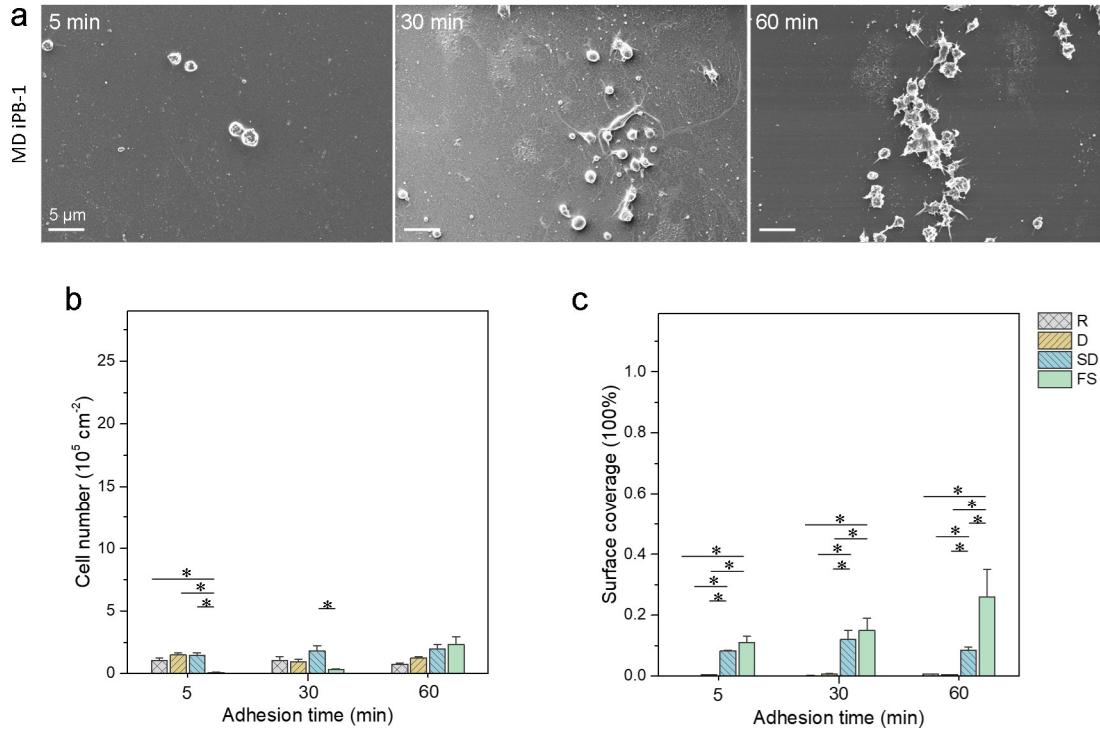


Figure 31. Platelets adhesion on MD iPB-1. Representative SEM recordings for MD iPB-1 surfaces after 5, 30 and 60 minutes. (b) The number of platelets in millions per cm² over the adhesion time on MD iPB-1. (c) Surface coverage percentage of platelets on MD iPB-1. R, D, SD, and FS indicate rest, dendritic, spread dendritic and fully spread. The stars indicate a significant difference (P<0.05).

According to the size and shape of the platelets on MD iPB-1 after 60 minutes, the cells could be incomplete activated granules and small aggregates of platelets. Taking into account the “side-on” orientation of HPF molecules on MD iPB-1, not only the primary binding sites, C terminus of γ chains, but also the supplementary binding sites, A α sequences on D-domains, are significantly reduced. This leads to an apparent inhibition of platelet adhesion and activation. However, the small platelet aggregates might be attributed to the locally high amount of binding sites on adsorbed HPF layers. On the one hand, the activation and morphology change of the platelets is associated with the activation of the platelets and the adhesion of other platelets. On the other hand, the platelet aggregations are one of the evolving risk factors to thrombosis. Therefore, this behavior would be doubtful and require a more in-depth understanding.

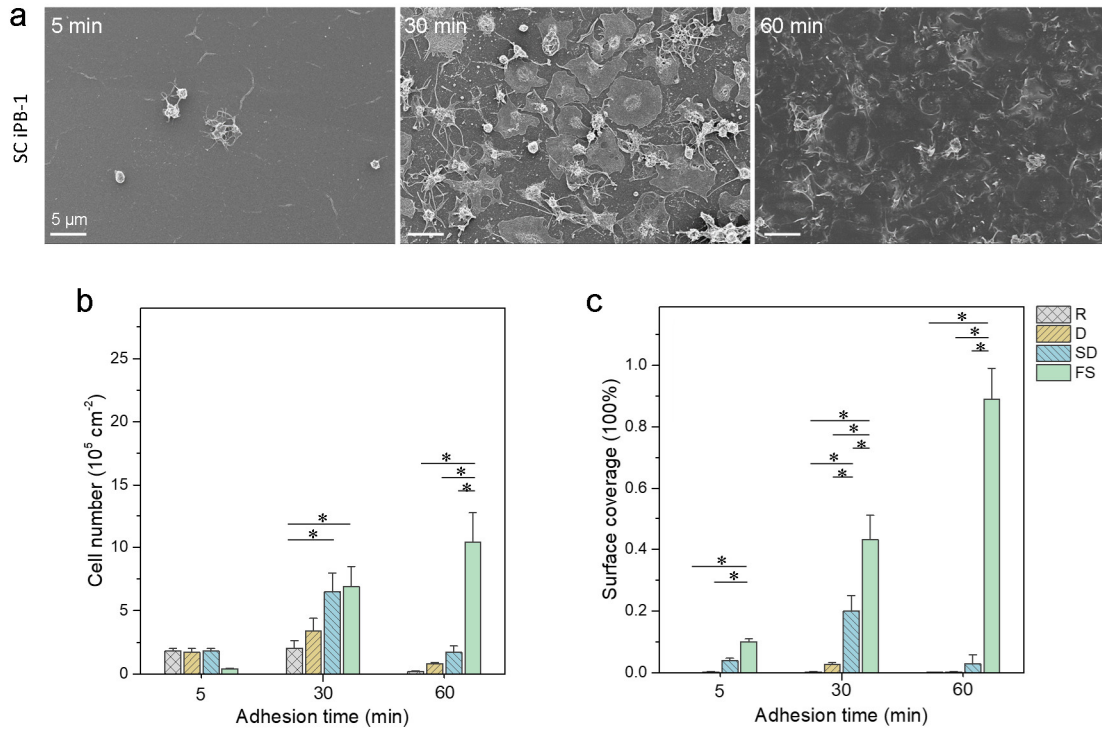


Figure 32. Platelets adhesion on SC iPB-1. Representative SEM recordings for SC iPB-1 surfaces in 5, 30 and 60 minutes. (b) The number of platelets in millions per cm² over the adhesion time on SC iPB-1. (c) Surface coverage percentage of platelets on SC iPB-1. R, D, SD, and FS indicate rest, dendritic, spread dendritic and fully spread. The stars indicate a significant difference (P<0.05).

On SC iPB-1 films, the number of D and SD platelets increases slightly from 5 to 30 minutes, shown in Fig. 32. However, this increase is somewhat stronger in 30 minutes. Occasional FS cells can be observed in this film after 5 minutes. In the period of 30 to 60 minutes, the number of D and SD platelets nearly disappear, whereas the FS platelets increase significantly. This can be explained by the considerable number of D or SD platelets in the early stage.

On the MD HDPE surfaces, D, SD, and FS cells present already in 5 min (Fig. 33), earlier than those on MD and SC iPB-1. As the same trends in other films, the numbers of D and SD cells slightly decrease over time or remain constant, while FS cells increase. It is notable that, on this HPF-immobilized surface, the number of FS cells does not increase significantly with adhesion time.

The evolutions of platelet morphologies based on the previous observation are reflected in Fig. 33b and c. The development begins in each case with a small amount of R, D, or SD cells that are not yet activated. Distinct from MD and SC iPB-1, several minutes later, most of the platelets are fully activated and form FS cells.

After fully spread, the early-adhered granules of FS cells are already emptied and stimulate other platelets for adhesion. As the incubation time progresses, the surfaces are covered with more FS cells.

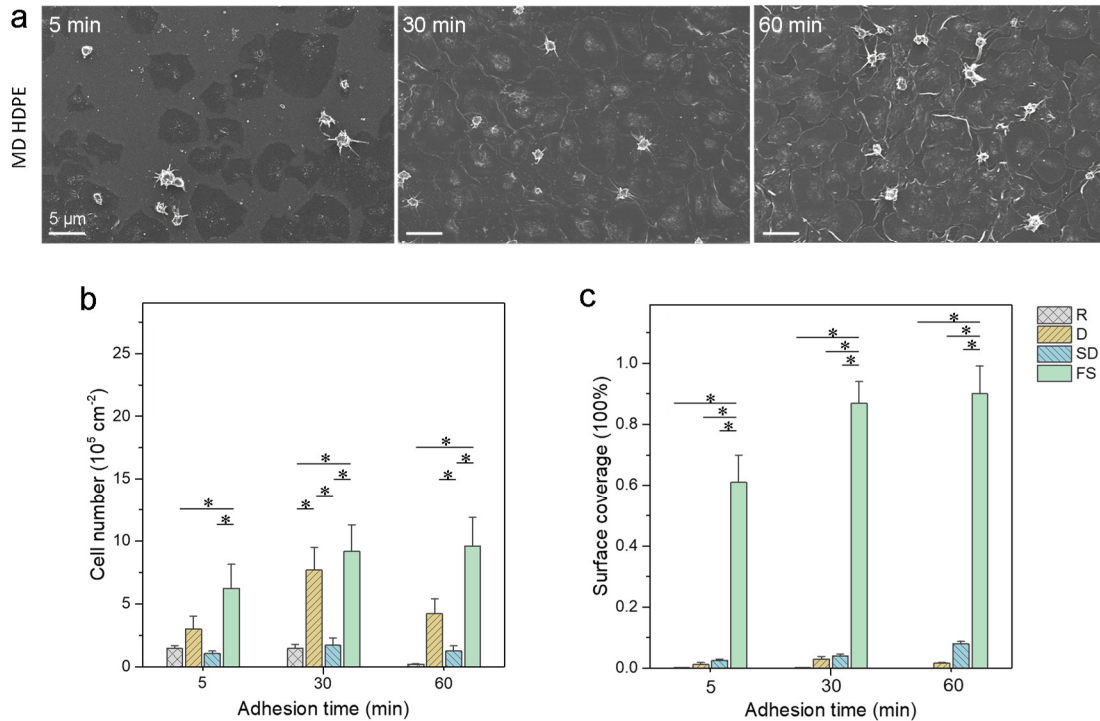


Figure 33. Platelets adhesion on MD HDPE. Representative SEM recordings for MD HDPE surfaces in 5, 30, and 60 minutes. (b) The number of platelets in millions per cm² over the adhesion time on MD HDPE. (c) Surface coverage percentage of platelets on MD HDPE. R, D, SD, and FS indicate rest, dendritic, spread dendritic and fully spread. The stars indicate a significant difference (P<0.05).

In a comprehensive work by Koh *et al.*, [226] the platelet adhesion were found increase with the width of PLGA nanopillars, attributing to the increased contact area with the tips of nanopillars. Whereas, in our work, increased platelet adhesion and activation on SC iPB-1 might be induced by the distinct conformations of immobilized HPF molecules.

To further understand the platelet adhesion behaviors on surfaces, platelet adhesion mechanism (Fig. 34) was proposed. The availability of binding sites on the HPF layer to platelet membrane integrin determines the adhesion and activation of platelet cells. These binding sites include both primary (γ 12) and secondary (RGD) binding sites, located on γ C and α C domains, respectively. As described in section 5.1, the different nanotopographies influenced not only the amount of proteins but also the protein conformations.

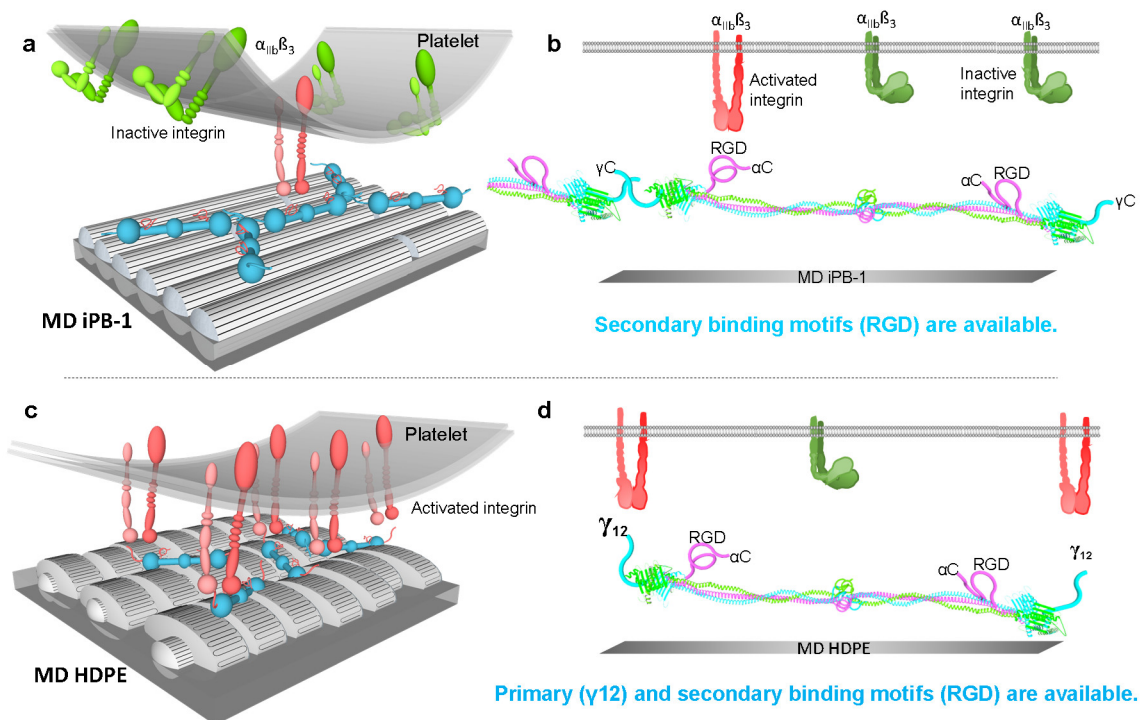


Figure 34. Sketches of platelets adhesion on HPF adsorbed surfaces. (a,b) Strong protein-protein interaction inhibits the binding of platelet integrin. (c,d) Few protein-protein interactions facilitate the binding of integrin. MD iPB-1 and MD HDPE show NLCs and SKCs, respectively. The connected three blue balls indicate HPF molecules. The pink strings on HPF indicate the available binding sites to platelets. The paired green and red integrin display inactive and activated states of $\alpha_{IIb}\beta_3$.

On MD iPB-1, the “eyelet” network structures with “side-on” HPF conformation on MD iPB-1 surface occupied the primary binding sites. The reason is that the D-D interactions are facilitated by the seven amino acid units in γ_C , named as γ_{XL} (QHHLGGA). The γ_{XL} partially overlaps with the amino acid sequences with primary binding sites, γ_{12} (HHLGGAKQAGDV). Only the secondary binding sites RGD are available to the platelet cells, and thus the platelet adhesion and activation processes are hindered. In contrast, the SC iPB-1 surfaces are covered by SD and FS cells in a much higher speed than that on MD iPB-1 surfaces. Till 60 min, their surfaces are fully covered by FS cells. On SC iPB-1, HPF adsorbs in a more tightly packed with “end-on” conformation than on MD iPB-1. It is known that the amino acid sequences of the HPF gamma chains, i.e., $\gamma_{392-411}$, located on the D-domains of HPF molecules, are the preferred platelet ligands. [304, 305] Therefore, it appears that both the primary and secondary binding sites within the HPF layer on SC iPB-1 surfaces are more accessible to the platelets. Thus, the HPF molecules on SC iPB-1 present favorable conformation and more binding sites to the platelets,

and as a result, promote the platelets adhesion and activation. Similar to the HPF layers on SC iPB-1, the packed HPF molecules on MD HDPE presents lots of binding sites accessible to the platelets and thus result in a high number of adhered platelets. Furthermore, it remains to be clarified how comparable is the platelet adhesion performed here with that in the human body. According to the University Hospital Jena and guidelines of the transfusion law of the Federal Republic of Germany, the platelet concentrates used in this work contain at least 2×10^{11} platelets per 250 mL unit. 1 mL of this concentrate, i.e., 8×10^8 platelets, was added to each sample. This concentrate was relatively higher than that in 1 mL blood of an adult human, which contains 1.5 to 4.0×10^8 platelets. [306, 307] However, it should be noticed that significantly more blood per unit area comes into contact with the biomaterial after insertion of the implant, resulting in more platelets overall. Thus, the experimental conditions in this work are well comparable to the circumstances in the human body.

5.3.5 Conclusion

This section aimed to investigate how the subsequent biological responses are mediated by the nanostructures and the surface-immobilized protein molecules. Results showed that the platelet adhesion was inhibited on MD iPB-1, comparing to that on SC iPB-1 and MD HDPE. From the topographical point of view, inhibited adhesion of platelets on MD iPB-1 is mainly due to the uniform network formation of HPF molecules on the NLCs with small size and curvature. However, the HPF conformations, i.e., randomly-distributed HPF on SC iPB-1 and loosely-packed HPF layer on MD HDPE, lead to more exposed binding sites and further result in higher numbers of the adhered and activated platelets. Direct observations of amount and morphology changes in activated platelet cells were able to confirm the hypothesis that the nanostructures alter the conformation, and thus bioactivities of the adsorbed HPF molecules, which affect the adhesion behavior and activation of platelets. Meanwhile, these findings reveal that the conformation of the surface-immobilized proteins and the binding site available to the platelets can be controlled by the specific design of surface topography. These preliminary studies underscore the possibility that controlled HPF adsorption may serve to prevent the thrombosis of the implants or blood contact biomaterials. To make the observations more clear, table 3 is presented to illustrate the distinct protein adsorption

behaviors on nanostructured polymer surfaces and their influence on the following platelet adhesion and activation.

Table 3 Platelet adhesion and activation influenced by HPF adsorbed surfaces.

Polymers	MD iPB-1	SC iPB-1	MD HDPE
Patterns	NLCs (width 22 ± 8 nm)	LCs (width 50 ± 11 nm)	SKCs (width 13 ± 2 nm)
Contact angle	$103.04 \pm 3.16^\circ$	$106.2 \pm 1.96^\circ$	$99.4 \pm 1.25^\circ$
HPF Adsorption	“Eyelet” network structures; Side-on conformation; Anisotropic orientation; Single HPF diffusion along the short axis of NLCs.	HPF did not form networks; More end-on conformation; Loosely packed HPF layer.	Densely packed HPF layer; More end-on conformation; Loosely packed HPF layer; Single HPF diffusion along the short axis of SKCs.
Binding sites	Secondary	Primary and secondary	Primary and secondary
Platelet adhesion	Slow activation of platelets; Low adhesion number of platelets; Small surface coverage.	Slow activation of platelets; High adhesion number of platelets; Large surface coverage after one hour.	Fast activation of platelets; High adhesion number of platelets; Large surface coverage after 30 min.

6

Summary

Human plasma fibrinogen (HPF) network formation is the critical factor to initiate blood clotting or coagulation, which can be either life-saving or life-risking, encountered by artificial implant surfaces. Studies showed that the biocompatibility for a blood-contacting material could be mediated by surface nanostructures. Therefore, to control HPF adsorption and network formation on polymeric surfaces with precisely-defined and easily-processed nanostructures is of vital importance in biomedical and tissue engineering fields. In this work, the nanostructures on polymers, i.e., isotactic polybutene-1 (iPB-1) and high-density polyethylene (HDPE), were demonstrated to be able to guide the adsorption of HPF and the subsequent platelet adhesion.

The melt-drawn isotactic polybutene-1 (MD iPB-1) surface featured close-packed longitudinal needle-like crystals, NLCs, which exhibited a lateral dimension lower than the length of the HPF molecules. This unique nanostructure supported the HPF into uniform protein layer with “side-on” conformation, in which the major axis of HPF was parallel to the surface plane. Interestingly, a preferential alignment of HPF molecules concerning the axial direction of the NLCs and high anisotropy of the HPF network assembly were observed and investigated with an orientation analysis on both “single” and multiprotein (“eyelets”) level.

Aiming at elucidating the relationships between the anisotropic “eyelet” network formation and HPF diffusion on MD iPB-1 surface, the adsorption dynamics of single HPF molecules were tracked and recorded with mapping using accumulated probe trajectories (MAPT) technique. The captured trajectories revealed the anisotropic diffusion of HPF on MD iPB-1. This was ascribed to the confinement of individual HPF molecules on the crystalline regions. Furthermore, HPF diffusion was found independent of the anisotropic friction characteristic of the surface. This

suggested that HPF molecules confined on the nanosized iPb-1 NLCs undergoes partial detachment and diffuse via a Sansetsukon-like nanocrawling mechanism. Also, the preferential HPF diffusion direction perpendicular to its major axis was explained by high conformational flexibility of the HPF in the coiled-coil regions favored by the presence of two hinges. Based on these results, it is believed that nanostructured surfaces that support nanoconfinement and anisotropic protein diffusion are more likely to lead to the formation of ordered protein assemblies.

On the spin-coated isotactic polybutene-1 (SC iPb-1) surface, lamellar crystals (LCs) presented and expressed a lateral size comparable to the length of HPF molecules. Randomly packed monolayer assembly was observed on SC iPb-1. Combining with the QCM-D data, the information pointed out that HPF adsorbed with an “end-on” conformation on SC iPb-1 surface, in which the major axis of HPF lay perpendicular to the surface plane. Contrary to the NLCs, which modulated the affinity of HPF molecules for protein-protein and protein-surface interactions in a balanced manner, the nanostructure LCs on SC iPb-1 blocked the “end-to-end” protein-protein interaction and thus hindered the uniform layer formation.

Different from MD and SC iPb-1, the MD HDPE surface presented shish-kebab crystals (SKCs) with kebab crystals overgrowth along with the extended shish crystals. The size of the kebab crystals was comparable to the dimension of HPF molecules. This distinct nanostructures on MD HDPE led to packed HPF layer without visible “eyelet” networks.

The biofunctionality of the surface-immobilized HPF molecules was tested via platelets adhesion on the HPF-adsorbed nanostructured surfaces. Distinct adhesion behaviors of platelets were detected via platelet morphological changes on HPF-immobilized surfaces. It was observed that the platelet number and surface coverage were reduced on MD iPb-1, which was immobilized with uniform HPF networks, comparing to those on SC iPb-1 and MD HDPE. As expected, on the “eyelet” networks on MD iPb-1, the HPF layers with occupied binding sites to platelets prevented the adhesion and activation of platelet cells. However, there were small platelet aggregates formed after half an hour. On SC iPb-1 surface, the immobilized HPF molecules resulted in a higher amount of platelet adhesion and activation, which could be considered as a potential risk for the biomaterial implantation. Similarly, a high number of the fully spread cell were identified on

MD HDPE surface, indicating that the HPF conformation was favorable for platelet adhesion. These observations revealed that the conformations of the adsorbed HPF molecules were mediated by the specific design of surface nanostructure.

The observed changes in HPF adsorption on NLCs, LCs, and SKCs unambiguously showed an overall picture that the nanostructures altered the conformation and thus the bioactivities of the adsorbed HPF molecules, which further affected the adhesion behavior and activation of platelets. Although the polymeric films display subtle variations in surface chemistry, their ability to form oriented protein layers demonstrated that surface nanotopography played a vital role in the surface assembly of HPF. Specifically, the surface topographical factors, such as structure width, curvature, and aspect ratio, all influenced the protein interaction preferences. The knowledge gained through this current study demonstrates that the ordered protein layer formation and platelet adhesion *in vitro* under physiological conditions point toward several clinical solutions. They include, i), possible mechanisms of clot formation and implant integration *in vivo*; ii), initial judgements of biocompatibility and hemocompatibility of the implants without complicated procedures; iii), more comprehensive models for thrombogenesis studies without the involvement of thrombin; and iv), new strategies for preventing thrombosis and implant failure in the absence of anticoagulant agents.

Last but not least, although the overall picture indicates an anti-thrombotic nature of MD iPB-1 substrate, there is still much subsequent work to be done in evaluating the biofunctionality of these immobilized HPF molecules. Therefore, aiming at determining the behaviors of nanostructure-mediated protein and platelet adhesion in blood contact biomaterials, further bioactivity confirmation of HPF molecules and *in vivo* studies of the films are of vital importance.

References

- [1] A. Choukourov, A. Grinevich, N. Saito, O. Takai, SPM analysis of fibrinogen adsorption on solid surfaces, *Surface Science*, 601 (2007) 3948-3951.
- [2] R. Langer, D.A. Tirrell, Designing materials for biology and medicine, *Nature*, 428 (2004) 487-492.
- [3] N.A. Peppas, R. Langer, New challenges in biomaterials, *Science*, 263 (1994) 1715-1720.
- [4] B.D. Ratner, A.S. Hoffman, F.J. Schoen, J.E. Lemons, *Biomaterials science: an introduction to materials in medicine*, Elsevier 2004.
- [5] L.L. Hench, J.M. Polak, Third-generation biomedical materials, *Science*, 295 (2002) 1014-1017.
- [6] P. Roach, D. Farrar, C.C. Perry, Interpretation of protein adsorption: surface-induced conformational changes, *Journal of the American Chemical Society*, 127 (2005) 8168-8173.
- [7] S. Patil, A. Sandberg, E. Heckert, W. Self, S. Seal, Protein adsorption and cellular uptake of cerium oxide nanoparticles as a function of zeta potential, *Biomaterials*, 28 (2007) 4600-4607.
- [8] J. Andrade, V. Hlady, Protein adsorption and materials biocompatibility: a tutorial review and suggested hypotheses, *Biopolymers/Non-Exclusion HPLC*, Springer 1986, pp. 1-63.
- [9] I. Firkowska-Boden, X. Zhang, K.D. Jandt, Controlling protein adsorption through nanostructured polymeric surfaces, *Advanced healthcare materials*, 7 (2018) 1700995.
- [10] J.M. Anderson, A. Rodriguez, D.T. Chang, Foreign body reaction to biomaterials, *Seminars in immunology*, Elsevier, 2008, pp. 86-100.
- [11] W.B. Kannel, P.A. Wolf, W.P. Castelli, R.B. D'Agostino, Fibrinogen and risk of cardiovascular disease: the Framingham Study, *Jama*, 258 (1987) 1183-1186.
- [12] E. Ernst, K.L. Resch, Fibrinogen as a cardiovascular risk factor: a meta-analysis and review of the literature, *Annals of internal medicine*, 118 (1993) 956-963.
- [13] M. Mosesson, Fibrinogen and fibrin structure and functions, *Journal of Thrombosis and Haemostasis*, 3 (2005) 1894-1904.
- [14] T.A. Horbett, Principles underlying the role of adsorbed plasma proteins in blood interactions with foreign materials, *Cardiovascular Pathology*, 2 (1993) 137-148.
- [15] M.S. Lord, M. Foss, F. Besenbacher, Influence of nanoscale surface topography on protein adsorption and cellular response, *Nano Today*, 5 (2010) 66-78.
- [16] H. Staudinger, Über polymerisation, *Berichte der deutschen chemischen Gesellschaft (A and B Series)*, 53 (1920) 1073-1085.

- [17] D. Rickert, Polymeric implant materials for the reconstruction of tracheal and pharyngeal mucosal defects in head and neck surgery, *GMS current topics in otorhinolaryngology, head and neck surgery*, 8 (2009).
- [18] P. Flory, *Principles of polymer chemistry* Ithaca, NY: Cornell University, (1953).
- [19] D.E. Szilagyi, L.C. France, R.F. Smith, J.G. Whitcomb, The clinical use of an elastic dacron prosthesis, *AMA archives of surgery*, 77 (1958) 538-551.
- [20] D.N. Theodorou, U.W. Suter, Detailed molecular structure of a vinyl polymer glass, *Macromolecules*, 18 (1985) 1467-1478.
- [21] T. Aida, E. Meijer, S.I. Stupp, Functional supramolecular polymers, *Science*, 335 (2012) 813-817.
- [22] M.J. Kasser, Regulation of UHMWPE biomaterials in total hip arthroplasty, *Journal of Biomedical Materials Research Part B: Applied Biomaterials*, 101 (2013) 400-406.
- [23] J.E. Mark, *Physical properties of polymers handbook*, Springer 2007.
- [24] Y. Doi, Structure and stereochemistry of atactic polypropylenes. Statistical model of chain propagation, *Die Makromolekulare Chemie, Rapid Communications*, 3 (1982) 635-641.
- [25] M. Pascual, O. Plastre, B. Montdargent, D. Labarre, J.A. Schifferli, Specific interactions of polystyrene biomaterials with factor D of human complement, *Biomaterials*, 14 (1993) 665-670.
- [26] S.J. Lee, J. San Choi, K.S. Park, G. Khang, Y.M. Lee, H.B. Lee, Response of MG63 osteoblast-like cells onto polycarbonate membrane surfaces with different micropore sizes, *Biomaterials*, 25 (2004) 4699-4707.
- [27] S. Ramakrishna, J. Mayer, E. Wintermantel, K.W. Leong, Biomedical applications of polymer-composite materials: a review, *Composites science and technology*, 61 (2001) 1189-1224.
- [28] P. Torricelli, M. Fini, G. Giavaresi, R. Botter, D. Beruto, R. Giardino, Biomimetic PMMA-based bone substitutes: A comparative in vitro evaluation of the effects of pulsed electromagnetic field exposure, *Journal of Biomedical Materials Research Part A: An Official Journal of The Society for Biomaterials, The Japanese Society for Biomaterials, and The Australian Society for Biomaterials and the Korean Society for Biomaterials*, 64 (2003) 182-188.
- [29] R. Nathawat, A. Kumar, N. Acharya, Y. Vijay, XPS and AFM surface study of PMMA irradiated by electron beam, *Surface and Coatings Technology*, 203 (2009) 2600-2604.
- [30] B. Schrauwen, L.v. Breemen, A. Spoelstra, L. Govaert, G. Peters, H. Meijer, Structure, deformation, and failure of flow-oriented semicrystalline polymers, *Macromolecules*, 37 (2004) 8618-8633.

- [31] D.A. Ivanov, B. Nysten, A.M. Jonas, Atomic force microscopy imaging of single polymer spherulites during crystallization: application to a semi-crystalline blend, *Polymer*, 40 (1999) 5899-5905.
- [32] A.T. Jones, J.M. Aizlewood, D. Beckett, Crystalline forms of isotactic polypropylene, *Die Makromolekulare Chemie: Macromolecular Chemistry and Physics*, 75 (1964) 134-158.
- [33] P.J. Flory, Molecular morphology in semicrystalline polymers, *Nature*, 272 (1978) 226-229.
- [34] J. Koenig, D. Witenhafer, Infrared studies of polymer chain folding I. Linear polyethylene, *Die Makromolekulare Chemie: Macromolecular Chemistry and Physics*, 99 (1966) 193-201.
- [35] A.T. Jones, Polybutene-1-type II crystalline form, *Journal of Polymer Science Part B: Polymer Letters*, 1 (1963) 455-456.
- [36] C. De Rosa, O. Ruiz de Ballesteros, F. Auriemma, R. Di Girolamo, C. Scarica, G. Giusto, S. Esposito, S. Guidotti, I. Camurati, Polymorphic behavior and mechanical properties of isotactic 1-butene-ethylene copolymers from metallocene catalysts, *Macromolecules*, 47 (2014) 4317-4329.
- [37] V. Holland, R.L. Miller, Isotactic polybutene-1 single crystals: morphology, *Journal of Applied Physics*, 35 (1964) 3241-3248.
- [38] S. Hugger, R. Thomann, T. Heinzl, T. Thurn-Albrecht, Semicrystalline morphology in thin films of poly (3-hexylthiophene), *Colloid and Polymer Science*, 282 (2004) 932-938.
- [39] I.M. Ward, J. Sweeney, *Mechanical properties of solid polymers*, John Wiley & Sons 2012.
- [40] M.F. Talbott, G.S. Springer, L.A. Berglund, The effects of crystallinity on the mechanical properties of PEEK polymer and graphite fiber reinforced PEEK, *Journal of Composite Materials*, 21 (1987) 1056-1081.
- [41] L. Mandelkern, The crystalline state, *Physical properties of polymers*, 3 (2004) 209-315.
- [42] K. Jandt, T. McMaster, M. Miles, J. Petermann, Scanning force microscopy of melt-crystallized, metal-evaporated poly (butene-1) ultrathin films, *Macromolecules*, 26 (1993) 6552-6556.
- [43] R. Baughman, Solid-state synthesis of large polymer single crystals, *Journal of Polymer Science: Polymer Physics Edition*, 12 (1974) 1511-1535.
- [44] F. Reding, J. Faucher, R. Whitman, Glass transitions in ethylene copolymers and vinyl homopolymers and copolymers, *Journal of Polymer Science*, 57 (1962) 483-498.
- [45] H. Tanaka, H. Hasegawa, T. Hashimoto, Ordered structure in mixtures of a block copolymer and homopolymers. 1. Solubilization of low molecular weight homopolymers, *Macromolecules*, 24 (1991) 240-251.

- [46] K.I. Winey, E.L. Thomas, L.J. Fetters, Swelling of lamellar diblock copolymer by homopolymer: influences of homopolymer concentration and molecular weight, *Macromolecules*, 24 (1991) 6182-6188.
- [47] M.R. Bockstaller, R.A. Mickiewicz, E.L. Thomas, Block copolymer nanocomposites: perspectives for tailored functional materials, *Advanced materials*, 17 (2005) 1331-1349.
- [48] A. Noshay, J.E. McGrath, *Block copolymers: overview and critical survey*, Elsevier 2013.
- [49] K. Schmidt, H.G. Schoberth, M. Ruppel, H. Zettl, H. Hänsel, T.M. Weiss, V. Urban, G. Krausch, A. Böker, Reversible tuning of a block-copolymer nanostructure via electric fields, *Nature materials*, 7 (2008) 142-145.
- [50] F.S. Bates, G.H. Fredrickson, Block copolymer thermodynamics: theory and experiment, *Annual review of physical chemistry*, 41 (1990) 525-557.
- [51] L. Leibler, Theory of microphase separation in block copolymers, *Macromolecules*, 13 (1980) 1602-1617.
- [52] R.D. Groot, T.J. Madden, Dynamic simulation of diblock copolymer microphase separation, *The Journal of chemical physics*, 108 (1998) 8713-8724.
- [53] M. Li, C.A. Coenjarts, C.K. Ober, Patternable block copolymers, *Block Copolymers II*, Springer 2005, pp. 183-226.
- [54] H.-C. Kim, S.-M. Park, W.D. Hinsberg, Block copolymer based nanostructures: materials, processes, and applications to electronics, *Chemical reviews*, 110 (2009) 146-177.
- [55] I. Hamley, Nanostructure fabrication using block copolymers, *Nanotechnology*, 14 (2003) R39.
- [56] Y. Okazaki, E. Gotoh, Comparison of metal release from various metallic biomaterials in vitro, *Biomaterials*, 26 (2005) 11-21.
- [57] H. Matsuno, A. Yokoyama, F. Watari, M. Uo, T. Kawasaki, Biocompatibility and osteogenesis of refractory metal implants, titanium, hafnium, niobium, tantalum and rhenium, *Biomaterials*, 22 (2001) 1253-1262.
- [58] W. Billotte, *Ceramic biomaterials*, Biomaterials, CRC Press 2012, pp. 40-73.
- [59] M.P. Staiger, A.M. Pietak, J. Huadmai, G. Dias, Magnesium and its alloys as orthopedic biomaterials: a review, *Biomaterials*, 27 (2006) 1728-1734.
- [60] V. dos Santos, R.N. Brandalise, M. Savaris, *Biomaterials: Characteristics and properties*, Engineering of Biomaterials, Springer 2017, pp. 5-15.
- [61] P. Roach, D. Eglin, K. Rohde, C.C. Perry, Modern biomaterials: a review—bulk properties and implications of surface modifications, *Journal of Materials Science: Materials in Medicine*, 18 (2007) 1263-1277.

- [62] J.Y. Lim, H.J. Donahue, Cell sensing and response to micro-and nanostructured surfaces produced by chemical and topographic patterning, *Tissue engineering*, 13 (2007) 1879-1891.
- [63] G. Wei, P.X. Ma, Nanostructured biomaterials for regeneration, *Advanced functional materials*, 18 (2008) 3568-3582.
- [64] L.S. Nair, C.T. Laurencin, Biodegradable polymers as biomaterials, *Progress in polymer science*, 32 (2007) 762-798.
- [65] R.J. Mondschein, A. Kanitkar, C.B. Williams, S.S. Verbridge, T.E. Long, Polymer structure-property requirements for stereolithographic 3D printing of soft tissue engineering scaffolds, *Biomaterials*, 140 (2017) 170-188.
- [66] M.S. Shoichet, Polymer scaffolds for biomaterials applications, *Macromolecules*, 43 (2009) 581-591.
- [67] R. Richmond, T.V. Macfarlane, J.F. McCord, An evaluation of the surface changes in PMMA biomaterial formulations as a result of toothbrush/dentifrice abrasion, *Dental Materials*, 20 (2004) 124-132.
- [68] J. Jagur-Grodzinski, Polymers for tissue engineering, medical devices, and regenerative medicine. Concise general review of recent studies, *Polymers for advanced technologies*, 17 (2006) 395-418.
- [69] W.F. Mousa, M. Kobayashi, S. Shinzato, M. Kamimura, M. Neo, S. Yoshihara, T. Nakamura, Biological and mechanical properties of PMMA-based bioactive bone cements, *Biomaterials*, 21 (2000) 2137-2146.
- [70] D.F. Farrar, J. Rose, Rheological properties of PMMA bone cements during curing, *Biomaterials*, 22 (2001) 3005-3013.
- [71] M. Herring, A. Gardner, J. Glover, A single-staged technique for seeding vascular grafts with autogenous endothelium, *Surgery*, 84 (1978) 498-504.
- [72] J.W. Boretos, W.S. Pierce, Segmented polyurethane: a new elastomer for biomedical applications, *Science*, 158 (1967) 1481-1482.
- [73] I. Hisamatsu T., Catheter, in: D.U.S.P.a.T.O. Washington (Ed.) U.S. Patent U.S., 2003.
- [74] I. T., Catheter tube and a method of processing the inner surface of a tube, in: D.U.S.P.a.T.O. Washington (Ed.), 1997.
- [75] F.A. Barber, M.A. Herbert, F.A. Schroeder, J. Aziz-Jacobo, M.J. Sutker, Biomechanical Testing of New Meniscal Repair Techniques Containing Ultra High Molecular Weight Polyethylene Suture (SS-35), *Arthroscopy*, 25 (2009) e19.
- [76] H. OL, B. M, B. F, R. CM, Lieberman]R, H. MH, S. EA, Polyethylene and metal debris generated by non-articulating surfaces of modular acetabular components, *The Journal of Bone and Joint Surgery. British volume*, 76-B (1994) 568-574.

- [77] B. Klosterhalfen, K. Junge, U. Klinge, The lightweight and large porous mesh concept for hernia repair, *Expert Review of Medical Devices*, 2 (2005) 103-117.
- [78] W. Stone Gregg, G. Ellis Stephen, A. Cox David, J. Hermiller, C. O'Shaughnessy, T. Mann James, M. Turco, R. Caputo, P. Bergin, J. Greenberg, J. Popma Jeffrey, E. Russell Mary, One-Year Clinical Results With the Slow-Release, Polymer-Based, Paclitaxel-Eluting TAXUS Stent, *Circulation*, 109 (2004) 1942-1947.
- [79] K. Rezwan, Q.Z. Chen, J.J. Blaker, A.R. Boccaccini, Biodegradable and bioactive porous polymer/inorganic composite scaffolds for bone tissue engineering, *Biomaterials*, 27 (2006) 3413-3431.
- [80] U. Klinge, B. Klosterhalfen, V. Birkenhauer, K. Junge, J. Conze, V. Schumpelick, Impact of Polymer Pore Size on the Interface Scar Formation in a Rat Model, *Journal of Surgical Research*, 103 (2002) 208-214.
- [81] D. Knoll, J. Hermans, Polymer-protein interactions. Comparison of experiment and excluded volume theory, *Journal of Biological Chemistry*, 258 (1983) 5710-5715.
- [82] M.J. Dalby, M.O. Riehle, H.J.H. Johnstone, S. Affrossman, A.S.G. Curtis, Polymer-Demixed Nanotopography: Control of Fibroblast Spreading and Proliferation, *Tissue Engineering*, 8 (2002) 1099-1108.
- [83] P. Kim, K.W. Kwon, M.C. Park, S.H. Lee, S.M. Kim, K.Y. Suh, Soft lithography for microfluidics: a review, (2008).
- [84] F.A. Denis, P. Hanarp, D.S. Sutherland, Y.F. Dufrêne, Fabrication of Nanostructured Polymer Surfaces Using Colloidal Lithography and Spin-Coating, *Nano Letters*, 2 (2002) 1419-1425.
- [85] B.W. Maynor, S.F. Filocamo, M.W. Grinstaff, J. Liu, Direct-Writing of Polymer Nanostructures: Poly(thiophene) Nanowires on Semiconducting and Insulating Surfaces, *Journal of the American Chemical Society*, 124 (2002) 522-523.
- [86] R. Glass, M. Arnold, J. Blümmel, A. Küller, M. Möller, J.P. Spatz, Micro-Nanostructured Interfaces Fabricated by the Use of Inorganic Block Copolymer Micellar Monolayers as Negative Resist for Electron-Beam Lithography, *Advanced Functional Materials*, 13 (2003) 569-575.
- [87] S.Y. Chou, P.R. Krauss, P.J. Renstrom, Imprint of sub-25 nm vias and trenches in polymers, *Applied Physics Letters*, 67 (1995) 3114-3116.
- [88] J.-H. Lim, C.A. Mirkin, Electrostatically Driven Dip-Pen Nanolithography of Conducting Polymers, *Advanced Materials*, 14 (2002) 1474-1477.
- [89] E. Menard, M.A. Meitl, Y. Sun, J.-U. Park, D.J.-L. Shir, Y.-S. Nam, S. Jeon, J.A. Rogers, Micro- and Nanopatterning Techniques for Organic Electronic and Optoelectronic Systems, *Chemical Reviews*, 107 (2007) 1117-1160.

- [90] K.-B. Lee, S.-J. Park, C.A. Mirkin, J.C. Smith, M. Mrksich, Protein Nanoarrays Generated By Dip-Pen Nanolithography, *Science*, 295 (2002) 1702-1705.
- [91] D. Yun, J. Park, H. Kim, J. Mun, S. Kim, K. Kim, G. Yeom, Improvement of a block copolymer (PS-b-PMMA)-masked silicon etch profile using a neutral beam, *Nanotechnology*, 27 (2016) 384002.
- [92] D.-Y. Khang, H.H. Lee, Sub-100 nm Patterning with an Amorphous Fluoropolymer Mold, *Langmuir*, 20 (2004) 2445-2448.
- [93] A.M. Urbas, M. Maldovan, P. DeRege, E.L. Thomas, Bicontinuous Cubic Block Copolymer Photonic Crystals, *Advanced Materials*, 14 (2002) 1850-1853.
- [94] Z. Nie, E. Kumacheva, Patterning surfaces with functional polymers, *Nature Materials*, 7 (2008) 277.
- [95] R.K. Pal, A.A. Farghaly, M.M. Collinson, S.C. Kundu, V.K. Yadavalli, Photolithographic Micropatterning of Conducting Polymers on Flexible Silk Matrices, *Advanced Materials*, 28 (2016) 1406-1412.
- [96] T. Ito, S. Okazaki, Pushing the limits of lithography, *Nature*, 406 (2000) 1027-1031.
- [97] D. Bratton, D. Yang, J. Dai, C.K. Ober, Recent progress in high resolution lithography, *Polymers for Advanced Technologies*, 17 (2006) 94-103.
- [98] V. Auzelyte, C. Dais, P. Farquet, D.A. Gruetzmacher, L.J. Heyderman, F. Luo, S. Olliges, C. Padeste, P. Sahoo, T. Thomson, A. Turchanin, C. David, H.H. Solak, Extreme ultraviolet interference lithography at the Paul Scherrer Institut, *Journal of Micro/Nanolithography, MEMS, and MOEMS*, 8 (2009) 1-10.
- [99] J.A. Rogers, K.E. Paul, R.J. Jackman, G.M. Whitesides, Using an elastomeric phase mask for sub-100 nm photolithography in the optical near field, *Applied Physics Letters*, 70 (1997) 2658-2660.
- [100] B.D. Gates, Q. Xu, M. Stewart, D. Ryan, C.G. Willson, G.M. Whitesides, New Approaches to Nanofabrication: Molding, Printing, and Other Techniques, *Chemical Reviews*, 105 (2005) 1171-1196.
- [101] M.D. Levenson, N.S. Viswanathan, R.A. Simpson, Improving resolution in photolithography with a phase-shifting mask, *IEEE Transactions on Electron Devices*, 29 (1982) 1828-1836.
- [102] Y. Mai, A. Eisenberg, Self-assembly of block copolymers, *Chemical Society Reviews*, 41 (2012) 5969-5985.
- [103] S. Ouk Kim, H.H. Solak, M.P. Stoykovich, N.J. Ferrier, J.J. de Pablo, P.F. Nealey, Epitaxial self-assembly of block copolymers on lithographically defined nanopatterned substrates, *Nature*, 424 (2003) 411-414.

- [104] R.A. Segalman, Patterning with block copolymer thin films, *Materials Science and Engineering: R: Reports*, 48 (2005) 191-226.
- [105] J.N.L. Albert, T.H. Epps, Self-assembly of block copolymer thin films, *Materials Today*, 13 (2010) 24-33.
- [106] G. Singh, K.G. Yager, B. Berry, H.-C. Kim, A. Karim, Dynamic Thermal Field-Induced Gradient Soft-Shear for Highly Oriented Block Copolymer Thin Films, *ACS Nano*, 6 (2012) 10335-10342.
- [107] L. Li, C.-M. Chan, K.L. Yeung, J.-X. Li, K.-M. Ng, Y. Lei, Direct Observation of Growth of Lamellae and Spherulites of a Semicrystalline Polymer by AFM, *Macromolecules*, 34 (2001) 316-325.
- [108] R.L. Miller, *Polymer single crystals (Polymer reviews)*, Interscience, New York, 1963.
- [109] G. Reiter, Some unique features of polymer crystallisation, *Chemical Society Reviews*, 43 (2014) 2055-2065.
- [110] B.S. Hsiao, L. Yang, R.H. Somani, C.A. Avila-Orta, L. Zhu, Unexpected Shish-Kebab Structure in a Sheared Polyethylene Melt, *Physical Review Letters*, 94 (2005) 117802.
- [111] J. Petermann, R.M. Gohil, A new method for the preparation of high modulus thermoplastic films, *Journal of Materials Science*, 14 (1979) 2260-2264.
- [112] J. Petermann, H. Gleiter, Direct observation of amorphous and crystalline regions in polymers by defocus imaging, *The Philosophical Magazine: A Journal of Theoretical Experimental and Applied Physics*, 31 (1975) 929-934.
- [113] K.D. Jandt, L.M. Eng, J. Petermann, H. Fuchs, Scanning force microscopy of nanostructured uniaxially oriented ultra thin film surfaces of isotactic polystyrene, *Polymer*, 33 (1992) 5331-5333.
- [114] K.D. Jandt, M. Buhk, J. Petermann, Microscopic aspects of polymer-metal epitaxy, *Journal of Materials Science*, 31 (1996) 1779-1788.
- [115] T. Keller, M. Grosch, K.D. Jandt, Nanoscale Surface Lamellar Orientation and Lamellar Doubling in Ultrathin UHMW-PE Films, *Macromolecules*, 40 (2007) 5812-5819.
- [116] T.F. Keller, J. Schönfelder, J. Reichert, N. Tuccitto, A. Licciardello, G.M.L. Messina, G. Marletta, K.D. Jandt, How the Surface Nanostructure of Polyethylene Affects Protein Assembly and Orientation, *ACS Nano*, 5 (2011) 3120-3131.
- [117] M.M.L. Arras, C. Schillai, T.F. Keller, R. Schulze, K.D. Jandt, Alignment of multi-wall carbon nanotubes by disentanglement in ultra-thin melt-drawn polymer films, *Carbon*, 60 (2013) 366-378.
- [118] A.J. Pennings, Lamellar and fibrillar crystallization of polymers, *Die Makromolekulare Chemie*, 2 (1979) 99-142.

- [119] T. Nagasawa, Y. Shimomura, Mechanism of formation of shish kebab structures, *Journal of Polymer Science: Polymer Physics Edition*, 12 (1974) 2291-2308.
- [120] J.L. Brash, Exploiting the current paradigm of blood-material interactions for the rational design of blood-compatible materials, *Journal of Biomaterials Science, Polymer Edition*, 11 (2000) 1135-1146.
- [121] H.T. Spijker, R. Graaff, P.W. Boonstra, H.J. Busscher, W. van Oeveren, On the influence of flow conditions and wettability on blood material interactions, *Biomaterials*, 24 (2003) 4717-4727.
- [122] G.A. Herzlinger, R.D. Cumming, Role of complement activation in cell adhesion to polymer blood contact surfaces, *ASAIO Journal*, 26 (1980) 165-171.
- [123] P. Kim, D.H. Kim, B. Kim, S.K. Choi, S.H. Lee, A. Khademhosseini, R. Langer, K.Y. Suh, Fabrication of nanostructures of polyethylene glycol for applications to protein adsorption and cell adhesion, *Nanotechnology*, 16 (2005) 2420-2426.
- [124] Y. Nishizuka, The role of protein kinase C in cell surface signal transduction and tumour promotion, *Nature*, 308 (1984) 693-698.
- [125] M. Amiji, K. Park, Prevention of protein adsorption and platelet adhesion on surfaces by PEO/PPO/PEO triblock copolymers, *Biomaterials*, 13 (1992) 682-692.
- [126] R.D. Petsko G. A., *Protein structure and function*, New Science Press, London, 2004.
- [127] G.N. Ramachandran, V. Sasisekharan, *Conformation of Polypeptides and Proteins***The literature survey for this review was completed in September 1967, with the journals which were then available in Madras and the preprinta which the authors had received.††By the authors' request, the publishers have left certain matters of usage and spelling in the form in which they wrote them, in: C.B. Anfinsen, M.L. Anson, J.T. Edsall, F.M. Richards (Eds.) *Advances in Protein Chemistry*, Academic Press 1968, pp. 283-437.
- [128] F.M. Richards, Areas, Volumes, Packing, and Protein Structure, *Annual review of biophysics and bioengineering*, 6 (1977) 151-176.
- [129] C. Chothia, The Classification and Origins of Protein Folding Patterns, *Annual review of biochemistry*, 59 (1990) 1007-1035.
- [130] H.P. Baden, L.D. Lee, Fibrous Protein of Human Epidermis, *Journal of Investigative Dermatology*, 71 (1978) 148-151.
- [131] C.N. Pace, The stability of globular proteins, *CRC Crit Rev Biochem*, 3 (1975) 1-43.
- [132] N. Shaklai, R.L. Garlick, H.F. Bunn, Nonenzymatic glycosylation of human serum albumin alters its conformation and function, *Journal of Biological Chemistry*, 259 (1984) 3812-3817.

- [133] S.D. Westerheide, R.I. Morimoto, Heat Shock Response Modulators as Therapeutic Tools for Diseases of Protein Conformation, *Journal of Biological Chemistry*, 280 (2005) 33097-33100.
- [134] A.G. Murzin, S.E. Brenner, T. Hubbard, C. Chothia, SCOP: A structural classification of proteins database for the investigation of sequences and structures, *Journal of Molecular Biology*, 247 (1995) 536-540.
- [135] P.A. Karplus, Experimentally observed conformation-dependent geometry and hidden strain in proteins, *Protein Science*, 5 (1996) 1406-1420.
- [136] M.W. Mosesson, The roles of fibrinogen and fibrin in hemostasis and thrombosis, *Semin Hematol*, 29 (1992) 177-188.
- [137] B. Blombäck, B. Hessel, D. Hogg, L. Therkildsen, A two-step fibrinogen–fibrin transition in blood coagulation, *Nature*, 275 (1978) 501-505.
- [138] M. Mittermayr, Hemostatic Changes After Crystalloid or Colloid Fluid Administration During Major Orthopedic Surgery: The Role of Fibrinogen Administration, *Anesthesia and analgesia*, 105 (2007) 905-917.
- [139] K.N. Jeejeebhoy, Albumin, fibrinogen and transferrin synthesis in isolated rat hepatocyte suspensions. A model for the study of plasma protein synthesis, *Biochemical journal*, 146 (1975) 141-155.
- [140] T.W. Meade, R. Chakrabarti, A.P. Haines, W.R. North, Y. Stirling, Characteristics affecting fibrinolytic activity and plasma fibrinogen concentrations, *British Medical Journal*, 1 (1979) 153-156.
- [141] S. Köhler, F. Schmid, G. Settanni, The Internal Dynamics of Fibrinogen and Its Implications for Coagulation and Adsorption, *PLoS Computational Biology*, 11 (2015) e1004346.
- [142] C.E. Hall, H.S. Slayter, The Fibrinogen Molecule: Its Size, Shape, and Mode of Polymerization, *The Journal of Biophysical and Biochemical Cytology*, 5 (1959) 11-27.
- [143] R.F. Doolittle, Fibrinogen and Fibrin, *Scientific American*, 245 (1981) 126-135.
- [144] G. Spraggon, S.J. Everse, R.F. Doolittle, Crystal structures of fragment D from human fibrinogen and its crosslinked counterpart from fibrin, *Nature*, 389 (1997) 455-462.
- [145] C.J. Wilson, R.E. Clegg, D.I. Leavesley, M.J. Pearcy, Mediation of Biomaterial–Cell Interactions by Adsorbed Proteins: A Review, *Tissue Engineering*, 11 (2005) 1-18.
- [146] M.W. Mosesson, K.R. Siebenlist, J.P. DiOrio, M. Matsuda, J.F. Hainfeld, J.S. Wall, The role of fibrinogen D domain intermolecular association sites in the polymerization of fibrin and fibrinogen Tokyo II (γ 275 Arg \rightarrow Cys), *The Journal of Clinical Investigation*, 96 (1995) 1053-1058.

- [147] J.W. Weisel, L. Medved, The Structure and Function of the α C Domains of Fibrinogen, *Annals of the New York Academy of Sciences*, 936 (2001) 312-327.
- [148] M.W. Mosesson, Fibrinogen functions and fibrin assembly, *Fibrinolysis and Proteolysis*, 14 (2000) 182-186.
- [149] M.W. Mosesson, K.R. Siebenlist, D.A. MEH, The Structure and Biological Features of Fibrinogen and Fibrin, *Annals of the New York Academy of Sciences*, 936 (2001) 11-30.
- [150] D.A. Cheresh, Human endothelial cells synthesize and express an Arg-Gly-Asp-directed adhesion receptor involved in attachment to fibrinogen and von Willebrand factor, *Proceedings of the National Academy of Sciences*, 84 (1987) 6471-6475.
- [151] B. Savage, E. Saldívar, Z.M. Ruggeri, Initiation of Platelet Adhesion by Arrest onto Fibrinogen or Translocation on von Willebrand Factor, *Cell*, 84 (1996) 289-297.
- [152] L. Zhang, B. Casey, D.K. Galanakis, C. Marmorat, S. Skoog, K. Vorvolakos, M. Simon, M.H. Rafailovich, The influence of surface chemistry on adsorbed fibrinogen conformation, orientation, fiber formation and platelet adhesion, *Acta Biomaterialia*, 54 (2017) 164-174.
- [153] Z.M. Ruggeri, Platelet Adhesion under Flow, *Microcirculation*, 16 (2009) 58-83.
- [154] B. Sivaraman, R.A. Latour, The relationship between platelet adhesion on surfaces and the structure versus the amount of adsorbed fibrinogen, *Biomaterials*, 31 (2010) 832-839.
- [155] R. Moriarty, C.A. McManus, M. Lambert, T. Tilley, M. Devocelle, M. Brennan, S.W. Kerrigan, D. Cox, A novel role for the fibrinogen Asn-Gly-Arg (NGR) motif in platelet function, *Thromb Haemost*, 114 (2015) 290-304.
- [156] R.A. Latour, Biomaterials: protein-surface interactions, *Encyclopedia of biomaterials and biomedical engineering*, 1 (2005) 270-278.
- [157] M. Rabe, D. Verdes, S. Seeger, Understanding protein adsorption phenomena at solid surfaces, *Advances in colloid and interface science*, 162 (2011) 87-106.
- [158] R.C. Graham Jr, M.J. Karnovsky, The early stages of absorption of injected horseradish peroxidase in the proximal tubules of mouse kidney: ultrastructural cytochemistry by a new technique, *Journal of Histochemistry & Cytochemistry*, 14 (1966) 291-302.
- [159] A.E. Cohen, W. Moerner, Controlling Brownian motion of single protein molecules and single fluorophores in aqueous buffer, *Optics express*, 16 (2008) 6941-6956.
- [160] D.J. Fink, T.B. Hutson, K.K. Chittur, R.M. Gendreau, Quantitative surface studies of protein adsorption by infrared spectroscopy: II. Quantification of adsorbed and bulk proteins, *Analytical Biochemistry*, 165 (1987) 147-154.
- [161] J.A. Schellman, Protein Stability in Mixed Solvents: A Balance of Contact Interaction and Excluded Volume, *Biophysical Journal*, 85 (2003) 108-125.

- [162] L. Vroman, A.L. Adams, G.C. Fischer, P.C. Munoz, Interaction of high molecular weight kininogen, factor XII, and fibrinogen in plasma at interfaces, *Blood*, 55 (1980) 156-159.
- [163] S.-Y. Jung, S.-M. Lim, F. Albertorio, G. Kim, M.C. Gurau, R.D. Yang, M.A. Holden, P.S. Cremer, The Vroman Effect: A Molecular Level Description of Fibrinogen Displacement, *Journal of the American Chemical Society*, 125 (2003) 12782-12786.
- [164] C.F. Wertz, M.M. Santore, Effect of Surface Hydrophobicity on Adsorption and Relaxation Kinetics of Albumin and Fibrinogen: Single-Species and Competitive Behavior, *Langmuir*, 17 (2001) 3006-3016.
- [165] J.-W. Shen, T. Wu, Q. Wang, H.-H. Pan, Molecular simulation of protein adsorption and desorption on hydroxyapatite surfaces, *Biomaterials*, 29 (2008) 513-532.
- [166] I. Lundström, H. Elwing, Simple kinetic models for protein exchange reactions on solid surfaces, *Journal of Colloid and Interface Science*, 136 (1990) 68-84.
- [167] W. Norde, Driving forces for protein adsorption at solid surfaces, *Macromolecular Symposia*, 103 (1996) 5-18.
- [168] K.L. Jones, C.R. O'Melia, Protein and humic acid adsorption onto hydrophilic membrane surfaces: effects of pH and ionic strength, *Journal of Membrane Science*, 165 (2000) 31-46.
- [169] F. Höök, M. Rodahl, B. Kasemo, P. Brzezinski, Structural changes in hemoglobin during adsorption to solid surfaces: Effects of pH, ionic strength, and ligand binding, *Proceedings of the National Academy of Sciences*, 95 (1998) 12271-12276.
- [170] W. Norde, J. Lyklema, The adsorption of human plasma albumin and bovine pancreas ribonuclease at negatively charged polystyrene surfaces: I. Adsorption isotherms. Effects of charge, ionic strength, and temperature, *Journal of Colloid and Interface Science*, 66 (1978) 257-265.
- [171] F.-Y. Lin, C.-S. Chen, W.-Y. Chen, S. Yamamoto, Microcalorimetric studies of the interaction mechanisms between proteins and Q-Sepharose at pH near the isoelectric point (pI): Effects of NaCl concentration, pH value, and temperature, *Journal of Chromatography A*, 912 (2001) 281-289.
- [172] M.B. Ulmschneider, M.S.P. Sansom, Amino acid distributions in integral membrane protein structures, *Biochimica et Biophysica Acta (BBA) - Biomembranes*, 1512 (2001) 1-14.
- [173] P. ARGOS, J. PALAU, Amino acid distribution in protein secondary structures, *International Journal of Peptide and Protein Research*, 19 (1982) 380-393.
- [174] R.A. Hartvig, M. van de Weert, J. Østergaard, L. Jorgensen, H. Jensen, Protein Adsorption at Charged Surfaces: The Role of Electrostatic Interactions and Interfacial Charge Regulation, *Langmuir*, 27 (2011) 2634-2643.

- [175] M. Binazadeh, Zeng, H., Unsworth, L. D., Inhibiting Nonspecific Protein Adsorption: Mechanisms, Methods, and Materials, in: J.M.a.J.R.-C. A. Taubert (Ed.) *Biomaterials Surface Science*, Wiley-VCH Verlag GmbH & Co. KGaA, Weinheim, Germany, 2013, pp. 45-61.
- [176] H. Zhu, M. Snyder, Protein chip technology, *Current Opinion in Chemical Biology*, 7 (2003) 55-63.
- [177] L. Tang, P. Thevenot, W. Hu, Surface Chemistry Influences Implant Biocompatibility, *Current Topics in Medicinal Chemistry*, 8 (2008) 270-280.
- [178] W. Khan, M. Kapoor, N. Kumar, Covalent attachment of proteins to functionalized polypyrrole-coated metallic surfaces for improved biocompatibility, *Acta Biomaterialia*, 3 (2007) 541-549.
- [179] Q. Wei, T. Becherer, S. Angioletti-Uberti, J. Dzubiella, C. Wischke, A.T. Neffe, A. Lendlein, M. Ballauff, R. Haag, Protein Interactions with Polymer Coatings and Biomaterials, *Angewandte Chemie International Edition*, 53 (2014) 8004-8031.
- [180] P. Roach, D. Farrar, C.C. Perry, Surface Tailoring for Controlled Protein Adsorption: Effect of Topography at the Nanometer Scale and Chemistry, *Journal of the American Chemical Society*, 128 (2006) 3939-3945.
- [181] K. Cai, J. Bossert, K.D. Jandt, Does the nanometre scale topography of titanium influence protein adsorption and cell proliferation?, *Colloids and Surfaces B: Biointerfaces*, 49 (2006) 136-144.
- [182] F.A. Denis, P. Hanarp, D.S. Sutherland, J. Gold, C. Mustin, P.G. Rouxhet, Y.F. Dufrêne, Protein Adsorption on Model Surfaces with Controlled Nanotopography and Chemistry, *Langmuir*, 18 (2002) 819-828.
- [183] H. Shi, W.-B. Tsai, M.D. Garrison, S. Ferrari, B.D. Ratner, Template-imprinted nanostructured surfaces for protein recognition, *Nature*, 398 (1999) 593-597.
- [184] I. Lynch, K.A. Dawson, Protein-nanoparticle interactions, *Nano Today*, 3 (2008) 40-47.
- [185] P. Kim, Fabrication of nanostructures of polyethylene glycol for applications to protein adsorption and cell adhesion, *Nanotechnology*, 16 (2005) 2420-2426.
- [186] K. Rechendorff, M.B. Hovgaard, M. Foss, V.P. Zhdanov, F. Besenbacher, Enhancement of Protein Adsorption Induced by Surface Roughness, *Langmuir*, 22 (2006) 10885-10888.
- [187] G. Hammarin, H. Persson, A.P. Dabkowska, C.N. Prinz, Enhanced laminin adsorption on nanowires compared to flat surfaces, *Colloids and Surfaces B: Biointerfaces*, 122 (2014) 85-89.
- [188] T. Xie, A. Vora, P.J. Mulcahey, S.E. Nancu, M. Singh, D.S. Choi, J.K. Huang, C.-C. Liu, D.P. Sanders, J.-i. Hahn, Surface Assembly Configurations and Packing Preferences of

Fibrinogen Mediated by the Periodicity and Alignment Control of Block Copolymer Nanodomains, *ACS Nano*, 10 (2016) 7705-7720.

[189] N. Dragneva, O. Rubel, W.B. Floriano, Molecular Dynamics of Fibrinogen Adsorption onto Graphene, but Not onto Poly(ethylene glycol) Surface, Increases Exposure of Recognition Sites That Trigger Immune Response, *Journal of Chemical Information and Modeling*, 56 (2016) 706-720.

[190] Z. Tang, C. He, H. Tian, J. Ding, B.S. Hsiao, B. Chu, X. Chen, Polymeric nanostructured materials for biomedical applications, *Progress in Polymer Science*, 60 (2016) 86-128.

[191] G.M.L. Messina, C. Satriano, G. Marletta, Confined protein adsorption into nanopore arrays fabricated by colloidal-assisted polymer patterning, *Chemical Communications*, (2008) 5031-5033.

[192] X. Zhang, C. Helbing, M.M.L. Arras, K.D. Jandt, I. Firkowska-Boden, Nanocrystal Width Controls Fibrinogen Orientation and Assembly Kinetics on Poly(butene-1) Surfaces, *Langmuir*, 33 (2017) 6563-6571.

[193] P. Jonkheijm, D. Weinrich, H. Schröder, C.M. Niemeyer, H. Waldmann, Chemical Strategies for Generating Protein Biochips, *Angewandte Chemie International Edition*, 47 (2008) 9618-9647.

[194] J.Y. Lim, H.J. Donahue, Cell Sensing and Response to Micro- and Nanostructured Surfaces Produced by Chemical and Topographic Patterning, *Tissue Engineering*, 13 (2007) 1879-1891.

[195] J.H. Lee, J. Kopecek, J.D. Andrade, Protein-resistant surfaces prepared by PEO-containing block copolymer surfactants, *Journal of Biomedical Materials Research*, 23 (1989) 351-368.

[196] K.H.A. Lau, J. Bang, D.H. Kim, W. Knoll, Self-assembly of Protein Nanoarrays on Block Copolymer Templates, *Advanced Functional Materials*, 18 (2008) 3148-3157.

[197] N. Kumar, J.-i. Hahm, Nanoscale Protein Patterning Using Self-Assembled Diblock Copolymers, *Langmuir*, 21 (2005) 6652-6655.

[198] S. Song, K. Ravensbergen, A. Alabanza, D. Soldin, J.-i. Hahm, Distinct Adsorption Configurations and Self-Assembly Characteristics of Fibrinogen on Chemically Uniform and Alternating Surfaces including Block Copolymer Nanodomains, *ACS Nano*, 8 (2014) 5257-5269.

[199] N. Kumar, O. Parajuli, A. Gupta, J.-i. Hahm, Elucidation of Protein Adsorption Behavior on Polymeric Surfaces: Toward High-Density, High-Payload Protein Templates, *Langmuir*, 24 (2008) 2688-2694.

- [200] M. Matsusaki, M. Omichi, K. Kadowaki, B.H. Kim, S.O. Kim, I. Maruyama, M. Akashi, Protein nanoarrays on a highly-oriented lamellar surface, *Chemical Communications*, 46 (2010) 1911-1913.
- [201] S.H. Baxamusa, K.K. Gleason, Random Copolymer Films with Molecular-Scale Compositional Heterogeneities that Interfere with Protein Adsorption, *Advanced Functional Materials*, 19 (2009) 3489-3496.
- [202] S. Song, T. Xie, K. Ravensbergen, J.-i. Hahm, Ascertaining effects of nanoscale polymeric interfaces on competitive protein adsorption at the individual protein level, *Nanoscale*, 8 (2016) 3496-3509.
- [203] R. Piner, R. Reifengerger, D.C. Martin, E.L. Thomas, R.P. Apkarian, A scanning tunneling microscope study of single crystal polyethylene, *Journal of Polymer Science Part C: Polymer Letters*, 28 (1990) 399-410.
- [204] C. Helbing, R. Stoeßel, D.A. Hering, M.M.L. Arras, J. Bossert, K.D. Jandt, pH-Dependent Ordered Fibrinogen Adsorption on Polyethylene Single Crystals, *Langmuir*, 32 (2016) 11868-11877.
- [205] N.R. Washburn, K.M. Yamada, C.G. Simon, S.B. Kennedy, E.J. Amis, High-throughput investigation of osteoblast response to polymer crystallinity: influence of nanometer-scale roughness on proliferation, *Biomaterials*, 25 (2004) 1215-1224.
- [206] H.K. Kim, T.G. Park, Comparative study on sustained release of human growth hormone from semi-crystalline poly(l-lactic acid) and amorphous poly(d,l-lactic-co-glycolic acid) microspheres: morphological effect on protein release, *Journal of Controlled Release*, 98 (2004) 115-125.
- [207] M. Kastantin, T.F. Keller, K.D. Jandt, D.K. Schwartz, Single-Molecule Tracking of Fibrinogen Dynamics on Nanostructured Poly(ethylene) Films, *Advanced Functional Materials*, 22 (2012) 2617-2623.
- [208] F.R. Rosendaal, Venous thrombosis: a multicausal disease, *The Lancet*, 353 (1999) 1167-1173.
- [209] P. Prandoni, A.W.A. Lensing, A. Cogo, S. Cuppini, S. Villalta, M. Carta, A.M. Cattelan, P. Polistena, E. Bernardi, M.H. Prins, The Long-Term Clinical Course of Acute Deep Venous Thrombosis, *Annals of Internal Medicine*, 125 (1996) 1-7.
- [210] I. Iakovou, T. Schmidt, E. Bonizzoni, L. Ge, G.M. Sangiorgi, G. Stankovic, F. Airolidi, A. Chieffo, M. Montorfano, M. Carlino, I. Michev, N. Corvaja, C. Briguori, U. Gerckens, E. Grube, A. Colombo, Incidence, Predictors, and Outcome of Thrombosis After Successful Implantation of Drug-Eluting Stents, *JAMA*, 293 (2005) 2126-2130.

- [211] L. Mauri, W.-h. Hsieh, J.M. Massaro, K.K.L. Ho, R. D'Agostino, D.E. Cutlip, Stent Thrombosis in Randomized Clinical Trials of Drug-Eluting Stents, *New England Journal of Medicine*, 356 (2007) 1020-1029.
- [212] L.A. Mermel, B.M. Farr, R.J. Sherertz, I.I. Raad, N. O'Grady, J.S. Harris, D.E. Craven, Guidelines for the Management of Intravascular Catheter-Related Infections, *Infection Control & Hospital Epidemiology*, 22 (2001) 222-242.
- [213] C.W. Akins, D.C. Miller, M.I. Turina, N.T. Kouchoukos, E.H. Blackstone, G.L. Grunkemeier, J.J.M. Takkenberg, T.E. David, E.G. Butchart, D.H. Adams, D.M. Shahian, S. Hagl, J.E. Mayer, B.W. Lytle, Guidelines for reporting mortality and morbidity after cardiac valve interventions, *European Journal of Cardio-Thoracic Surgery*, 33 (2008) 523-528.
- [214] B. Pérez-Saborido, D. Pacheco-Sánchez, A. Barrera-Rebollo, E. Asensio-Díaz, P. Pinto-Fuentes, J.C. Sarmentero-Prieto, P. Rodríguez-Vielba, R. Martínez-Díaz, M. Gonzalo-Martín, M. Rodríguez, H. Calero-Aguilar, R. Pintado-Garrido, F. García-Pajares, A. Anta-Román, Incidence, Management, and Results of Vascular Complications After Liver Transplantation, *Transplantation Proceedings*, 43 (2011) 749-750.
- [215] R.K. Andrews, M.C. Berndt, Platelet physiology and thrombosis, *Thrombosis Research*, 114 (2004) 447-453.
- [216] J.M. Gibbins, Platelet adhesion signalling and the regulation of thrombus formation, *Journal of Cell Science*, 117 (2004) 3415.
- [217] Z.M. Ruggeri, Mechanisms initiating platelet thrombus formation, *Thromb Haemostas*, 78 (1997) 611-616.
- [218] M.R.C.s.G.P.R. Framework., Thrombosis prevention trial: randomised trial of low-intensity oral anticoagulation with warfarin and low-dose aspirin in the primary prevention of ischaemic heart disease in men at increased risk, *The Lancet*, 351 (1998) 233-241.
- [219] C.W. Colwell, Jr., M.I. Froimson, M.A. Mont, M.A. Ritter, R.T. Trousdale, K.C. Buehler, A. Spitzer, T.K. Donaldson, D.E. Padgett, Thrombosis prevention after total hip arthroplasty: a prospective, randomized trial comparing a mobile compression device with low-molecular-weight heparin, *The Journal of bone and joint surgery. American volume*, 92 (2010) 527-535.
- [220] G.N. Chironi, C.M. Boulanger, A. Simon, F. Dignat-George, J.-M. Freyssinet, A. Tedgui, Endothelial microparticles in diseases, *Cell and Tissue Research*, 335 (2008) 143-151.
- [221] J.D. Pearson, Endothelial cell function and thrombosis, *Best Practice & Research Clinical Haematology*, 12 (1999) 329-341.

- [222] K. Adamson, E. Spain, U. Prendergast, R.J. Forster, N. Moran, T.E. Keyes, Ligand capture and activation of human platelets at monolayer modified gold surfaces, *Biomaterials Science*, 2 (2014) 1509-1520.
- [223] A. Campbell Robert, A. Overmyer Katherine, C.R. Bagnell, S. Wolberg Alisa, Cellular Procoagulant Activity Dictates Clot Structure and Stability as a Function of Distance From the Cell Surface, *Arteriosclerosis, Thrombosis, and Vascular Biology*, 28 (2008) 2247-2254.
- [224] A. Dibra, A. Kastrati, J. Mehilli, J. Pache, R. von Oepen, J. Dirschinger, A. Schömig, Influence of stent surface topography on the outcomes of patients undergoing coronary stenting: A randomized double-blind controlled trial, *Catheterization and Cardiovascular Interventions*, 65 (2005) 374-380.
- [225] T.T. Pham, S. Wiedemeier, S. Maenz, G. Gastrock, U. Settmacher, K.D. Jandt, J. Zanow, C. Lüdecke, J. Bossert, Hemodynamic aspects of reduced platelet adhesion on bioinspired microstructured surfaces, *Colloids and Surfaces B: Biointerfaces*, 145 (2016) 502-509.
- [226] L.B. Koh, I. Rodriguez, S.S. Venkatraman, A novel nanostructured poly(lactic-co-glycolic-acid)-multi-walled carbon nanotube composite for blood-contacting applications: Thrombogenicity studies, *Acta Biomaterialia*, 5 (2009) 3411-3422.
- [227] J.Y. Park, C.H. Gemmel, J.E. Davies, Platelet interactions with titanium: modulation of platelet activity by surface topography, *Biomaterials*, 22 (2001) 2671-2682.
- [228] L.B. Koh, I. Rodriguez, S.S. Venkatraman, The effect of topography of polymer surfaces on platelet adhesion, *Biomaterials*, 31 (2010) 1533-1545.
- [229] T. Sun, H. Tan, D. Han, Q. Fu, L. Jiang, No Platelet Can Adhere—Largely Improved Blood Compatibility on Nanostructured Superhydrophobic Surfaces, *Small*, 1 (2005) 959-963.
- [230] M. Stüber, L. Niederberger, F. Danneil, H. Leiste, S. Ulrich, A. Welle, M. Marin, H. Fischer, Surface Topography, Surface Energy and Wettability of Magnetron-Sputtered Amorphous Carbon (a-C) Films and Their Relevance for Platelet Adhesion, *Advanced Engineering Materials*, 9 (2007) 1114-1122.
- [231] M. Hulander, A. Lundgren, L. Faxälv, T.L. Lindahl, A. Palmquist, M. Berglin, H. Elwing, Gradients in surface nanotopography used to study platelet adhesion and activation, *Colloids and Surfaces B: Biointerfaces*, 110 (2013) 261-269.
- [232] B. Bhushan, K. Koch, Y.C. Jung, Nanostructures for superhydrophobicity and low adhesion, *Soft Matter*, 4 (2008) 1799-1804.
- [233] J.N. Lindon, G. McManama, L. Kushner, E.W. Merrill, E.W. Salzman, Does the conformation of adsorbed fibrinogen dictate platelet interactions with artificial surfaces?, *Blood*, 68 (1986) 355-362.

- [234] T.P. Ugarova, A.Z. Budzynski, S.J. Shattil, Z.M. Ruggeri, M.H. Ginsberg, E.F. Plow, Conformational changes in fibrinogen elicited by its interaction with platelet membrane glycoprotein GPIIb-IIIa, *Journal of Biological Chemistry*, 268 (1993) 21080-21087.
- [235] J.W. Weisel, C. Nagaswami, G. Vilaire, J.S. Bennett, Examination of the platelet membrane glycoprotein IIb-IIIa complex and its interaction with fibrinogen and other ligands by electron microscopy, *Journal of Biological Chemistry*, 267 (1992) 16637-16643.
- [236] L.-C. Xu, J.W. Bauer, C.A. Siedlecki, Proteins, platelets, and blood coagulation at biomaterial interfaces, *Colloids and Surfaces B: Biointerfaces*, 124 (2014) 49-68.
- [237] T. Xie, J. Chatteraj, P.J. Mulcahey, N.P. Kelleher, E. Del Gado, J.-i. Hahn, Revealing the principal attributes of protein adsorption on block copolymer surfaces with direct experimental evidence at the single protein level, *Nanoscale*, 10 (2018) 9063-9076.
- [238] M.S. Lord, J.M. Whitelock, A. Simmons, R.L. Williams, B.K. Milthorpe, Fibrinogen adsorption and platelet adhesion to silica surfaces with stochastic nanotopography, *Biointerphases*, 9 (2014) 041002.
- [239] H. Wang, P. Akcora, Confinement effect on the structure and elasticity of proteins interfacing polymers, *Soft Matter*, 13 (2017) 1561-1568.
- [240] G. Binnig, C.F. Quate, C. Gerber, Atomic Force Microscope, *Physical Review Letters*, 56 (1986) 930-933.
- [241] F.J. Giessibl, Advances in atomic force microscopy, *Reviews of Modern Physics*, 75 (2003) 949-983.
- [242] G. Meyer, N.M. Amer, Novel optical approach to atomic force microscopy, *Applied Physics Letters*, 53 (1988) 1045-1047.
- [243] B. Cappella, G. Dietler, Force-distance curves by atomic force microscopy, *Surface Science Reports*, 34 (1999) 1-104.
- [244] E. Meyer, Atomic force microscopy, *Progress in Surface Science*, 41 (1992) 3-49.
- [245] M.J. Higgins, C.K. Riener, T. Uchihashi, J.E. Sader, R. McKendry, S.P. Jarvis, Frequency modulation atomic force microscopy: a dynamic measurement technique for biological systems, *Nanotechnology*, 16 (2005) S85-S89.
- [246] C.F.Q. F. J. Giessibl, Exploring the nanoworld with atomic force microscopy, *Physics today*, 59 (2006) 44-50.
- [247] B. Anczykowski, B. Gotsmann, H. Fuchs, J.P. Cleveland, V.B. Elings, How to measure energy dissipation in dynamic mode atomic force microscopy, *Applied Surface Science*, 140 (1999) 376-382.
- [248] U. Rabe, S. Amelio, M. Kopycinska, S. Hirsekorn, M. Kempf, M. Göken, W. Arnold, Imaging and measurement of local mechanical material properties by atomic force acoustic microscopy, *Surface and Interface Analysis*, 33 (2002) 65-70.

- [249] Y. Song, B. Bhushan, Atomic force microscopy dynamic modes: modeling and applications, *Journal of Physics: Condensed Matter*, 20 (2008) 225012.
- [250] S.N. Magonov, V. Elings, M.H. Whangbo, Phase imaging and stiffness in tapping-mode atomic force microscopy, *Surface Science*, 375 (1997) L385-L391.
- [251] R. García, A. San Paulo, Attractive and repulsive tip-sample interaction regimes in tapping-mode atomic force microscopy, *Physical Review B*, 60 (1999) 4961-4967.
- [252] C.A.J. Putman, K.O.V.d. Werf, B.G.D. Grooth, N.F.V. Hulst, J. Greve, Tapping mode atomic force microscopy in liquid, *Applied Physics Letters*, 64 (1994) 2454-2456.
- [253] T.G. Kuznetsova, M.N. Starodubtseva, N.I. Yegorenkov, S.A. Chizhik, R.I. Zhdanov, Atomic force microscopy probing of cell elasticity, *Micron*, 38 (2007) 824-833.
- [254] M. Radmacher, R.W. Tillmann, M. Fritz, H.E. Gaub, From molecules to cells: imaging soft samples with the atomic force microscope, *Science*, 257 (1992) 1900-1905.
- [255] D.F. Ogletree, R.W. Carpick, M. Salmeron, Calibration of frictional forces in atomic force microscopy, *Review of Scientific Instruments*, 67 (1996) 3298-3306.
- [256] R.M. Overney, E. Meyer, J. Frommer, D. Brodbeck, R. Lüthi, L. Howald, H.J. Giintherodt, M. Fujihira, H. Takano, Y. Gotoh, Friction measurements on phase-separated thin films with a modified atomic force microscope, *Nature*, 359 (1992) 133-135.
- [257] M.E. McConney, S. Singamaneni, V.V. Tsukruk, Probing Soft Matter with the Atomic Force Microscopies: Imaging and Force Spectroscopy, *Polymer Reviews*, 50 (2010) 235-286.
- [258] R. Buzio, C. Boragno, U. Valbusa, Contact mechanics and friction of fractal surfaces probed by atomic force microscopy, *Wear*, 254 (2003) 917-923.
- [259] W.A. Ducker, T.J. Senden, R.M. Pashley, Direct measurement of colloidal forces using an atomic force microscope, *Nature*, 353 (1991) 239-241.
- [260] A. Halperin, E.B. Zhulina, Atomic Force Microscopy of Polymer Brushes: Colloidal versus Sharp Tips, *Langmuir*, 26 (2010) 8933-8940.
- [261] S. Pasche, M. Textor, L. Meagher, N.D. Spencer, H.J. Griesser, Relationship between Interfacial Forces Measured by Colloid-Probe Atomic Force Microscopy and Protein Resistance of Poly(ethylene glycol)-Grafted Poly(l-lysine) Adlayers on Niobia Surfaces, *Langmuir*, 21 (2005) 6508-6520.
- [262] J. Malmström, H. Agheli, P. Kingshott, D.S. Sutherland, Viscoelastic Modeling of Highly Hydrated Laminin Layers at Homogeneous and Nanostructured Surfaces: Quantification of Protein Layer Properties Using QCM-D and SPR, *Langmuir*, 23 (2007) 9760-9768.
- [263] A. Dolatshahi-Pirouz, K. Rechendorff, M.B. Hovgaard, M. Foss, J. Chevallier, F. Besenbacher, Bovine serum albumin adsorption on nano-rough platinum surfaces studied by QCM-D, *Colloids and Surfaces B: Biointerfaces*, 66 (2008) 53-59.

- [264] A.A. Feiler, A. Sahlholm, T. Sandberg, K.D. Caldwell, Adsorption and viscoelastic properties of fractionated mucin (BSM) and bovine serum albumin (BSA) studied with quartz crystal microbalance (QCM-D), *Journal of Colloid and Interface Science*, 315 (2007) 475-481.
- [265] M. Rodahl, F. Höök, C. Fredriksson, C. A. Keller, A. Krozer, P. Brzezinski, M. Voinova, B. Kasemo, Simultaneous frequency and dissipation factor QCM measurements of biomolecular adsorption and cell adhesion, *Faraday Discussions*, 107 (1997) 229-246.
- [266] M. Rodahl, F. Höök, B. Kasemo, QCM Operation in Liquids: An Explanation of Measured Variations in Frequency and Q Factor with Liquid Conductivity, *Analytical Chemistry*, 68 (1996) 2219-2227.
- [267] M. Rodahl, B. Kasemo, Frequency and dissipation-factor responses to localized liquid deposits on a QCM electrode, *Sensors and Actuators B: Chemical*, 37 (1996) 111-116.
- [268] K.A. Marx, The Quartz Crystal Microbalance and the Electrochemical QCM: Applications to Studies of Thin Polymer Films, Electron Transfer Systems, Biological Macromolecules, Biosensors, and Cells, in: A. Janshoff, C. Steinem (Eds.) *Piezoelectric Sensors*, Springer Berlin Heidelberg, Berlin, Heidelberg, 2007, pp. 371-424.
- [269] M.V. Voinova, M. Jonson, B. Kasemo, 'Missing mass' effect in biosensor's QCM applications, *Biosensors and Bioelectronics*, 17 (2002) 835-841.
- [270] B.D. Vogt, E.K. Lin, W.-l. Wu, C.C. White, Effect of Film Thickness on the Validity of the Sauerbrey Equation for Hydrated Polyelectrolyte Films, *The Journal of Physical Chemistry B*, 108 (2004) 12685-12690.
- [271] L. Rodriguez-Pardo, J.F. Rodriguez, C. Gabrielli, H. Perrot, R. Brendel, Sensitivity, noise, and resolution in QCM sensors in liquid media, *IEEE Sensors Journal*, 5 (2005) 1251-1257.
- [272] N. Chandrasekaran, S. Dimartino, C.J. Fee, Study of the adsorption of proteins on stainless steel surfaces using QCM-D, *Chemical Engineering Research and Design*, 91 (2013) 1674-1683.
- [273] M.J. Kasser, Regulation of UHMWPE biomaterials in total hip arthroplasty, *Journal of Biomedical Materials Research Part B: Applied Biomaterials*, 101B (2013) 400-406.
- [274] I. Reviakine, D. Johannsmann, R.P. Richter, Hearing What You Cannot See and Visualizing What You Hear: Interpreting Quartz Crystal Microbalance Data from Solvated Interfaces, *Analytical Chemistry*, 83 (2011) 8838-8848.
- [275] F. Höök, J. Vörös, M. Rodahl, R. Kurrat, P. Böni, J.J. Ramsden, M. Textor, N.D. Spencer, P. Tengvall, J. Gold, B. Kasemo, A comparative study of protein adsorption on titanium oxide surfaces using in situ ellipsometry, optical waveguide lightmode spectroscopy, and quartz crystal microbalance/dissipation, *Colloids and Surfaces B: Biointerfaces*, 24 (2002) 155-170.

- [276] J. Hu, D. Yang, Q. Kang, D. Shen, Estimation the kinetics parameters for non-specific adsorption of fibrinogen on quartz surface from the response of an electrode-separated piezoelectric sensor, *Sensors and Actuators B: Chemical*, 96 (2003) 390-398.
- [277] M. Kastantin, D.K. Schwartz, Connecting Rare DNA Conformations and Surface Dynamics Using Single-Molecule Resonance Energy Transfer, *ACS Nano*, 5 (2011) 9861-9869.
- [278] A. Honciuc, D.K. Schwartz, Probing Hydrophobic Interactions Using Trajectories of Amphiphilic Molecules at a Hydrophobic/Water Interface, *Journal of the American Chemical Society*, 131 (2009) 5973-5979.
- [279] M. Kastantin, B.B. Langdon, E.L. Chang, D.K. Schwartz, Single-Molecule Resolution of Interfacial Fibrinogen Behavior: Effects of Oligomer Populations and Surface Chemistry, *Journal of the American Chemical Society*, 133 (2011) 4975-4983.
- [280] R. Walder, N. Nelson, D.K. Schwartz, Super-resolution surface mapping using the trajectories of molecular probes, *Nature Communications*, 2 (2011) 515-522.
- [281] M. Kastantin, R. Walder, D.K. Schwartz, Identifying Mechanisms of Interfacial Dynamics Using Single-Molecule Tracking, *Langmuir*, 28 (2012) 12443-12456.
- [282] R.T.T. Gettens, Z. Bai, J.L. Gilbert, Quantification of the kinetics and thermodynamics of protein adsorption using atomic force microscopy, *Journal of Biomedical Materials Research Part A*, 72A (2005) 246-257.
- [283] S.H. Kristensen, G.A. Pedersen, L.N. Nejsun, D.S. Sutherland, Protein Adsorption at Nanopatterned Surfaces Studied by Quartz Crystal Microbalance with Dissipation and Surface Plasmon Resonance, *The Journal of Physical Chemistry B*, 117 (2013) 10376-10383.
- [284] H. Jung, J.-Y. Kim, Y. Kim, G. Tae, Y.H. Kim, D. Johannsmann, QCM and AFM Analysis of Anticoagulant Activities of Sulfonated Polymers against Fibrin Formation, *Langmuir*, 25 (2009) 7032-7041.
- [285] O. Mellbring, S. Kihlman Øiseth, A. Krozer, J. Lausmaa, T. Hjertberg, Spin Coating and Characterization of Thin High-Density Polyethylene Films, *Macromolecules*, 34 (2001) 7496-7503.
- [286] P.S. Sit, R.E. Marchant, Surface-dependent differences in fibrin assembly visualized by atomic force microscopy, *Surface Science*, 491 (2001) 421-432.
- [287] A.D. Protopopova, N.A. Barinov, E.G. Zavyalova, A.M. Kopylov, V.I. Sergienko, D.V. Klinov, Visualization of fibrinogen α C regions and their arrangement during fibrin network formation by high-resolution AFM, *Journal of Thrombosis and Haemostasis*, 13 (2015) 570-579.
- [288] P.H. Hermans, *Physics and Chemistry of Cellulose Fibres*, New York, 1949.

- [289] R. Rezakhaniha, A. Agianniotis, J.T.C. Schrauwen, A. Griffa, D. Sage, C.V.C. Bouten, F.N. van de Vosse, M. Unser, N. Stergiopoulos, Experimental investigation of collagen waviness and orientation in the arterial adventitia using confocal laser scanning microscopy, *Biomechanics and Modeling in Mechanobiology*, 11 (2012) 461-473.
- [290] Z. Gu, Z. Yang, Y. Chong, C. Ge, J.K. Weber, D.R. Bell, R. Zhou, Surface Curvature Relation to Protein Adsorption for Carbon-based Nanomaterials, *Scientific Reports*, 5 (2015) 10886-10895.
- [291] Y. Zhang, Y. Fung, H. Sun, D. Zhu, S. Yao, Study of protein adsorption on polymer coatings surface by combining quartz crystal microbalance with electrochemical impedance methods, *Sensors and Actuators B: Chemical*, 108 (2005) 933-942.
- [292] S. Jiang, Y. Duan, L. Li, D. Yan, E. Chen, S. Yan, An AFM study on the structure and melting behavior of melt-crystallized isotactic poly(1-butene), *Polymer*, 45 (2004) 6365-6374.
- [293] Z. Adamczyk, J. Barbasz, M. Cieřła, Mechanisms of Fibrinogen Adsorption at Solid Substrates, *Langmuir*, 27 (2011) 6868-6878.
- [294] L. Guicai, S. Xiaoli, Y. Ping, Z. Ansha, H. Nan, Investigation of fibrinogen adsorption on solid surface by quartz crystal microbalance with dissipation(QCM-D) and ELISA, *Solid State Ionics*, 179 (2008) 932-935.
- [295] M. Kumar Vyas, K. Schneider, B. Nandan, M. Stamm, Switching of friction by binary polymer brushes, *Soft Matter*, 4 (2008) 1024-1032.
- [296] J.M. Kollman, L. Pandi, M.R. Sawaya, M. Riley, R.F. Doolittle, Crystal Structure of Human Fibrinogen, *Biochemistry*, 48 (2009) 3877-3886.
- [297] I.S. Yermolenko, V.K. Lishko, T.P. Ugarova, S.N. Magonov, High-Resolution Visualization of Fibrinogen Molecules and Fibrin Fibers with Atomic Force Microscopy, *Biomacromolecules*, 12 (2011) 370-379.
- [298] J.W. Weisel, R.I. Litvinov, Fibrin Formation, Structure and Properties, in: D.A.D. Parry, J.M. Squire (Eds.) *Fibrous Proteins: Structures and Mechanisms*, Springer International Publishing, Cham, 2017, pp. 405-456.
- [299] M.P. Heuberger, M.R. Widmer, E. Zobeley, R. Glockshuber, N.D. Spencer, Protein-mediated boundary lubrication in arthroplasty, *Biomaterials*, 26 (2005) 1165-1173.
- [300] F. Pourdanesh, A. Jebali, S. Hekmatimoghaddam, A. Allaveisie, In vitro and in vivo evaluation of a new nanocomposite, containing high density polyethylene, tricalcium phosphate, hydroxyapatite, and magnesium oxide nanoparticles, *Materials Science and Engineering: C*, 40 (2014) 382-388.
- [301] M. Prasitsilp, T. Siritwittayakorn, R. Molloy, N. Suebsanit, P. Siritwittayakorn, S. Veeranondha, Cytotoxicity study of homopolymers and copolymers of 2-hydroxyethyl

methacrylate and some alkyl acrylates for potential use as temporary skin substitutes, *Journal of Materials Science: Materials in Medicine*, 14 (2003) 595-600.

[302] J.E. Italiano, W. Bergmeier, S. Tiwari, H. Falet, J.H. Hartwig, K.M. Hoffmeister, P. André, D.D. Wagner, R.A. Shivdasani, Mechanisms and implications of platelet discoid shape, *Blood*, 101 (2003) 4789-4796.

[303] M. Moser, B. Nieswandt, S. Ussar, M. Pozgajova, R. Fässler, Kindlin-3 is essential for integrin activation and platelet aggregation, *Nature Medicine*, 14 (2008) 325-330.

[304] D.H. Farrell, P. Thiagarajan, Binding of recombinant fibrinogen mutants to platelets, *Journal of Biological Chemistry*, 269 (1994) 226-231.

[305] D.H. Farrell, P. Thiagarajan, D.W. Chung, E.W. Davie, Role of fibrinogen alpha and gamma chain sites in platelet aggregation, *Proceedings of the National Academy of Sciences*, 89 (1992) 10729-10732.

[306] W.D. Callister Jr, D.G. Rethwisch, *Fundamentals of materials science and engineering: an integrated approach*, John Wiley & Sons 2012.

[307] K.C. Dee, D.A. Puleo, R. Bizios, *Tissue-biomaterial interactions*, Hoboken: Wiley, (2002).

Acknowledgments

First and foremost, I would like to thank my supervisor Prof. Klaus D. Jandt. It has been an honor to be his first Chinese Ph.D. student. All his contributions of time, ideas, and patience, especially funding during my tough time during the Ph.D. pursuit, are highly appreciated and stored up in my heart.

The members of the Jandt group have gifted me abundant friendships, efficient collaborations, and thoroughly advice through my life in Jena. I very much appreciate Dr. Izabela Firkowska-Boden for all the instructions, willingness, and revisions of manuscripts and thesis. I am especially grateful to Dr. Matthias M. L. Arras, Christian Helbing, Prof. Huiliang Cao, Prof. Bin Zhao, and Dr. Jörg Bossert for their enthusiasm, suggestions, and collaborations through my professional life. I also would like to acknowledge Ines Thiele, Heidrun Garlipp, Dr. Thomas Dauben, Felix Arendt, and Carolin Dewald who helped me with the part of the experimental works. Furthermore, I am also thankful for the beautiful memories with Mrs. Karin Jandt. Meanwhile, I would like to thank Robert Marvin for proofreading of the dissertation. Regarding the experimental instructions, I have appreciated the past and present group members, Ines Schildhauer, Ralf Wagner, Dr. Ranko Adjiski, Prof. Fuping Dong, Max Hennig, Dr. Tam Thanh Pham, Mike Mühlstädt, Dr. Robert Stößel, Michaela Schürmann, Karl Scheuer, Dr. Stefan Maenz, Katherine Su, Bojia He, Yuan Shen, Haifeng Xu, Michele Scholl, Dr. Tanatchaporn Sangfai, Jiaxin Lian, and Prof. Xin Wang.

I gratefully acknowledge the funding sources, China Scholarship Council (CSC) for giving a chance for my Ph.D. work in Germany. Last but most importantly, I would like to thank my family (Yaqing Zhang, Yuefang Hu, Yibo Zhang, Xiaoning Zhang, Peidong Zhang, and Zhichao Wang) as well as all my friends for their love, sincerity, patience, understanding, and faithful support.

Xiaoyuan Zhang

Curriculum Vitae

Personal Information

Name	Xiaoyuan Zhang
Date of Birth	23. November 1988
Place of Birth	Qinghai province, P. R. China
Nationality	People's Republic of China
E-mail	xiaoyuan.zhang@uni-jena.de
Address	Löbdergraben 32, E014, D-07743, Jena, Germany

Education

09/2013 - now	Ph.D. candidate in Material Science Friedrich-Schiller-Universität Jena (Jena, Germany)
09/2010 - 07/2013	Master in Polymer Chemistry and Physics Beijing University of Chemical Technology (Peking, P.R. China)
09/2005 - 07/2009	Bachelor in Polymer Science and Engineering Beijing University of Chemical Technology (Peking, P.R. China)

Projects

2013-now	“Protein adsorption on nanostructured polymer surfaces” Project, Chair of Materials Science, Otto Schott Institute of Materials Research (OSIM), Friedrich Schiller University Jena, Germany
2013	“Crystallization and Phase Separation Behavior of PE- <i>b</i> -PEO Diblock Copolymer and Nano-hybrids” Project, State Key Laboratory of Chemical Resource Engineering, BUCT, Peking, P.R. China
2012	I. “Electrospinning of Polymer Nanofibers Filled with Nanoparticles and Its Application in the Field of Non-Enzymatic Amperometric Biosensors” Project, BUCT, Peking, P.R. China II. “Reactive Blending as Effective Method in Promoting Nucleation Efficiency of Polymeric Nucleating Agents in Isotactic Polypropylene” Project, BUCT, Peking, P.R. China III. “Surface Structure Regulation and Biological Application of Amphipathic Diblock Copolymers” project for the “Natural Science Foundation of China” (NSFC), BUCT, Peking, P.R. China

2009 “Crystallization Behavior of Isotactic Polypropylene/Clay Nano-composites” Project, State Key Laboratory of Polymer Physics and Chemistry, Institute of Chemistry, Chinese Academy of Sciences (ICCAS), Peking, P.R. China

Publications

2018 “Influence of Network Structure on the Crystallization Behavior in Chemically Crosslinked PEG Hydrogels” *Polymers* 2018, 10(9): 970.

Zhenfang Zhang, Qian Li, Cigdem Yesildag, Christoph Bartsch, *Xiaoyuan Zhang*, Wei Liu, Axel Loebus, Zhiqiang Su*, Marga Lensen*

“Controlling Protein Adsorption through Nanostructured Polymeric Surfaces” *Advance healthcare material* 2018, 7 (1), 1700995. (Cover)

Izabela Firkowska-Boden, *Xiaoyuan Zhang*, Klaus D. Jandt*

“Nanoconfinement and Sansetsukon-like Nanocrawling Govern Fibrinogen Dynamics and Self-Assembly on Nanostructured Polymeric Surfaces” *Langmuir* 2018, 34(47), 14309-14316. (Cover)

Xiaoyuan Zhang[‡], Izabela Firkowska-Boden[‡], Matthias Michael Lothar Arras, Mark Kastantin, Christian Helbing, Alper Özoğul, Enrico Gnecco, Daniel K Schwartz, Klaus D Jandt*

2017 “Nanocrystal Width Controls Fibrinogen Orientation and Assembly Kinetics on Poly (butane-1) Surfaces” *Langmuir* 2017 (33) 6563–6571.

Xiaoyuan Zhang, Christian Helbing, Matthias M. L. Arras, Klaus D. Jandt*, and Izabela Firkowska-Boden

2015 “Graphene film doped with silver nanoparticles: self-assembly formation, structural characterizations, antibacterial ability, and biocompatibility” Published online. *Biomater. Sci.* 2015 3 852-860.

Panpan Zhang, Haixia Wang, *Xiaoyuan Zhang*, Wei Xu, Yang Li, Qing Li, Gang Wei* and Zhiqiang Su*

2014 1. “Path-way Mediated Microstructures and Phase Morphologies of Asymmetric Double Crystalline Co-Oligomer” *RSC Advances*, 2014 (4) 7900-7910.

Xiaoyuan Zhang, Zhaofei Ouyang, Robert Schulze, Thomas F. Keller, Klaus D. Jandt* and Zhiqiang Su*

2. “How Different Mesophases Affect the Interactive Crystallisation of a Block Co-oligomer” Published online.

Xiaoyuan Zhang, Robert Schulze, Panpan Zhang, Claudia Lüdecke, Xiuqin Zhang*, Zhiqiang Su*, Klaus D. Jandt

- 2013
-
1. "A highly effective reactive liquid crystal for the improved β -nucleation of isotactic polypropylene" Published online.
Qing Li[†], *Xiaoyuan Zhang*[†], Jingfeng Li, Zhaofei Ouyang, Zhiqiang Su* and Gang Wei*
-
2. "One-pot green synthesis, characterizations, and biosensor application of self-assembled reduced graphene oxide -gold nanoparticle hybrid membranes" *J. Mater. Chem. B* 2013 (1) 6525-6531.
Panpan Zhang, *Xiaoyuan Zhang*, Siyu Zhang, Xin Lu, Qing Li, Zhiqiang Su* and Gang Wei*
-
3. "Self-assembled reduced graphene oxide/gold nanoparticle hybrid membrane by one-pot green synthesis for a novel H₂O₂ biosensor" *Journal of Materials Chemistry B* 2013 (47) 6525-6531.
Panpan Zhang, *Xiaoyuan Zhang*, Siyu Zhang, Xin Lu, Qing Li, Zhiqiang Su* and Gang Wei*
-
4. "Synthesis, characterization and drug release application of carbon nanotube-polymer nanosphere composites" *RSC Advances*, 2013, 3(24): 9304-9310.
Haixia Wang, Jingfeng Li, *Xiaoyuan Zhang*, Zhaofei Ouyang, Qing Li, Zhiqiang Su* and Gang Wei*
-
5. "Electrospinning polyurethane nanofibers filled with carbon nanotubes and silver nanoparticles on the electrode for the non-enzymatic amperometric sensor of hydrogen peroxide" *Journal of Materials Chemistry B*, 2013, 1: 2415-2424.
Zhaofei Ouyang, Jingfeng Li, Jinhui Wang, Tongyang Ni, *Xiaoyuan Zhang*, Haixia Wang, Qing Li, Zhiqiang Su*, and Gang Wei

Conferences

-
- 2019 Thüringer Werkstofftag 2019 (poster)
-
- 2018 CGCA® East forum 2018 (attendance)
Thüringer Werkstofftag 2018 (poster)
CGCA® 30th annual conference (talk)
-
- 2017 Thüringer Werkstofftag 2017 (poster)
Biomat 2017 (poster)
CGCA® 29th annual conference (talk)
JSMC Symposium 2017 (talk)
-
- 2016 CGCA® South forum 2016 (talk)
Thüringer Werkstofftag 2016 (poster)
CGCA® 28th annual conference (talk)

	Ministry of Education of the P. R. China 'Chunhui' Plan (talk)	
	CGCA® East forum 2016 (talk)	
	JSMC Symposium 2016 (talk)	
2015	Thüringer Werkstofftag 2015 (poster)	
	Biomat 2015 (attendance)	
	CGCA® East forum 2015 (talk)	
	JSMC Retreat 2015 (talk and poster)	

Honors and Awards

2017	Young researchers up to 30 years, in BioMAT 2017, Second Prize (top two)	Once
2016	“Chunhui” Plan, the Ministry of Education of the P.R. China (top 1%)	Once
2013-2017	Award poster presentations in Thueringer Werkstofftag (top three)	Twice
2013	China Scholarship Council (CSC) for PhD student	Once
2011-2012	Tuition Scholarship, Second Prize (top 5%)	Twice
2007-2008	People Scholarship, Third Prize (top 10%)	Twice
2006-2007	Social Practice Advanced Individual Award (top 1%)	Once
2006	PowerPoint Design Competition, Third Prize (top 2%)	Once
